AIRBORNE ELECTROMAGNETIC SEA ICE SOUNDER OPERATIONAL SENSITIVITY AND ERROR ANALYSIS

J.S. Holladay

Ocean Sciences Division
Maritimes Region
Fisheries and Oceans Canada

Bedford Institute of Oceanography
P.O. Box 1006
Dartmouth, Nova Scotia
Canada B2Y 4A2

1999

Canadian Contractor Report of Hydrography and Ocean Sciences 54

Fisheries and Oceans | Pêches et Océans

Canada

Canadian Contractor Report of
Hydrography and Ocean Sciences 54

1999

Airborne Electromagnetic Sea Ice Sounder Operational Sensitivity and Error Analysis

by

J.S. Holladay*

Ocean Sciences Division
Maritimes Region
Fisheries and Oceans Canada

Bedford Institute of Oceanography
PO Box 1006
Dartmouth, Nova Scotia
Canada, B2Y 4A2

* Vanguard Geophysics Inc.
66 Mann Avenue
Toronto, Ontario M4S 2Y3

Cat. No. Fs97-17/54 E ISSN 0711-6748

Correct Citation for this publication:

Holladay, J.S., 1999, Airborne Electromagnetic Sea Ice Sounder Operational Sensitivity and Error Analysis , Can. Contract. Rep. Hydrogr. Ocean Sci. 54: xi + 85 p.

TABLE OF CONTENTS

ABSTRACT

Holladay, J.S., 1999, Airborne Electromagnetic Sea Ice Sounder Operational Sensitivity and Error Analysis , Can. Contract. Rep. Hydrogr. Ocean Sci. 54: xi + 85 p.

The Canadian Coast Guard airborne Electromagnetic Ice Sounder (EIS) estimates the thickness and electrical conductivity of floating sea ice using an electromagnetic (EM) sensor towed beneath a helicopter. Considerable operational experience has been accumulated with the EIS over the last four years, and with predecessor systems since the early 1990's. In order to facilitate the transition of the sensor from demonstration status to a robust, fully-operational tool for ice monitoring, a detailed analysis of EIS sensitivity and error characteristics was conducted. This study substantiated earlier estimates of the sensitivity of EIS calibration and operational accuracy to EM error, altitude and orientation effects, leading to the formulation of error budgets for calibration and operational use of the system, both in real time and for post-processed datasets. Calibration of the sensor over open water was also investigated through analysis of field examples. Field examples were used to clarify the importance of key error sources for operational cases. Finally, work on a Quality index was started which synthesises the contributions to ice conductivity and thickness error of sensor altitude, EM drift, sensor motion and observed fitting error into a single quantity which in future can be generated in real time or in post-processing. The principal conclusion regarding EIS accuracy was that the original planned accuracy of +/- 10 cm is achieved over FY and MY ice most of the time. Larger errors occur over thinner ice (<10 cm). When enhanced ice thickness or conductivity accuracies are required, maintaining a relatively low survey altitude (10-15 m) is critical, as is the correct timing of background measurements for EM drift removal. An improved pilot display incorporating digital and analogue information on sensor altitude, orientation and Quality index on a sunlight-visible unit would improve operational data quality and consistency substantially. EM drift is the most troublesome error source in the present implementation of the system: a test program for analysis and reduction of drift error would substantially improve the productivity and accuracy of routine operations. If an order of magnitude or greater improvement in EM drift levels can be achieved, enhanced accuracies would be obtainable at a considerably greater height, which would reduce the effort required of the helicopter pilot. It should also be possible to improve real-time accuracy by more accurate prediction of EM drift.

RÉSUMÉ

Holladay, J.S., 1999, Airborne Electromagnetic Sea Ice Sounder Operational Sensitivity and Error Analysis , Can. Contract. Rep. Hydrogr. Ocean Sci. 54: xi + 85 p.

Le sondeur de glace électromagnétique (EIS) aéroporté de la Garde côtière canadienne estime l'épaisseur et la conductivité électrique de la glace marine flottante au moyen d'un capteur électromagnétique (EM) suspendu à un hélicoptère. Ces quatre dernières années, on a acquis une expérience opérationnelle considérable avec l'EIS, et depuis le début des années 90 avec des systèmes précurseurs. Afin de permettre la transition du capteur d'un outil à l'état de démonstration à un robuste outil entièrement opérationnel pour la surveillance des glaces, on a mené une analyse détaillée de la sensibilité et des erreurs caractéristiques de l'EIS. Cette analyse a confirmé des estimations antérieures de la sensibilité de l'étalonnage et de la précision opérationnelle de l'EIS aux effets de l'erreur EM, de l'altitude et de l'orientation, ce qui a donné lieu à la pondération des erreurs pour l'étalonnage et l'utilisation opérationnelle du système, tant en temps réel que pour des ensembles de données de post-traitement. On a également étudié l'étalonnage du capteur par-dessus la mer libre par analyse d'exemples de conditions réelles. Des exemples de conditions d'exploitation ont été utilisés pour déterminer l'importance de sources d'erreurs clés pour les dossiers opérationnels. Enfin, on a commencé l'élaboration d'un indice de qualité qui synthétise les contributions à l'erreur de conductivité et d'épaisseur des glaces de l'altitude du capteur, de la dérive EM, du mouvement du capteur et de l'erreur d'ajustement observée en une seule grandeur qui, à l'avenir, pourra être générée en temps réel ou en post-traitement. La principale conclusion concernant la précision de l'EIS était que la précision de +/- 10 cm prévue à l'origine avec la glace de première année ou de plusieurs années est obtenue dans la plupart des cas. Des erreurs plus grandes se produisent avec la glace plus mince (<10 cm). Lorsque des précisions d'épaisseur ou de conductivité supérieures sont requises, le maintien d'une altitude de sondage relativement basse (10-15 m) est crucial, tout comme l'est la synchronisation des mesures de bruit de fond pour éliminer la dérive EM. Un affichage pilote amélioré comprenant de l'information numérique et analogique sur l'altitude et l'orientation du capteur et l'indice de qualité sur un écran lisible en pleine lumière du jour améliorerait considérablement la qualité et l'uniformité des données opérationnelles. La dérive EM est la source d'erreur la plus gênante dans la réalisation actuelle du système : un programme d'essai pour l'analyse et la réduction de l'erreur de dérive améliorerait considérablement la productivité et la précision des opérations courantes. Si une réduction d'un ordre de grandeur ou supérieure des niveaux de dérive EM peut être réalisée, des précisions supérieures seraient possibles à une hauteur nettement plus grande, ce qui

réduirait l'effort demandé au pilote d'hélicoptère. Il devrait également être possible d'améliorer la précision en temps réel grâce à une prédiction plus précise de la dérive EM.

LIST OF FIGURES

LIST OF TABLES

1 Introduction

The Canadian Coast Guard (CCG) airborne Electromagnetic Ice Sounder (EIS), is a compact integrated sea ice measurement sensor which is deployed from a helicopter. The system has been used to acquire long profiles (up to 300 km per flight, and up to 50 km per continuous segment) of sea ice data over first year and multi-year ice in the Arctic, the Labrador Sea and the Gulf of St. Lawrence. It is based on Helicopter Electromagnetic technology, but incorporates an accurate and stable internal calibration system and the capability for real-time estimation of sea ice properties. The EIS system has been described and discussed in numerous reports and publications, including Holladay and Prinsenberg (1999a, 1999b), Holladay and Moucha (1998), Moucha *et al* (1998), Holladay *et al* (1999, 1998, 1997), Peterson *et al* (1997), and Prinsenberg *et al* (1996, 1993, 1992). This report summarises a detailed analysis of error in EIS measurements performed for the Department of Fisheries and Oceans (DFO). The purpose of this project was to categorise and analyse EIS error and to provide recommendations for further error reduction in future EIS measurement programs.

Figure 1.0.1: EIS sensor bird being towed by a Canadian Coast Guard helicopter.

1.1 Estimation of Ice Conductivity from EIS Raw Data

A highly schematic representation of the EIS system over a layer of ice floating on seawater is given in Figure 1.1.1. This particular model will be called the "Standard Model" for the purposes of this report. Its layer thicknesses and conductivities, which have been chosen to be representative of typical sea ice in the Labrador Sea and the Gulf of St. Lawrence, will be used as a reference example during the following analysis. A sensor altitude of 15 m will also be used for many of these cases.

Ice thickness estimation with the EIS system is relatively straightforward and easily visualised. At the fundamental level, EIS simply compares an accurate measurement of the sensor's distance above the ice/seawater interface made by the EM sensor with a corresponding distance to the top of the ice, measured by a laser rangefinder mounted in the sensor platform (Rossiter and Holladay, 1994).

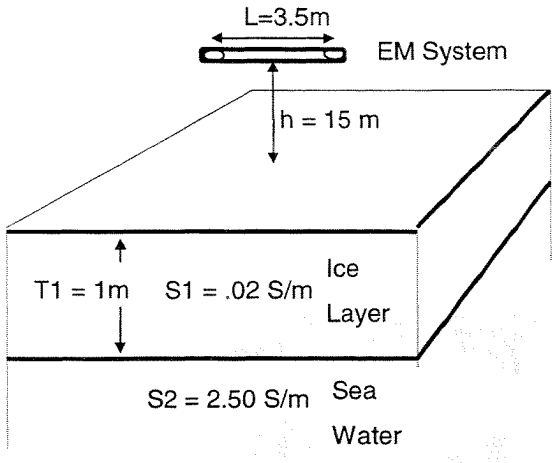

Figure 1.1.1: Standard Model for sensitivity and calibration analysis

The frequency response of the Standard Model for a system with the EIS geometry, *i.e.* a 3.5 m coil separation, with the transmitter and receiver coils mounted in a coplanar fashion in a horizontal plane, is given in Figure 1.1.2. It can be seen that the effect of nonzero conductivity in the ice layer is to progressively enhance the system's response at high frequencies.

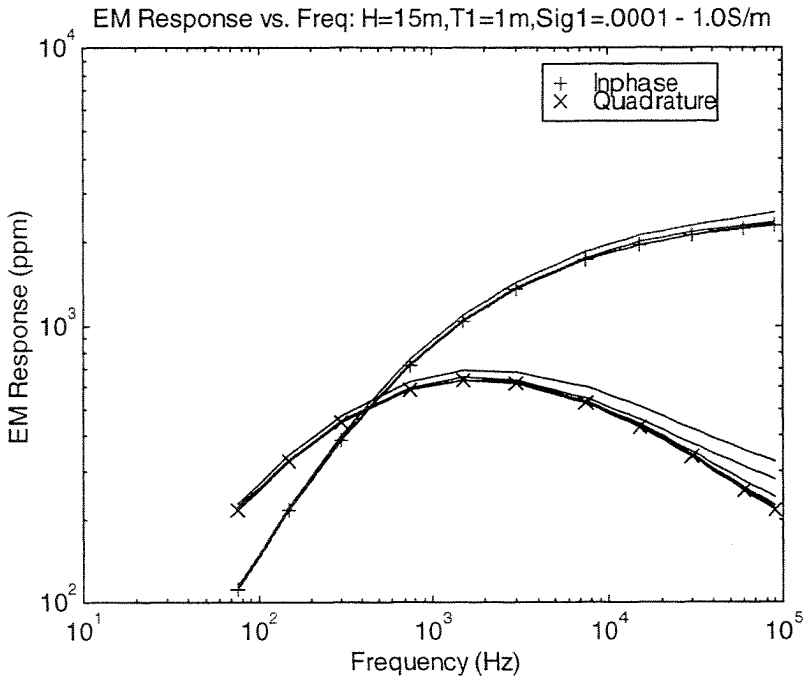

Figure 1.1.2: EM response of "Standard Model" at 15 m sensor altitude, varying ice conductivity as a parameter. Responses for conductive ice layers are enhanced at high frequency relative to that for a layer of negligible conductivity (symbols).

An improved mode of presentation of these data is shown in Figure 1.1.3. In this figure, the difference between the observed response at a given ice layer conductivity (identified by labels, *e.g.* 0.003 S/m) is subtracted from the response of the same model with negligible ice layer conductivity. Using this approach, it is immediately apparent that changes in the ice layer conductivity generate corresponding multiplicative increments in both the inphase and the quadrature responses. A thinner layer would yield smaller increments in the response for the same conductivity changes.

The log-log plotting format used here preserves detail even in small responses. It should be remembered that the EM noise levels are on the order of 0.6 ppm at F1 and 6 ppm at F2 (RMS), so that only responses that lie above these levels at those frequencies may be easily distinguished from noise. The 0.6 ppm level is shown by a dashed horizontal line for reference. Note that the normal operating frequencies of the EIS system are F1 = 3×10^4 and F2 = 9×10^4, as indicated at the lower left-hand corner of the plot. The 0.02 S/m ice conductivity of the Standard Model lies between the 0.03 and 0.01 S/m traces, well above the 0.6 ppm level at F1 and just below the 6 ppm level at F2.

The pattern of the responses is more uniform as a function of frequency for the quadrature (solid, with X symbols on the trace at bottom) than for the inphase

component (dashed, with + symbols.) The quadrature usually exhibits slightly lower drift and noise than the inphase at a given frequency.

This plot suggests that for the Standard Model geometrical parameters (height and layer thicknesses), the conductivity noise level for the system is approximately 0.003 S/m. F2 does not constrain low conductivities very well as does F1, despite its higher frequency, owing to its higher noise level. The noise level obtained from inversion of both frequencies for ice conductivity would be expected to be comparable to that seen at F1 in this case, since its noise level is much lower than at F2.

Note that the ice conductivity noise levels estimated here are instantaneous values: averages over longer periods will reduce the effects of random noise by $\sqrt{N}$, where N is the number of samples averaged. Thus, for a ten second (100 sample) average, the effective conductivity noise level would be reduced by a factor of 10, to about 0.0003 mS/m at F1 and 0.0025 S/m at F2.

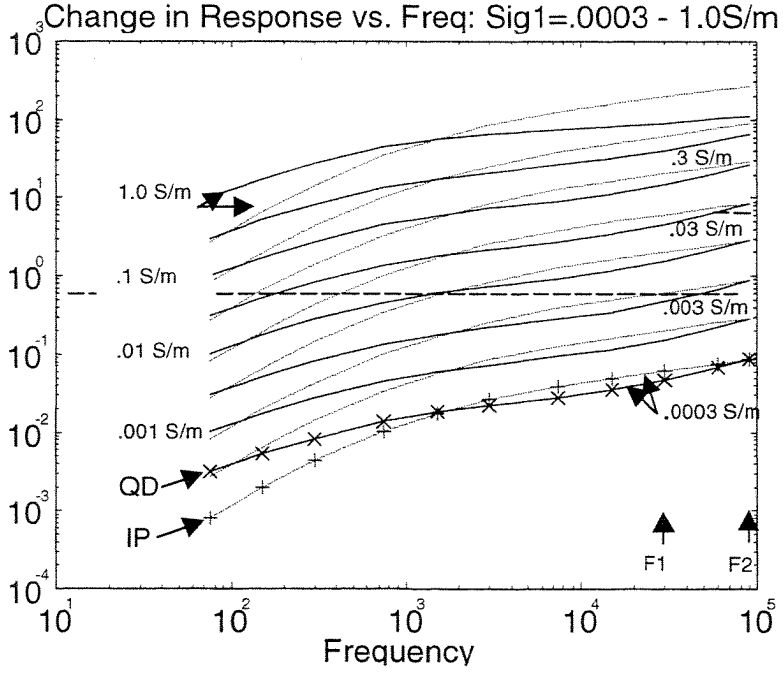

Figure 1.1.3: Change in EM response *vs* frequency relative to response for similar model with highly resistive ice layer. Sensor altitude is 15 m. The long horizontal dashed line indicates the 0.6 ppm RMS response level, while the short dashed line just above the .03 S/m label marks the 6 ppm noise level.

2 Definition of terms and assumptions used for this report

The technology for airborne electromagnetic ice sounding is relatively complex. The use of this technology in a survey methodology suitable for accurate measurement of ice thicknesses and conductivities should therefore be placed into context by defining the terms and assumptions implicit in the rest of this study. These will be listed in approximate order of significance.

1. Airborne data acquired under reasonable conditions:
   - survey altitude between say 5 m and 30 m, normally between 10 and 20 m
   - bird motion bandwidth small enough that Vector can monitor orientation
   - all sensors in system are operating nominally, without easily diagnosed noise, drift or other problems.
   - laser altimeter accuracy nominal over snow and ice
   - ice and snow thickness can be directly measured using auger and stick to ±1 cm point accuracy. For aliasing effects, it might be wise to assume ± 2 cm sampling error, based on experience-would be lower on bare new ice, higher on drifts or deformed ice.
   - ice conductivity estimate good to ± 20 mS/m
   - sub-ice seawater conductivity can be measured with a CTD to approx 1% accuracy, or 25 mS/m
   - ice conductivities not well known, but variable at least with temperature, brine inclusion density, thickness, manner of formation and deformation history
2. EM error consists of noise, drift and calibration error.
   - noise is defined as erroneous EM signal variations with periods of less than some tens of seconds.
   - drift is defined as erroneous EM signal variations having periods of more than some tens of seconds
   - EM error can contribute to calibration error, as can inaccuracies in the "calibration model" caused by spatial sampling error, rafting or other deformation, or departures in ice or seawater conductivity from the values used in the calibration model.
3. EM noise
   - noise has contributions from ambient EM signals, *e.g.* sferics, HF radio transmissions and power lines, as well as contributions from the relative motion of the transmitter and receiver coils, due to flexure of the bird or deformation of the coil mounts within the bird. Other potential

contributions, all of which appear to be negligible at the present time, include ripple on the power supplies from the helicopter, motion of the time-varying supply currents in the two cable relative to the receiver coil, motion of the currents induced in the conductors of the tow cable by the transmitted field relative to the receiver coil (through cable motion), and interference from electronic components mounted within the bird.

- in a properly designed EM system, there should be little sensitivity to signals above the frequency range at which the system nominally operates. It is possible for non-linear effects at the front end of the preamplifier to generate low-frequency signals from a mixture of moderate-intensity high-frequency signals and the high-intensity signals from the system's transmitter, but in this system these have been controlled through hash filtering at the input to the preamplifier.
- strong noise sources at frequencies lower than the system's nominal operating range can cause noise through harmonic generation. This has been minimised in the Coast Guard system through careful selection of the operating frequency. However, if power line noise is strong enough to cause system saturation at the preamplifier output, noise will appear in the system's outputs. This situation would be very unusual during normal operation of the system over sea ice.
- the system has been designed so that sferic noise (caused by distant lightning flashes) dominates the electronic noise of the receiver coil and receiver electronics under normal conditions.
- A noise component has been observed on occasion which may be related to the 1Hz real-time calibration sampling. Further assessment under controlled conditions will be required to investigate this possibility. However, the apparent noise amplitude is weak, so that this issue is not urgent.
- Unambiguous bird deformation noise has not been observed in this system. If it were present, it would only be seen during strong bird accelerations, which are not common during routine surveying.
- Noise due to motion of conductive elements or sensor coils within the bird have not been unambiguously observed. If present, such motion would generate strong inphase anomalies synchronised with bird accelerations.
- A type of noise which has sometimes appeared in the system appears to be due to weak electric- and magnetic-field coupling between the bird and its tow cable. For small changes in the bird-tow cable angle, the effect is weak. However, large gyrations of 5 degrees or more, particularly in bird pitch, have been observed to generate significant effects with amplitudes of 10 ppm or more at high EM frequencies. This is one reason for ensuring that the bird is flying in a stable manner after climbing to background altitude before initiating a background measurement. This

effect appears to have been essentially eliminated since the March, 1998 transmitter repair.

4. EM drift
   - typically arises from temperature variations in EM system components
   - quasi-linear with respect to time on sufficiently short time scales
   - degree of time-linearity dependent on rate of temperature change in system components. Approaching thermal equilibrium, drift rate approaches zero.
   - early in flight, drift rate higher than late in flight
   - EM system corrects some drift through the real-time calibration system. The drift component addressed in this report is residual after this correction.
   - Drift may be measured by briefly ascending to a height sufficient to render contributions from seawater response negligible. Such measurements are called "background measurements" or "backgrounds". Data which has been post-flight corrected for drift using background measurements has been "baselined" or "baseline drift corrected."
   - During real-time acquisition, drift is predicted based on its behaviour during previous background interval
5. EM real-time calibration system error
   - this subsystem calibrates all aspects of the receiver electronics from the preamplifier through the digital signal processing, and is activated once per second.
   - small systematic errors, on the order of 1%, are possible in this subsystem, particularly at higher frequencies. However, the subsystem should be extremely stable during normal operation, down to below the 0.1% level. Thus an accurate ground-truth calibration should serve to remove the systematic error, permitting continuing operation with accuracies at the 0.1% level or better.
6. Laser altimeter errors
   - It is assumed that the laser rangefinder (an Optech Alpha) performance matches its 1cm accuracy specification over normal snow and ice. Its performance over open water, or puddled water on ice, has not yet been fully characterised. The manufacturer has indicated that the dominant error mode over open water should be one of signal loss caused by the specular reflection of the laser beam away from the receiving optics by the smooth surface of the water. Under this model, wind-roughened water and brash ice should yield good ranges, which does agree with experience.

7. Orientation measurement errors

   - The Trimble TANS Vector system used for absolute orientation monitoring has a one-second update rate and apparently negligible lag. The nominal error level for this device is approximately 0.2° for the 1m baseline (across the bird) used for roll measurement. However, if the bird is rapidly gyrated by wind gusts or rough flight profiles, it is possible that the bird dynamics will briefly exceed the Vector's ability to track bird orientation. This is a good reason for avoiding large, abrupt course changes or other sudden flight profile adjustments during the course of normal data acquisition. Similarly, operation of the system in cross-wind conditions on gusty days may generate a small amount of orientation-related noise arising from tracking errors in the Vector output.

3 Categories of EIS calibration error sources

There are two levels of calibration practice in the EIS system. At the instrumental level, the EM sensor incorporates a calibration subsystem that monitors and corrects the EM output for small electronically-induced changes in calibration. This subsystem appears to be stable to the 0.1% level in amplitude (corresponding to snow-plus-ice thickness) and fractions of a degree in phase (which mainly affects ice conductivity estimates). However, the "absolute" calibration of the system, which relates its output to the snow plus ice thicknesses measured on the surface, must be set through "ground truth calibration." The ground truth calibration process entails the acquisition of EM data over a given ice/water structure which can be numerically modelled, typically a relatively thin, uniform thickness of ice overlying uniform seawater of known conductivity, and adjusting the EM calibration factors so that the calibrated EM response observed over the model matches the response calculated for the model. This process is subject to a number of errors, which are discussed below.

1. EM Calibration Subsystem error:

   - The EM calibration subsystem works by monitoring the output of a highly stable pickup coil which senses the time-varying "primary" magnetic field due to the transmitter. It also senses the "secondary" field reflected by the ice and water and by conductive elements within the bird. However, as long as the secondary responses are small in amplitude relative to the primary field at the location of the pickup coil, this effect is negligible. In the case of the EIS bird, the bucking coil located at the midpoint of the bird is used as the pickup coil.

   - The primary field as monitored at the pickup coil is sampled for approximately 0.1 s, once per second. This sampling is accomplished by using a relay in the preamplifier to switch the preamplifier input from the receiver-bucking coil combination (the usual state which monitors

secondary fields) to an attenuated version of the bucking coil output. At a 30 kHz base frequency, a 0.1 s sample comprises many transmitter waveforms' worth of data.

- These waveforms are "stacked", *i.e.* the average waveform over the interval is calculated, and the stacked waveform is transformed into its Fourier sine and cosine components at the frequencies of interest. In the case of EIS, this is typically at 30, 90 and 150 kHz. (In point of fact, since the Fourier transform is linear, the stacking can be done before or after transformation.)
- These Fourier components are then smoothed with an exponential filter to ensure that they are not unduly affected by short-period noise in the calibration signal.
- The smoothed Fourier components are then divided into their corresponding secondary field Fourier components, with appropriate factors to account for attenuation factors, amplifier gains and coil effective areas, to yield calibrated EM data.
- The calibration subsystem ensures that slow variations in transmitter amplitude or waveform shape, as well as variations in the gains or frequency responses of the transmitter coil, pickup coil, amplifiers and filters in the preamplifier and analog-digital conversion board, are removed from the calibrated EM output. In its present form, it cannot compensate for changes in EM output due to variations in the properties of the receiver coil or the cabling between the bucking coil and the receiver coil.

2. Other EM error:
   - EM noise and drift errors arising during measurements over the ground-truth calibration line will degrade the accuracy of the resulting ground-truth calibration.
   - For this reason, it is best to perform multiple passes over the calibration line and select the best one(s) for use in calibration calculations. A level bird altitude, preferably in the 10-15 m range, with minimal bird swing and good background measurements before and after the pass(es) are all positive factors in maximising the accuracy of the calibration procedure. Using a relatively low bird altitude maximises EM signal to noise ratios over the line, rendering the effects of small drift and noise errors less important.
   - It is best to perform more than one set of passes over the calibration line, with clean background measurements before and afterwards, in order to confirm the consistency of the factors being obtained.

3. Laser altimeter error:

   - The Optech laser altimeter used in the existing EIS bird (Model number 1-Alpha) is nominally accurate to 5 cm, with a 1 cm precision (and observed stability to 1 cm) for a wide range of target reflectances. These characteristics are superior to the Optech G150 used in the original two-frequency TDC system. Testing in the lab suggested that this accuracy claim was reasonable, but was not exhaustive. The IBEO PS100E that was used until 1996 and was destroyed during the bird crash also appeared to have excellent accuracy for a variety of target reflectances.

   - The performance of these devices has not been assessed over open water. From a consideration of the basic physics of their operation, it appears likely that they will measure the distance to the top of the water under normal circumstances. It remains to be established whether an accurate range may be obtained when the primary specular reflection from the water's surface is diverted from the rangefinder's receiver optics by undulations in the reflecting surface. It is possible that a weaker reflection may occur from suspended matter or air bubbles just below the water's surface under some circumstances. Such a reflection may be detected and processed by recent rangefinder models, and might provide a useful fallback in the case of primary signal loss.

4. Bird Orientation Measurement Error:

   - Errors in bird orientation measurement by the Vector are typically small. The systematic registration error between the Vector and the coil system has been estimated to be about 1°, while the random noise in the measurement should be less than 0.1°.

5. Surface Measurement Error and Positioning error:

   - The fundamental problem of ground-truth calibration is that, to achieve the highest possible calibration accuracy, a very thorough knowledge of snow plus ice thickness along the marked ground-truth line set out on the ice must be achieved. Since the bird cannot be repeatably towed along the entire length of the line, directly over the surface markings, it is in fact necessary to be able to project the surface measurement results to perhaps 10-20 m on either side of the marked line. This can be done practially with errors of about 1 cm or less if the ice is extremely uniform and lacks snow cover. In the presence of drifted snow, errors are increased substantially.

   - An ideal site for ground-truth calibration is on stable ice (so that it won't drift away), is logistically convenient, is extremely uniform in thickness, lacks snow cover, and has not been significantly deformed. Such conditions are often found in the Beaufort Sea in refrozen leads before the ice becomes highly mobile in late winter, and have been observed in the Southern Gulf on rare occasions.

- However, as observed by the author and others in the Southern Gulf of St. Lawrence or off Labrador, the more common situation is that apparently uniform pans of sea ice may be variable at the 5 cm level or beyond. Even sea ice which appears to the eye to be relatively level from the air or even on the surface can be remarkably variable in thickness. This is particularly true of pack ice, or land-fast ice which has been broken up and refrozen, but is also common in otherwise uniform ice which has been snow-covered, melted and refrozen a few times. Even smooth ice recently formed in leads will often be covered with a variable layer of snow, and older land-fast ice may have a substantial amount of snow cover.
- As a result, it is often difficult to locate a suitable pan of ice on which to set up a ground-truth calibration line, and less-than-ideal calibration conditions may be the result.
- A further factor which must be considered in the selection of ground truth calibration sites is that the minimum water depth beneath the sea ice should be in excess of 4 m (for a 30 kHz base frequency). The water beneath the ice should be uniform in its conductivity profile down to at least this depth. If the salinity and temperature conditions are such that the water conductivity varies significantly from 2.5 S/m over this depth interval, this fact must be used during the calibration calculations or an erroneous set of factors will result. Fresh water flows beneath the ice from rivers or surface melting are one hazard that must be guarded against during ground truth measurement programs. In areas with significant tidal variation, there may be some change in seawater conductivity as a function of the tidal cycle. Fresh water layers beneath sea ice have been observed in the Mackenzie Delta near Tuktoyaktuk and in the Bay of Exploits in Newfoundland. Similar effects may be encountered in Labrador estuaries.
- An alternative to ground-truth calibration using an ice-based calibration lines has been proposed, in which open water or extremely thin ("black") ice would be overflown with the system. Provided that the seawater conductivity is well-known and that the laser altimeter has no systematic error over such a low-reflectivity target, it should be possible to obtain a more accurate calibration under these circumstances than could be obtained using "traditional" calibration lines. A carefully controlled experiment is planned for the 1999 field season.

4 Categories of EIS errors for routine operations

The error sources observed during normal system operation include the following, listed in approximate order of their contribution to EIS systematic errors.

1. System Calibration error
2. EM Drift
3. Bird Orientation
4. EM Noise
5. Laser altimeter errors
6. Positioning errors

System Calibration:

System (hardware and ground-truth) calibration was addressed in the previous section and will not be discussed here. Calibration error is certainly the most important class of error for EIS, since improper calibration procedures could lead to the acquisition of large volumes of incorrect ice thickness data. Fortunately, most calibration problems can be corrected during post-processing of the raw survey data if proper records are kept.

EM Drift:

EM drift is important because it represents a relatively long-term (tens of seconds to tens of minutes) error in the EM response of the system which may result in systematic errors over similar time ranges in estimated snow plus ice thickness. It is the most serious type of error that is normally encountered during routine survey operations, but can be made negligible through proper survey methodology. Many drift problems can also be corrected during post-processing, provided that the survey lines were not too long and that adequate background measurements were obtained before and after each line.

It is appropriate to preface this discussion with a brief description of the drift correction methodology as presently practised. During normal system operation, the system is flown at survey altitude (typically 10-20 m) for ice measurement, interrupted by short background measurement runs, during which the system is taken to about 300 m altitude, held there for about 20 seconds, then returned to survey altitude. These background measurements are used to estimate the system's output in the absence of nearby conductors. This baseline level drifts slowly, mainly due to the effects of temperature changes in the receiver coil. Drift rates drop as the system approaches thermal equilibrium with its surroundings, so that after the first ten minutes of flight the drift rate is much lower than after five minutes, and so on. For example, after five to ten minutes of flight at

temperatures approximating those found at survey altitude, the drift rate drops enough that baseline drift can be predicted with sufficient accuracy to permit real-time estimation of sea ice thickness and conductivity for a survey run of about five minutes. After a second background measurement, the prediction is typically adequate for a ten minute run, and after a third and later background, twenty minute lines can normally be flown with acceptable drift error. An alternate survey methodology is employed for some types of ice reconnaissance missions, in which the system is normally flown at high altitude, with occasional short runs over selected ice floes or groups of floes.

EM drift error may be defined as a slow (*i.e.* with periods greater than tens of seconds) variation in the base or zero level of EM responses as measured by the system, excluding errors generated by shifts in bird orientation (which are addressed below). In a properly functioning EM system, drift is mainly due to temperature changes of components inside the bird. If such a system were flown in a uniform environment, far away from conductive materials, for an entire flight, the measured EM responses could be interpreted as "drift curves" for the flight. The drift curve for each frequency and phase component would be characterised by high rates of drift (as measured in parts-per-million EM units per hour) during the early part of the flight, with low drift rates being observed toward the end of the flight. This behaviour is typical of phenomena affected by the temperature of their environment: early in the flight, critical system elements are far from thermal equilibrium, so that their temperature changes rapidly and drift rates are high, while late in the flight, all system temperatures are approaching their steady-state condition and drift rates drop to negligible levels.

Removing the system from the vicinity of conductive features, followed by measurement of the baseline shift and a return to survey altitude, is the usual means by which drift can be estimated. This measured drift can then be interpolated backwards in time to the previous background measurement (normally straight-line interpolation as a function of time is used for this) to provide an estimate of drift for each sample obtained during the measurement run preceding the most recent background measurement.

There is a drawback to this approach, which is that under some atmospheric conditions there is a strong change in temperature between survey altitude (less than 30 m) and background altitude (300 m). Temperature differences of several degrees between these two heights have been measured in the southern Gulf. When strong thermal gradients are present, even a brief background measurement can result in a large enough temperature shift within the bird to generate detectable changes in system drift, while a prolonged period at high altitude can cause substantial errors in drift prediction. It is therefore not advisable to mix the two survey modes mentioned above: the system should spend most of its time either profiling at low altitude with brief background measurements, or flying at high altitude with brief low altitude runs, in order to minimise drift effects and errors in real-time drift prediction.

7. Bird Orientation:

Bird orientation may affect system performance in one of three ways:

- unusual orientation changes, particularly strong pitching, can distort EM measurements during background measurements, causing inaccurate EM drift predictions and corrections. This type of motion damps out quickly, and is rarely encountered during normal low-altitude surveying.
- very rapid bird orientation changes may not be tracked properly, leading to transient errors in altitude and EM correction for orientation effects.
- systematic errors in orientation could generate long-term, systematic errors in estimated snow plus ice thickness. These will not occur at a significant level in a properly assembled, undamaged and calibrated system.

The most important effect relating to bird orientation arises during background measurements. During the climb to background altitude, the bird tends to pitch nose-up about five to fifteen degrees, depending on the steepness of the climb. On reaching straight and level flight at the background altitude, the pitch normally returns to within a few degrees of normal, at which time it is safe to perform a background measurement. Ten seconds after the background measurement been completed, it is safe to return to survey altitude. During the descent, the bird tends to pitch between five to fifteen degrees nose down, then levels out rapidly when survey altitude is achieved.

Bird pitch (and to a lesser extent, roll) can affect the EM response. The effect, which is thought to be related to electric field radiation by the transmitter driver and coil, is strongest in the inphase components and at high frequencies. Strong coupling (with clearly visible orientation-related high-altitude anomalies of 20 ppm or more at 30 kHz) is a clear indication that there is a problem with the system, most likely related to the transmitter driver. Acceptable data can still be obtained under these circumstances, but care must be taken to minimise bird motion. The current performance of the system, as indicated by records obtained after the 1998 transmitter repairs, show virtually no effect in the EM responses that can be correlated with bird pitch and roll during background measurements. However, it remains prudent to verify that the bird is in straight and level flight (this can be done by the pilot using the slinging mirror) at the background height before the background measurement is initiated.

Rapid orientation changes are sometimes observed while flying under gusty conditions, particularly with a cross-wind, and are caused by gusts striking the bird's vertical and stabilisers. The usual effect is to create small-amplitude, short period (less than 2 seconds) noise in the bird roll, which does not generate serious errors in the estimated ice thickness. However, especially violent gusts may generate transient errors in ice thickness estimates by briefly exceeding the ability of the Vector GPS-based orientation monitoring system to track the motion.

Systematic errors in orientation measurement should be negligible using the Vector. Under rare circumstances, the GPS satellite configuration used by the instrument could be sufficiently poor that it will cease to provide orientation measurements, but this has not been observed to be a problem. The Vector's calibration appears to be extremely stable, and has not shown any signs of degradation after repeated disassembly and re-assembly of the bird.

8. EM Noise:

EM noise includes a variety of EM errors with periods of less than some tens of seconds and displaying zero mean amplitude. Noise measurements are best performed at background altitude, with the bird flying straight and level. . Under optimal circumstances, with the bird operating properly, low wind speeds and a smooth flight profile, the system's noise level is typically below 2.5 ppm peak-peak (*i.e.* range of excursion between peak and trough observed in the absence of secondary field at high altitude, abbreviated pk-pk) at 30 kHz, 15 ppm pk-pk at 90 kHz, and 30-40 ppm pk-pk at 150 kHz (more precise estimates are presented in a later section). The rule of thumb for conversion of random error expressed as standard deviations into pk-pk is to multiply by 6. Noise levels significantly higher than these values at 30 and 90 kHz may indicate a problem in system operation or survey methodology and should be referred to an expert for assessment. Noise levels observed on the ground may be slightly better, particularly at high frequencies, if the bird is located well away from conductive objects such as metal siding or roofs, power lines and fences, and if it is not being moved about by wind gusts. Only 30 and 90 kHz are used for routine ice measurement, as noise and drift in the 150 kHz are high enough to degrade overall accuracies. EM noise is most easily seen on the analogue chart plot generated by the system's GR33 graphic printer: otherwise it is necessary to extract the desired responses from the RAW data files generated by the system.

The effect of EM noise on snow plus ice thickness estimates is a function of altitude: at low altitudes, the EM response is very strong and easily swamps out moderate levels of noise. However, at the upper end of the flight envelope (25 m altitude) such noise becomes a significant fraction of the signal and some degradation of snow plus ice thickness accuracy is seen. Ice conductivity is not as strongly determined by the data as thickness, but is still fairly well estimated for bird altitudes of less than 20 m. Representative examples of these effects will be discussed in detail in a later section.

Most EM noise types have periods of less than two seconds. For this reason, it is not likely to be a significant factor in the systematic accuracy of the system, and instead appears as a factor in the noise level of the estimated snow plus ice thickness and ice conductivity.

9. Laser Altimetry:

Laser rangefinder technology has improved to the point that excellent absolute accuracies, on the order of 1-2 cm, may be obtained with relatively inexpensive devices from Optech and IBEO. The long-term stabilities of these units may be expected to improve on this, reaching 1 cm or better. Range noise levels at high sampling rates are generally higher, on the order of 5 to 10 cm at 20 to 30 Hz, though high-power models are available which reduce the scatter considerably. The footprint of most laser altimeters operating in this altitude range is small, on the order of 1-3 cm.

Computation of snow plus ice thickness is effectively accomplished by subtracting the laser-measured altitude from the EM-measured distance to the seawater surface below the aircraft. Since the EM response is averaged over a relatively large footprint with a diameter of about three times the flight height, the EM-measured height above seawater is considerably smoother than the tightly-focused laser-measured altitude above the snow/ice surface. This difference in footprints means that the estimated total thickness profile will contain features which are much narrower than the EM footprint, but that the "spot" accuracy of the snow-plus-ice thickness may be degraded from the system's nominal accuracy when profiling ice with strong lateral variations in thickness. Averaging the EIS snow-plus-ice thickness estimates over the width of the footprint (corresponding to about 1 second's worth of data at normal flight speeds and survey heights) should, however, yield a much more accurate value. An assessment of EM footprint/altitude ratios may be found in Kovacs *et al* (1995).

10. Positioning Errors:

Positioning of the EIS system is presently accomplished using the GPS position output by the Vector bird orientation sensor. These positions are subject to error due principally to Selective Availability (SA) dithering of the Global Positioning System (GPS) position and to time jitter of the position, apparently caused by processing delays within the Vector instrument coupled with its relatively low (~1 Hz) output sampling rate. Occasional dropouts caused by poor satellite constellations have been observed, but these can be predicted prior to a survey mission and so can often be avoided.

Selective Availability is a deliberate degradation of the positioning capability of the civilian GPS service. Typical modern GPS receivers yield SA positions within 70-80 m of the true value, 95% of the time, although the SA specification is to be within 100 m, 95% of the time. The Vector, which uses six-channel receivers (compared to the twelve channels used by most newer receivers), may be expected to display this somewhat lower accuracy.

5 Sensitivity Analysis for EIS Measurement and Calibration Accuracy

5.1 Methodology

A standard tool for analysing errors in measurement systems and geophysical methodologies is the "sensitivity analysis." This analysis uses numerical modelling techniques to investigate the behaviour of various measures of system performance. An instructive example is given in Figure 5.1.1, which shows the "standard error" (equivalent to standard deviation) levels estimated for the parameters of a two-layer model, based on random noise standard deviations of 1 ppm in the EM measurements. Higher noise levels generate correspondingly higher parameter error levels.

This method assumes that the problem is not extremely non-linear, as it utilises a quasi-linear approximation in the vicinity of the solution. In this case, the linearity assumption is justified and the estimated error levels are reasonable.

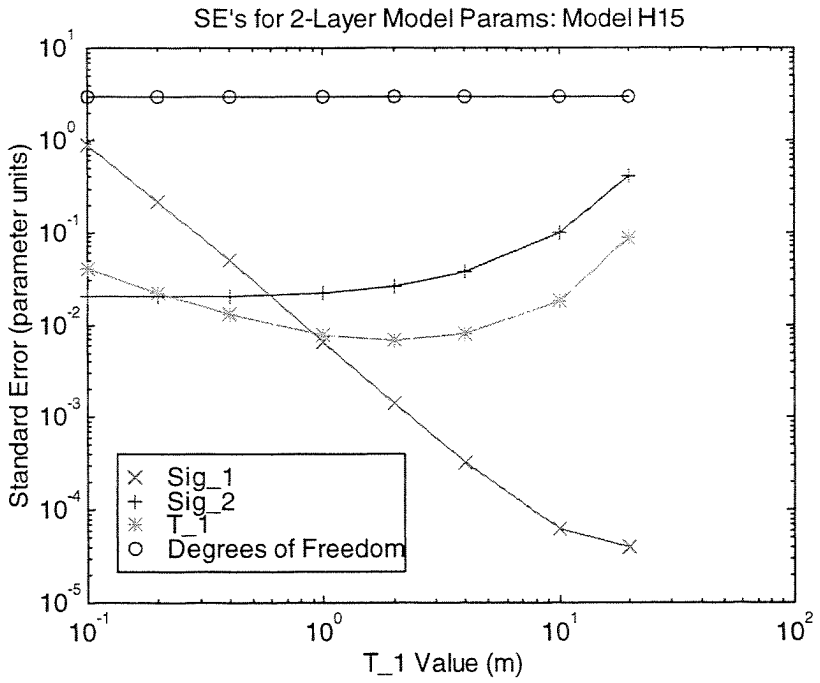

Figure 5.1.1: Parameter error estimates for Standard Model, assuming 1 ppm random EM noise.

The predicted error levels in the parameters Sig1, Sig2 and T1, corresponding to ice conductivity, seawater conductivity and snow plus ice thickness, are plotted with respect to the T1 value (T1 and T_1 are used interchangeably, as are Sig1 and Sig_1 and Sig2 and Sig_2.) It can be seen immediately that the parameter errors are functions of the snow plus ice thickness. For very thin ice, T1 error

increases by a factor of 2 relative to the error levels at 2 m, mainly due to the high degree of uncertainty in ice conductivity Sig1. For ice thicknesses of 1 m or greater, the Sig1 error levels drop rapidly below 0.01 S/m, at which point they have little effect on the uncertainty in T1. At T1 values greater than 10 m, the distance between the EM sensor and the ice/seawater interface increases rapidly, which reduces the amplitude of the EM response and increases error levels in the T1 estimate. The same phenomenon increases Sig2 error estimates for large values of T1. The term "degrees of freedom" as used in this report refers to the number of free parameters which are resolved by the data.

The effect on the derivative of EM response with respect to sensor altitude above the surface of the Standard Model, plotted *vs* altitude, is shown in Figure 5.1.2.

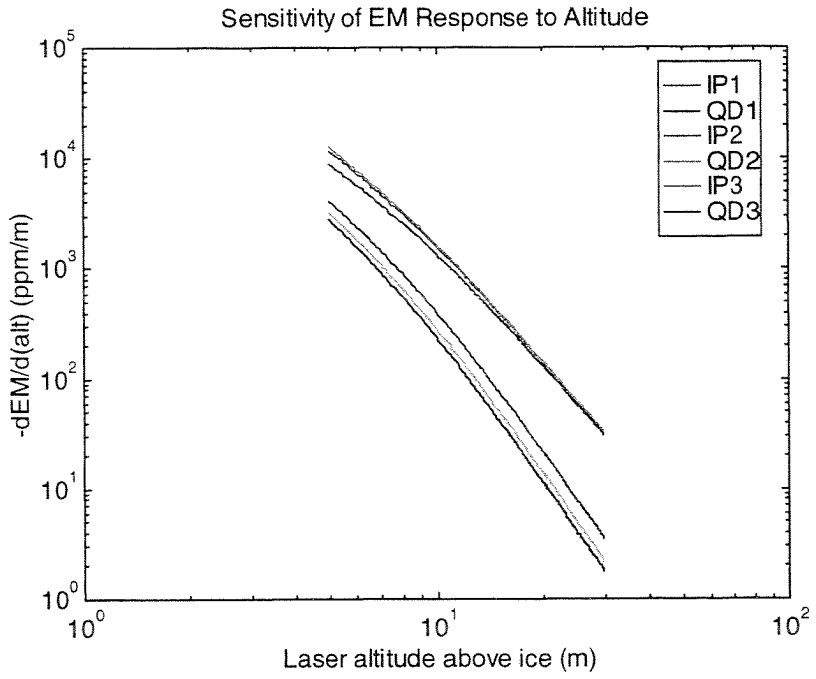

Figure 5.1.2: Sensitivity of EM response to altitude as a function of altitude.

Two aspects of this figure are of interest. First, the steepness of the dEM/d(alt) curves indicates that the sensitivity of the EM response to altitude drops off very rapidly with altitude, with slopes on the log-log plot of between -2.5 and -4.5.

A second interesting feature of these curves is that the derivatives of the quadrature components are considerably weaker than for the inphase components, and decay at a slightly higher rate. The dispersion seen between different frequencies, especially at altitudes of 10m or less, is apparently due to the effect of ice conductivity: for ice of zero conductivity, the curves would be much more tightly grouped.

The next two plots, Figure 5.1.3 and Figure 5.1.3, show the derivative of the EM response with respect to pitch and roll. As these are derived from numerical differences, some "chatter" is seen in these curves, particularly at low values.

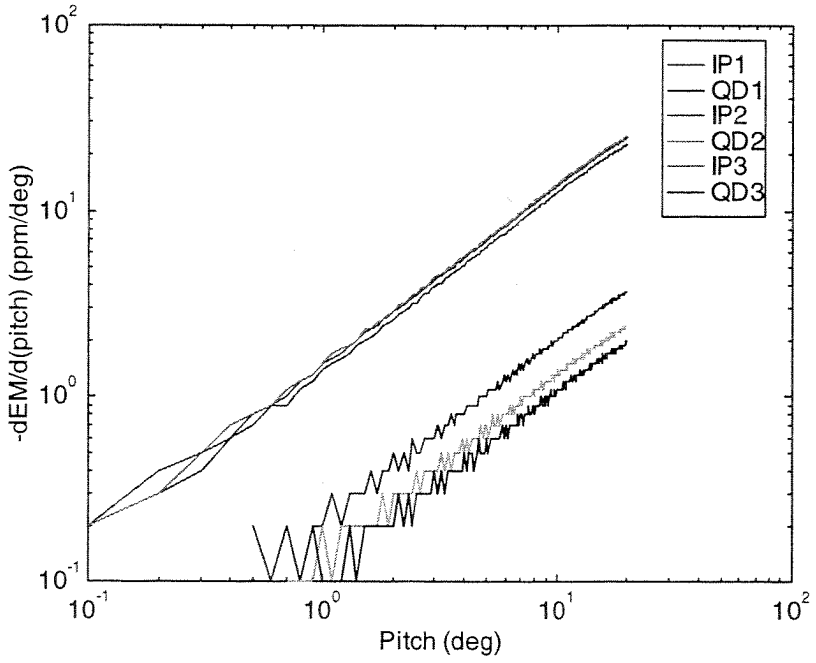

Figure 5.1.3: Sensitivity of EM response to pitch angle as a function of pitch. "Chatter" in curves at small values of ∂EM/∂Pitch are due to truncation in model response before numerical differentiation.

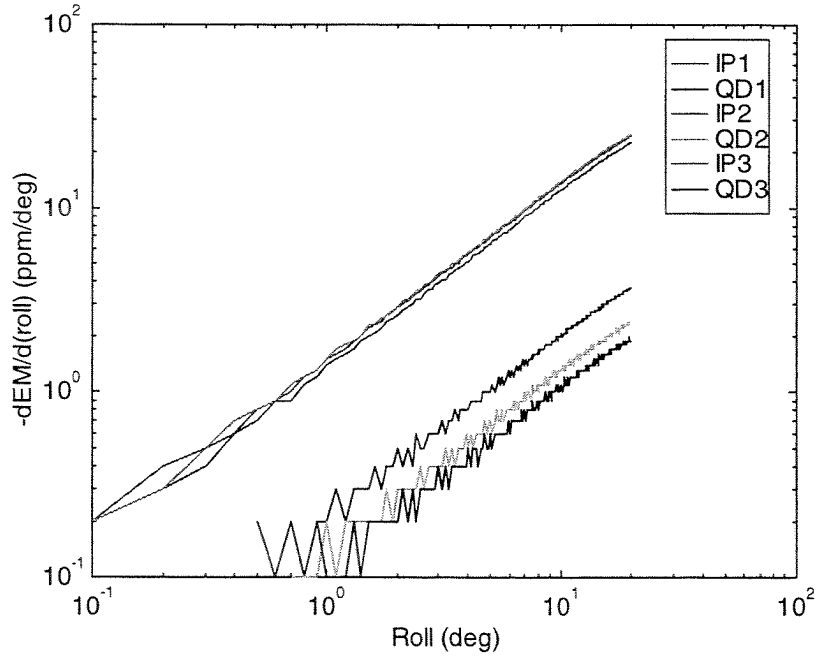

Figure 5.1.4: Sensitivity of EM response to roll angle as a function of roll.

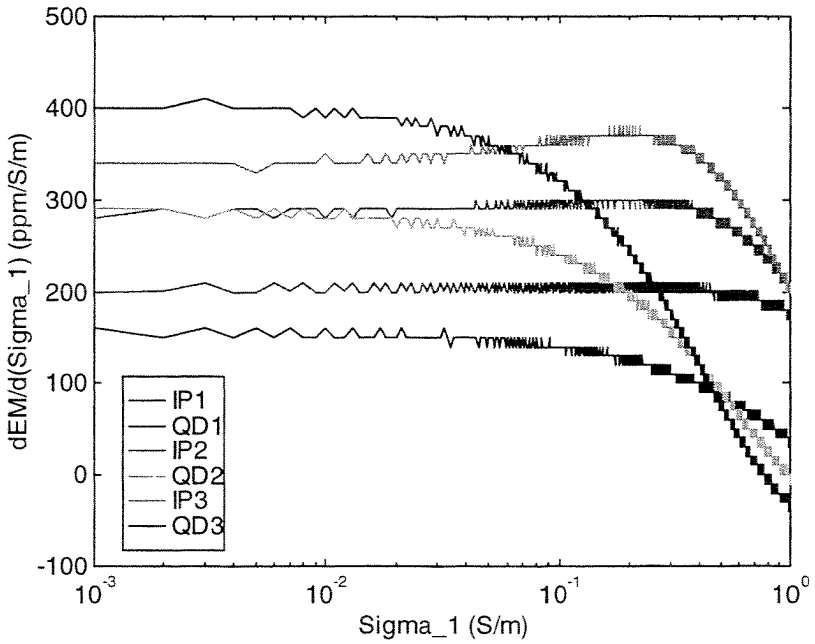

Figure 5.1.5: Sensitivity of EM to ice conductivity as a function of ice conductivity.

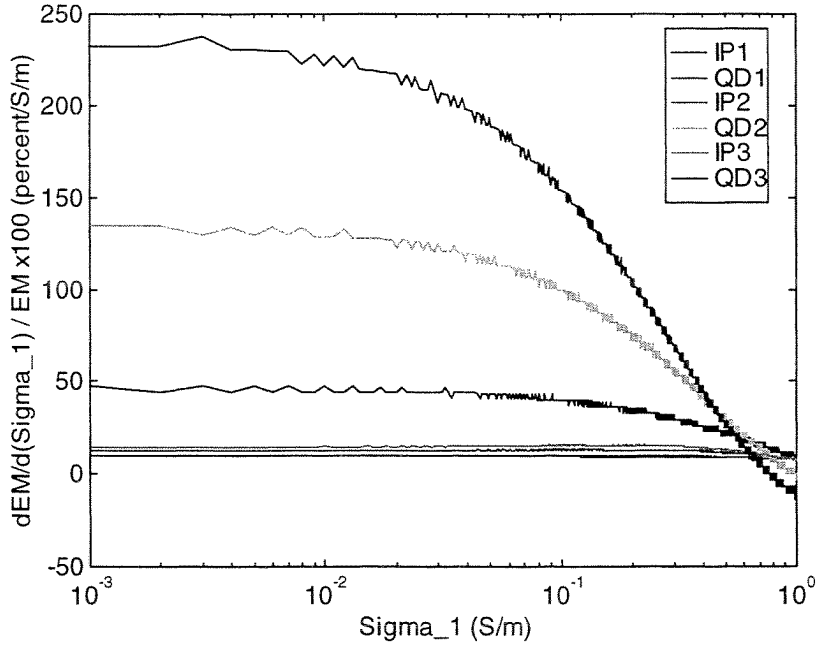

Figure 5.1.6: Sensitivity of EM IP and QD components to ice conductivity, expressed as a percentage of the amplitude of each component, as a function of ice conductivity.

Figure 5.1.5 and Figure 5.1.6 above display the derivative of the EM response with respect to ice conductivity Sig1 in two different formats. The first is a

straightforward plot of the amplitudes of the derivatives, while the second plots the derivative as a percentage of the EM amplitude for each component. The first plot is useful for extracting numerical estimates of derivative amplitudes, while the second shows that most of the sensitivity to ice conductivity, when viewed as a percentage of the measured amplitude, lies in the quadrature component at each frequency, and increases as a function of frequency.

Figure 5.1.7 below displays the derivative of the EM response with respect to water conductivity Sig2 as a function of water conductivity. Most of the curves display behaviour similar to power-law relationships with exponents of between -1 and -1.5.

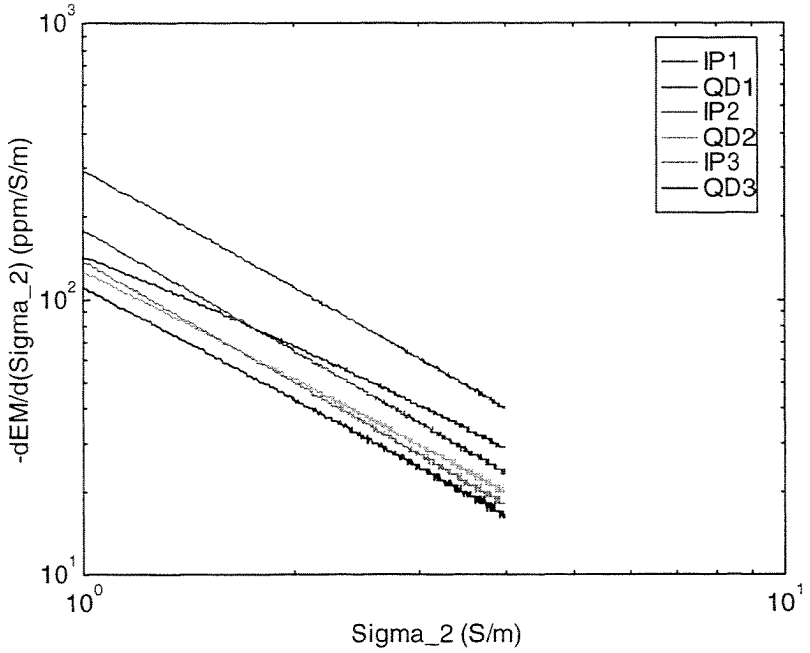

Figure 5.1.7: Sensitivity of EM response to water conductivity as a function of water conductivity.

Figure 5.1.8 below shows the derivative of the EM response with respect to ice thickness T1. These curves display more complexity than most of the preceding examples, but it is clear that the dominant sensitivity to ice thickness is in the inphase response, in contrast to Figure 5.1.5 where the quadrature component dominated. The behaviour becomes complex for large values of T1, as phase rotation and amplitude attenuation due to the nonzero conductivity of the ice become more important.

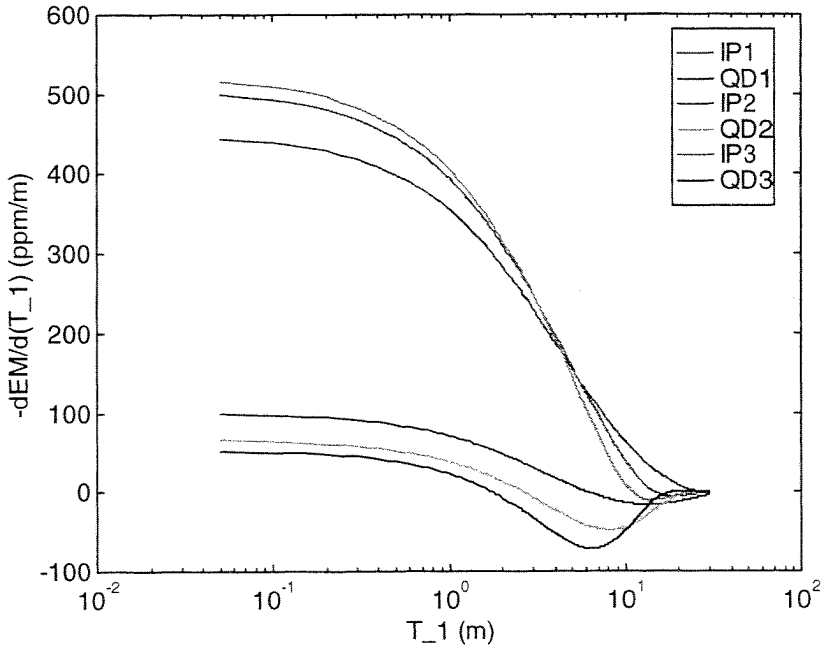

Figure 5.1.8: Sensitivity of EM response to ice thickness as a function of ice thickness.

5.2 Sensitivity Analysis for 3-layer Case

Another case that merits discussion is the three-layer case in which an ice layer overlies a shallow water layer and sea-bottom. Such situations have been observed, especially in relatively shallow water with rocks, sandbars or other obstructions coming close to the surface, or where a survey line runs up over the shore.

The model used for this analysis is shown in Figure 5.2.1 below. The sub-ice water depth is 2.5 m, and the ice thickness is again 1 m. A 10:1 conductivity contrast between seawater and sea-bottom was selected as being reasonable for sandy or granular bottom sediments.

Sensitivity plots, which assume 1 ppm EM noise levels as before, are presented for this three layer case in two formats and for two cases: in the first (Figure 5.2.2), *a priori* knowledge was assumed for the ice conductivity, which was set to 0.02 S/m. This permitted a unique solution for the remaining parameters. Sig3 is clearly the most poorly-determined parameter, with its error starting at 20% of the parameter value for thin ice and increasing rapidly for ice thicknesses of more than 2 m. In the second, both ice and water conductivities were assumed to be known and fixed. This reduced the error estimates for the remaining free parameters considerably.

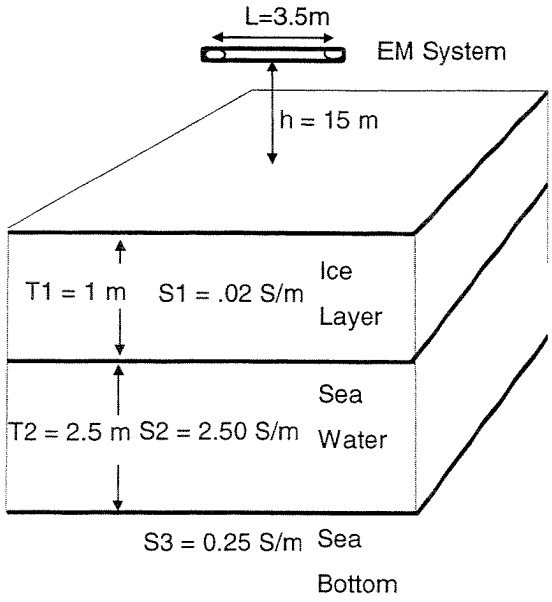

Figure 5.2.1: Three-layer model including ice, seawater and sea bottom layers for bathymetric sensitivity analysis.

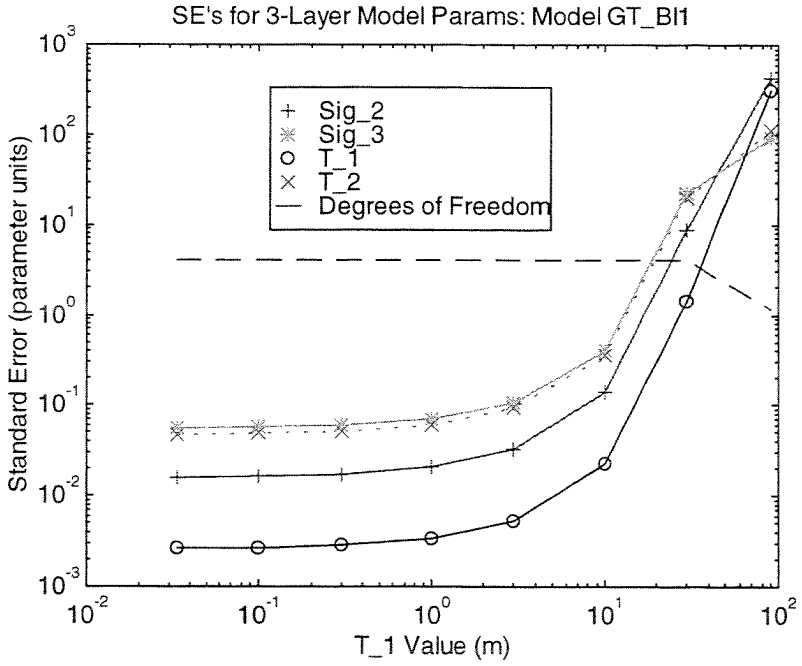

Figure 5.2.2: Sensitivity of model parameters to ice thickness for 3-layer case. *A priori* knowledge assumed for ice conductivity, fixed at 0.02 S/m.

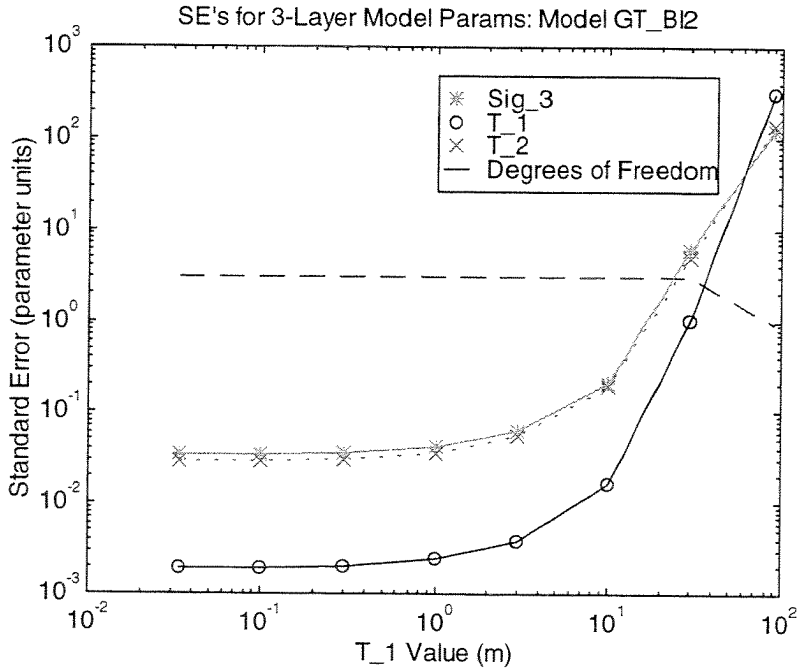

Figure 5.2.3: Sensitivity of model parameters to ice thickness for 3-layer case. *A priori* knowledge assumed for ice and water conductivities, fixed at 0.02 and 2.5 S/m.

An alternative view of these three-layer parameter sensitivities is provided in Figure 5.2.4 and Figure 5.2.5 below. In these plots, the parameter errors are plotted as a function of the sub-ice water conductivity Sig2. Again, the first plot assumes that ice conductivity is known *a priori*. The poor definition of T1, Sig2 and T2 for thin water layers are due to the lack of a substantial, strongly contrasting ice/water interface. As T2 increases beyond 1 m, the error estimates for these parameters reach practical levels. Further increases in T2 beyond 2 m lead to rapidly increasing error levels in T2 and Sig3, as the EM signal becomes highly attenuated at the bottom of the seawater layer.

In the second plot, both ice and water conductivities are assumed to be known and fixed. As a result, a major improvement is made in error levels all of the remaining free parameters until the seawater depth exceeds the 2 m point, at which case the T2 and Sig3 error levels increase rapidly due to EM screening effects.

The EIS sensor was not designed with bathymetric sounding as a significant mission goal. While a modified version of the system could be used for general bathymetric work, the existing system is certainly capable of sounding in shallow (< 2.5 m) water under good operational conditions, with or without the presence of sea ice.

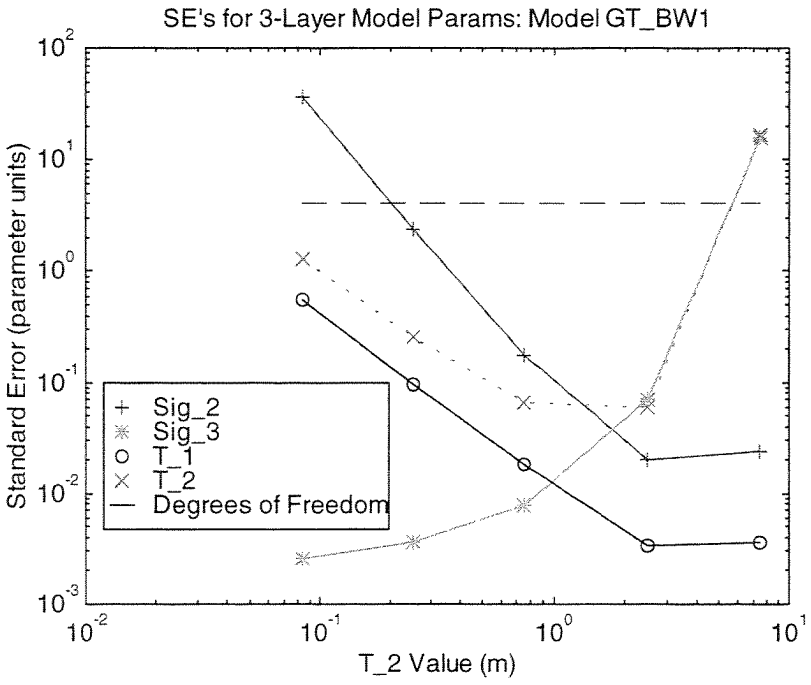

Figure 5.2.4: Sensitivity of model parameters to sub-ice water depth thickness for 3-layer case. *A priori* knowledge assumed for ice conductivity.

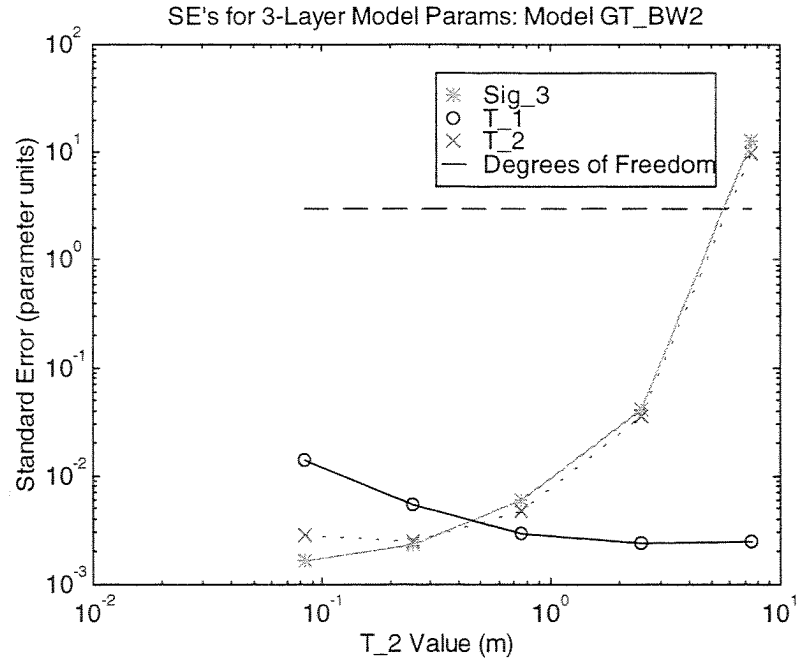

Figure 5.2.5: Sensitivity of model parameters to sub-ice water depth thickness for 3-layer case. *A priori* knowledge assumed for ice and seawater conductivities.

5.3 Eigen-Analysis for Selected Examples

Eigen-analysis or SVD analysis is a standard procedure for assessing the importance of model parameters to an inversion problem. Two cases are of interest: an ice-over-seawater case typical of deep water situations, and a three-layer case encountered in shoal areas. The method is based on singular-value decomposition of the matrix dEM/dParam and analysis of the singular values and eigenvectors.

Two-layer Case: Ice over Seawater

		Sig_1	Sig_2	T_1
dEM/dParam	IP1	204.018	79.9986	-357.217
	IP2	288.5305	46.7315	-396.349
	IP3	344.3159	35.8338	-407.693
	QD1	152.0765	-51.7384	-71.5444
	QD2	278.2033	-37.9837	-38.9976
	QD3	387.8022	-31.6981	-23.7652
	Sing. Vals	915.368	355.6177	55.5454
U Matrix	IP1	0.435	0.3615	0.4173
	IP2	0.5291	0.2507	-0.0961
	IP3	0.5809	0.1581	-0.1822
	QD1	0.1706	-0.191	-0.7881
	QD2	0.2464	-0.4828	-0.0724
	QD3	0.3217	-0.7155	0.3962
	Sing. Vals	915.368	355.6177	55.5454
V Matrix	Sig_1	0.7218	-0.6757	0.1497
	Sig_2	0.0568	0.2733	0.9602
	T_1	-0.6898	-0.6846	0.2356

In this case, the matrix ∂EM/∂Param (partial derivatives of the EM response with respect to the natural logarithm of the model parameters) is well conditioned, as can be seen by the modest 16:1 range of singular values. Taking the logs of the model parameters ensures that the parameters cannot become negative and enhances the conditioning of the matrix.

The good condition number of the matrix (defined as the ratio of the largest to the smallest singular value) means that all three parameters can be determined with good accuracy in the presence of moderate levels of data error. The columns of the "data eigenvector" matrix U and "parameter eigenvector" matrix V correspond to the singular values, with the best-determined parameter eigenvectors being those associated with the largest singular value, in this case 915. The first two

parameter eigenvectors determine between them the layer 1 conductivity and thickness, as expected (the first determines the conductivity/thickness ratio, and the second determines the conductivity-thickness ratio). The third parameter eigenvector, associated with a considerably smaller singular value, determines the seawater conductivity. Using a lower frequency much smaller than 30 kHz would improve the estimation of the water conductivity but degrade the accuracy of the ice thickness estimate, and would have increased overall EM noise levels and required bird weight considerably.

The data eigenvectors identify which data are associated with determination of a given eigenparameter. In this case, for example, the third column of U has its largest value in QD1, and its second largest value in IP1, indicating that the low-frequency quadrature is the most important piece of data in determining seawater conductivity, followed by the low frequency inphase.

Three-layer Case: Ice over Shallow Seawater and Sea Bottom

		Sig_1	Sig_2	Sig_3	T_1	T_2
dEM/dParam	IP1	192.7877	62.0466	-39.7839	-364.161	-35.7358
	IP2	286.6417	46.1651	2.1309	-396.062	-1.0623
	IP3	345.2274	36.7722	0.6944	-407.553	1.8366
	QD1	135.509	-67.6087	0.386	-72.0029	-28.2857
	QD2	281.6776	-34.2837	3.1516	-38.3851	7.206
	QD3	388.5318	-31.4225	-0.3527	-23.7988	0.5427
		U				
	Sing. Vals	912.049	358.9944	69.7684	46.4651	6.1738
U Matrix	IP1	0.4339	0.3791	-0.0039	-0.8015	-0.1498
	IP2	0.5296	0.2417	0.078	0.3645	0.4147
	IP3	0.5839	0.1456	0.0513	0.3864	-0.2527
	QD1	0.1584	-0.1651	-0.9645	-0.0136	0.1281
	QD2	0.2486	-0.4875	0.0158	0.0674	-0.713
	QD3	0.3217	-0.7153	0.2466	-0.2658	0.4657
	Sing. Vals	912.049	358.9944	69.7684	46.4651	6.1738
V Matrix	Sig_1	0.7165	-0.6825	0.1269	-0.0594	0.0348
	Sig_2	0.0477	0.2518	0.891	-0.2525	0.277
	Sig_3	-0.0164	-0.0441	-0.0008	0.7152	0.6973
	T_1	-0.6955	-0.6838	0.1809	-0.113	0.0565
	T_2	-0.0192	-0.0356	0.3967	0.639	-0.6577

This more complicated case displays many of the same basic characteristics as the two-layer case: for example, the first layer conductivity and thickness are still the best-determined parameters, followed by the water conductivity. However, the condition number of the complete partial derivative matrix has increased to

over 150, as a result of the greater number of unknowns and the relatively poor resolution of the third-layer conductivity by these measurements. If this parameter were known *a priori*, the condition number of the rest of the matrix would improve to 20, which is not much worse than the 16 of the two layer example. Conversely, this means that a reasonable approximation to the bottom conductivity can be used with little effect on the other model parameters.

This example represents a case which is sometimes encountered with the EIS system, particularly close to shore or in harbours such as Summerside Harbour southwest of Holman Island, where a zone of shoal water connects the island with MacCallums Point. A number of shoal effects have been seen with the system in Hillsborough Bay as well, particularly near Governors Island and St. Peters Island. Since the usual EIS thickness calculation uses a two-layer model and neglects bathymetric effects, erroneous ice thicknesses are reported over shoals: apparent thicknesses are increased, since there is less seawater beneath the ice to reflect the EM signal. In extreme cases where the ice is grounded, very large thickness in excess of 10 m are typically reported by the system. The same effect is noted when the system is flown over a small island or exposed rock. Extreme ice thickness values in shoal areas can therefore be assessed and discounted by reference to bathymetric charts of the area.

Eigen-analysis is an important tool for the investigation of "parameter equivalence," to be discussed in a later section.

5.4 Drift Behaviour of the System

EM drift is the one of the most serious sources of systematic error in the EIS method. This section examines some cases of EM drift from actual flight data.

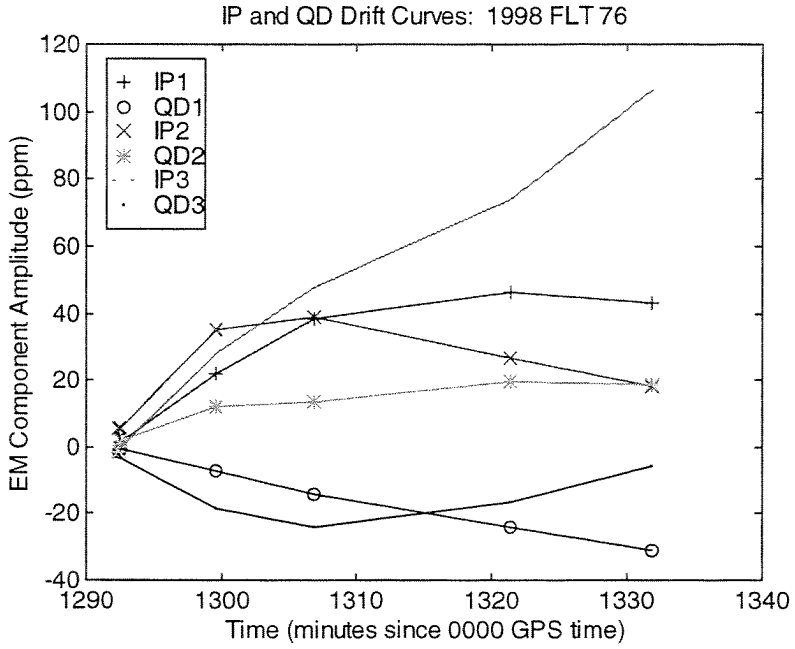

Figure 5.4.1: Estimated IP and QD drift curves, 1998 FLT 76.

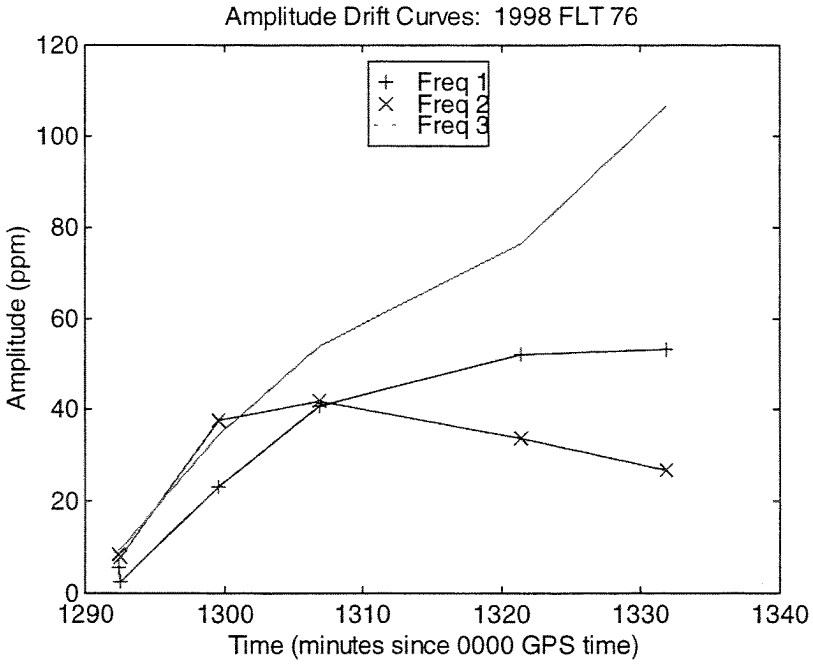

Figure 5.4.2: Amplitude plot of FLT076 drift.

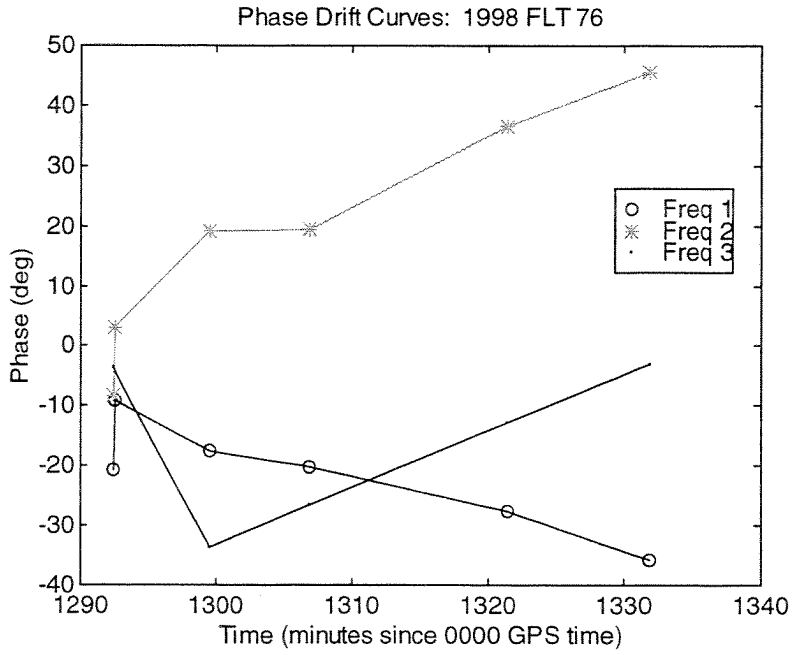

Figure 5.4.3: Phase plot of FLT076 drift.

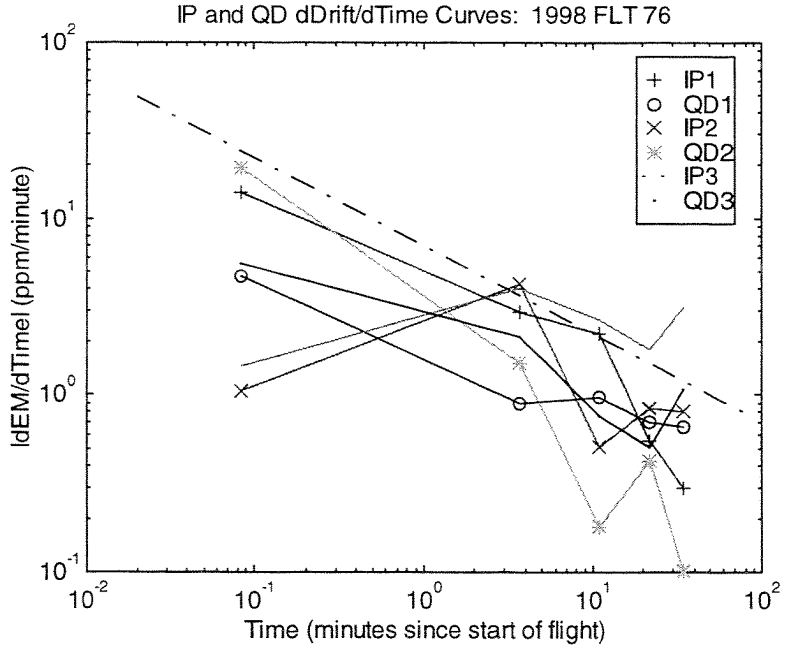

Figure 5.4.4: Absolute value of estimated time derivative of EM drift for FLT 76. The dashed black line at top represents a function proportional to $(\text{time})^{-1/2}$.

The first four plots above, Figure 5.4.1, Figure 5.4.2, Figure 5.4.3 and Figure 5.4.4, show the observed drift in inphase/quadrature, and as amplitude and

phase, followed by the absolute value of the time derivative of the drift for 1998 FLT 76 over the Northumberland Strait. Figure 5.4.5 is an inphase/quadrature plot and Figure 5.4.6 is a time derivative plot for FLT 78.

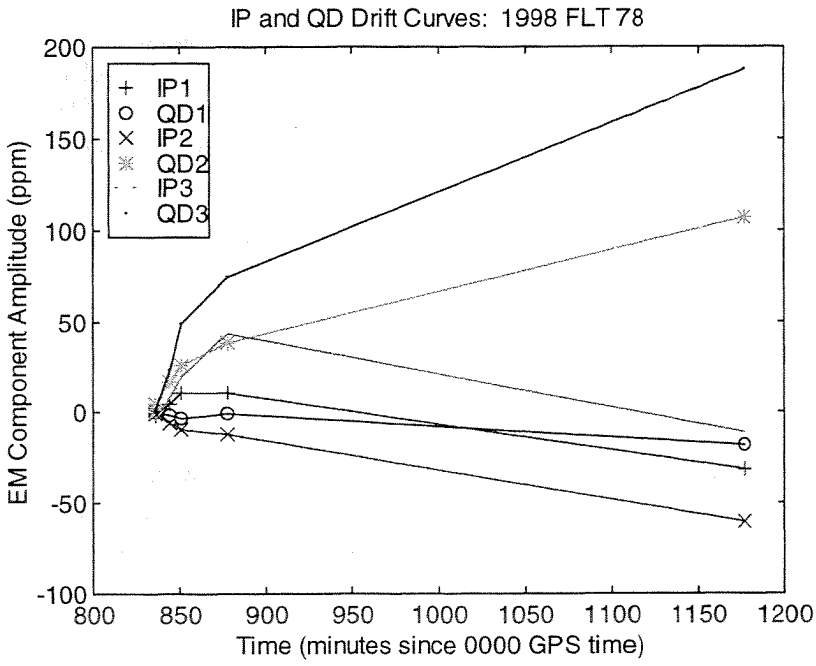

Figure 5.4.5: Drift curves for FLT 78.

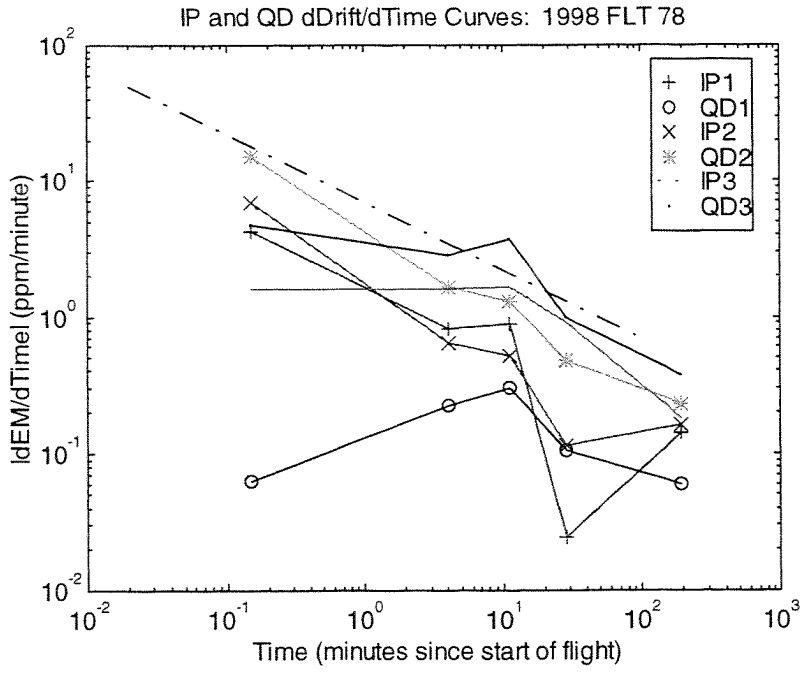

Figure 5.4.6: Time derivatives of drift curves for FLT 78 plotted with drift rate upper bound model.

Also shown on the time derivative plots is a "bounding function" (dashed line, no symbols) which represents an upper bound on the time rate of drift of the system. This bounding function shows that drift rates for "normal" flights not interrupted by long periods at high altitude or extended passages over land, both of which affect the process of temperature stabilisation within the bird, may be expected to be as good as or better than $10\ t^{-1/2}$ (the model plotted was actually for $7\ t^{-1/2}$: choosing a larger amplitude factor improves the confidence factor for the model.) This in turn permits the selection of a conservative background measurement schedule, which should ensure an acceptable level of performance.

In order to assess a given background measurement schedule, a plot such as that in Figure 5.4.7 is helpful. This figure shows the bounding function (integrated from the function for the time derivative of drift with an initial value of zero), together with a variety of drift estimates that can be used to remove drift to varying degrees of accuracy.

The simplest drift correction scheme, which can be applied in real-time or in post-processing, is simply to sample the baseline value at the high-altitude background measurement prior to a survey line, and hold that value until the next update. This is a strategy used in some data acquisition systems for sampling time-varying data, and is known as "sample-hold" prediction.

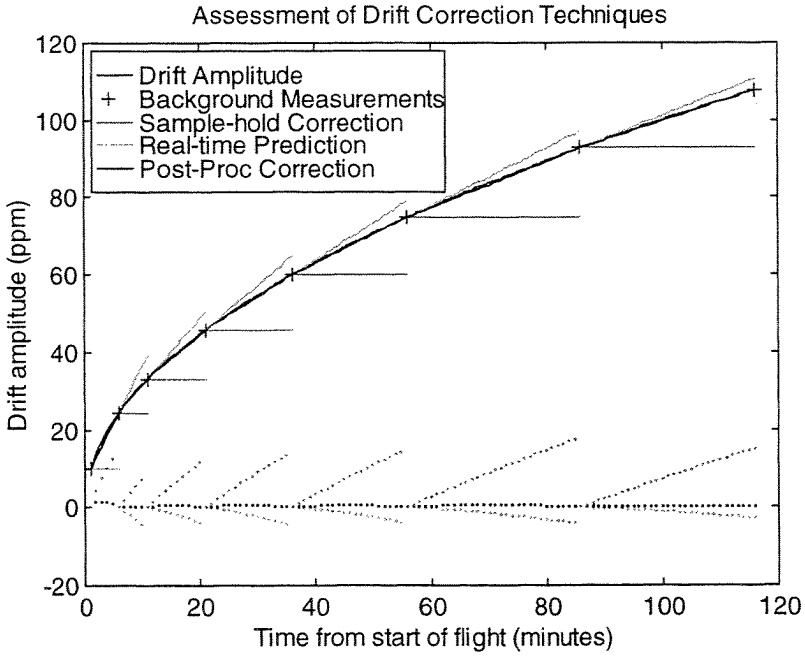

Figure 5.4.7: Theoretical drift curve with sample-hold, real-time prediction and post-processing interpolation corrections plotted.

A more sophisticated method is to look at the two background measurements prior to the current survey line, estimate the parameters for a straight line approximation to that prior background interval, and extrapolate it to the current

interval. This technique is used for real-time drift prediction in the EIS system, and has therefore been labelled "real-time" prediction.

The method used for post-processing drift removal makes use of the fact that the drift at both ends of a survey interval are already known. A straight-line interpolation between these two points can then be performed to yield an even better estimate of EM drift along the survey line. This method has been labelled the "Post-Proc" correction.

Each of these predictions and corrections is plotted in Figure 5.4.7. The error obtained by using each of these methods is shown in Figure 5.4.8. It should be clear that the sample-hold prediction yields large errors by the end of each background interval—only short survey intervals could therefore be performed using this technique if a given maximum level of EM drift could be tolerated. The Real-Time prediction is much more accurate, although prediction errors escalate rapidly toward the end of each interval. The Post-Proc method yields by far the best results, but has the disadvantage that it requires knowledge of both initial and final drift errors before the correction can be performed. It is thus not suitable for use in a real-time ice properties estimation sensor.

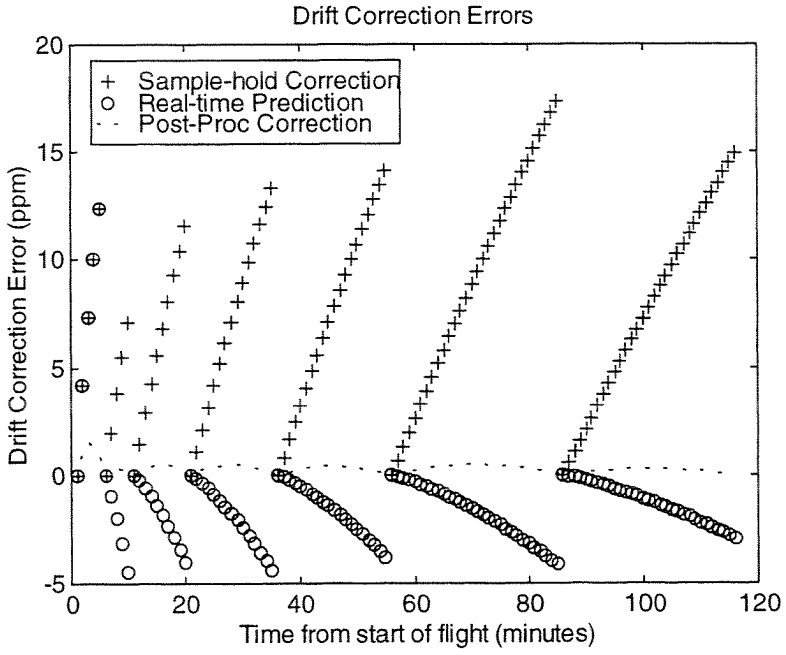

Figure 5.4.8: Drift error estimates obtained for sample-hold, real-time prediction and post-processing linear interpolation.

A direct estimate of the magnitude of drift-generated errors may be obtained by modelling the EM response of the Standard Model, adding progressively larger drift errors to a series of identical model results, and inverting the resulting EM dataset for the desired model parameters. This approach was used in the preparation of Figure 5.4.9 to Figure 5.4.12.

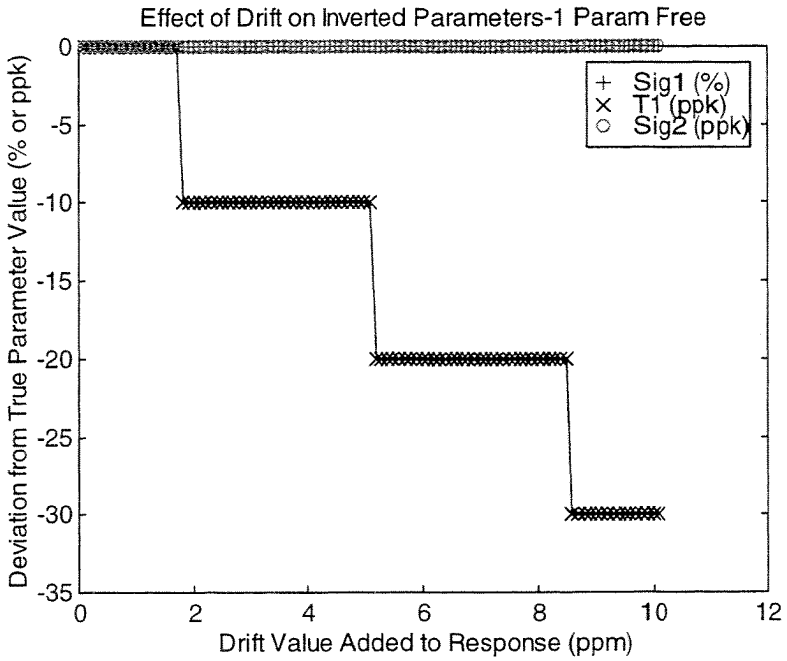

Figure 5.4.9: Inversion of Standard Model response with 0-10 ppm of drift added to EM data. T1 was left free in this case. Steps in T1 error are due to 1 cm changes in snow-plus-ice thickness. The 30 ppk error in T1 corresponds to a 3 cm error out of the 1m Standard Model thickness .

For Figure 5.4.9, only the snow plus ice thickness T1 was left free during inversion. As a result, all of the drift error was forced either into T1 or into the model misfit, which did rise rapidly as drift levels increased. An encouraging feature of this figure, which corresponds to the standard setup of the EIS system during routine surveys, is that the T1 error levels remain small even as drift errors reach and exceed 10 ppm in all frequencies of EM data. Each step in the T1 error curve represents an error of 1 cm, equal to 10 ppk in a 1 m ice thickness. Thus the maximum error seen, for 10 ppm of drift, is –3 cm, which lies well within the $\pm$ 5 cm nominal accuracy specification for the system.

If both T1 and Sig1 are allowed to vary during inversion, as was done in real time during the later part of the 1995 Resolute field program and in post-processing for all EIS survey work after 1994, the drift error biases the ice conductivity and generates negligible errors in the ice thickness—provided that the ice conductivity is allowed to vary over a wide enough range. The +200% error in Sig1 for 10 ppm of drift corresponds to a value of 0.06 S/m *vs* the true value of 0.02 S/m.

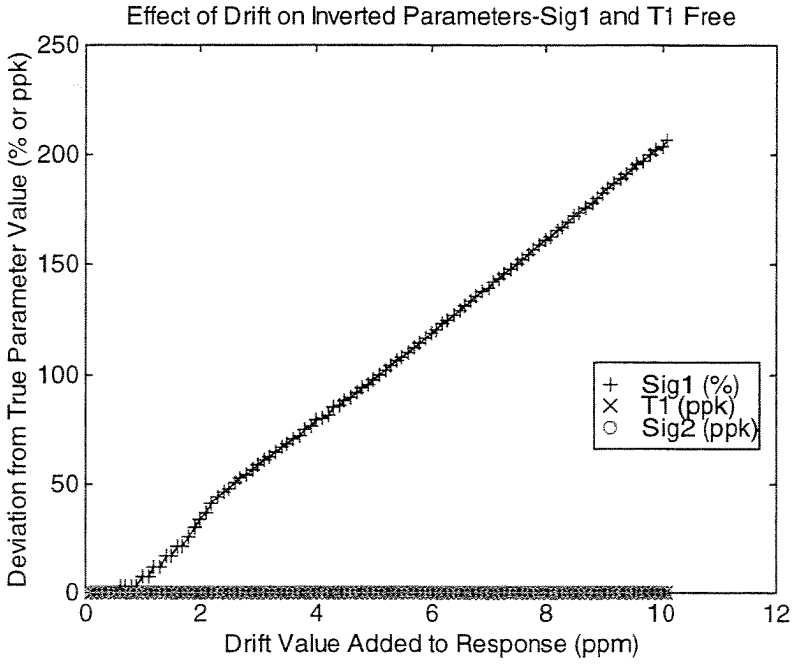

Figure 5.4.10: Inversion of Standard Model response with 0-10 ppm of drift added to EM data. Sig1 and T1 were left free. Inversion applies the error to Sig1 in this case, leaving T1 with zero apparent error. Errors in Sig1 are in %.

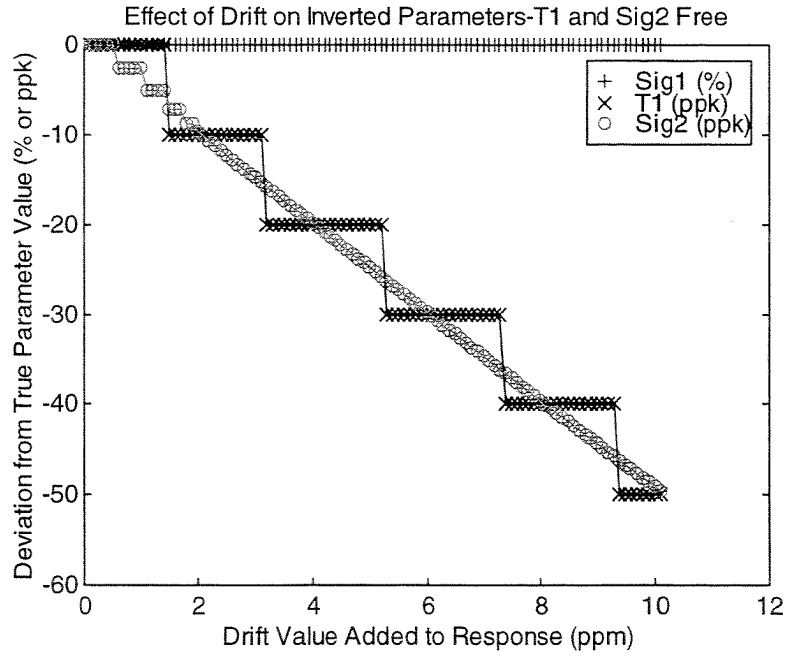

Figure 5.4.11: Inversion of Standard Model response with 0-10 ppm of drift added to EM data. T1 and Sig2 were left free. Note 1 cm error steps in T1.

Figure 5.1.2 shows the results of inversion when ice conductivity is fixed and the seawater conductivity is allowed to vary during inversion along with ice thickness. In this case, both free parameters vary at approximately the same rate in terms of their relative error. The maximum errors in this case are –5 cm for T1 and –0.125 S/m for Sig2.

When all three parameters are left free during inversion, Sig1 again absorbs most of the error, with T1 and Sig2 relative errors again tracking closely. In this case, for 10 ppm of error, the maximum errors in T1 are –2 cm, in Sig1 are +.024 S/m and in Sig2 are -.0625 S/m.

It should be noted that despite the apparent virtues of leaving multiple parameters free during inversion (*i.e.* reducing thickness error at the expense of ice and seawater conductivity error), there are drawbacks as well, particularly a greater susceptibility to random error, which indicate that the minimum practical number of parameters should be left free in most inversion applications.

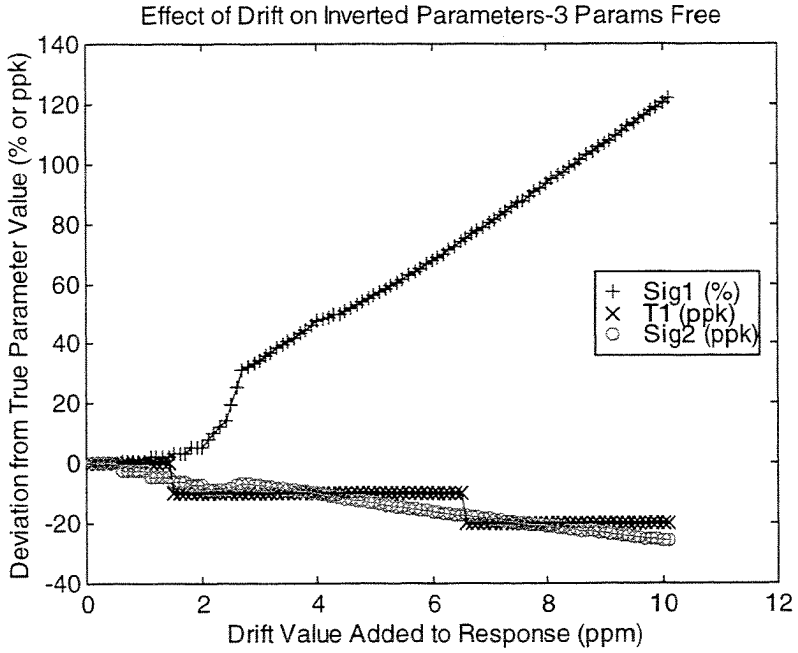

Figure 5.4.12: Inversion of Standard Model response with 0-10 ppm of drift added to EM data. All three model parameters were left free in this case. Steps in T1 curve are due to 1 cm changes in thickness. Note that errors in Sig1 are in percent, while T1 and Sig2 errors are in parts per thousand (ppk). Again, Sig1 is the parameter most subject to error due to drift.

5.5 Calibration Effects

The effects of a 1 ppk calibration error on applied to all EM data on the model parameter estimates are shown in Figure 5.5.1. A calibration error of this type yields results very similar to those for drift errors. This figure shows an alternative presentation of such errors, plotting them as a function of T1. Sig1 is most strongly affected by the error, which is expected since the signal component driving this parameter is weak and rides on top of the larger signals driving T1 and Sig2. The Sig1 error drops with increasing T1 because the signal component amplitude related to ice conductivity increases as the EM signal traverses a greater thickness of ice.

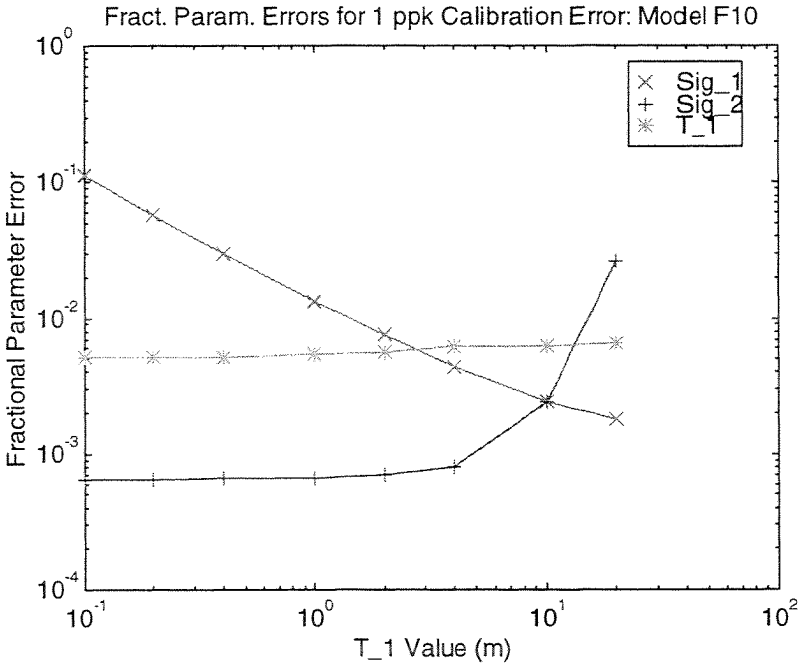

Figure 5.5.1: Fractional parameter error estimates for case with 1 part per thousand (ppk) calibration error applied to all data. The parameter most strongly affected is Sig1.

5.6 Altitude Effects

The effect of increasing sensor altitude is to decrease the amplitude of the EM response, thereby increasing the relative importance of errors such as those due to drift. This effect was anticipated in the formulas for both calibration and operational error budgets, as discussed earlier. In the three examples which follow, the effect of such errors on estimated ice thickness and conductivity are modelled.

The first example (Figure 5.6.1) shows the effect of changing altitude on estimated parameter errors, assuming 1 ppm random noise levels (with no

systematic component) in all EM data. Comparison of the error estimates in this plot at 15 m altitude with the identical error estimates for the 1 m Standard Model ice thickness in Figure 5.1.1 serves as a cross-check between the error estimates in the two figures.

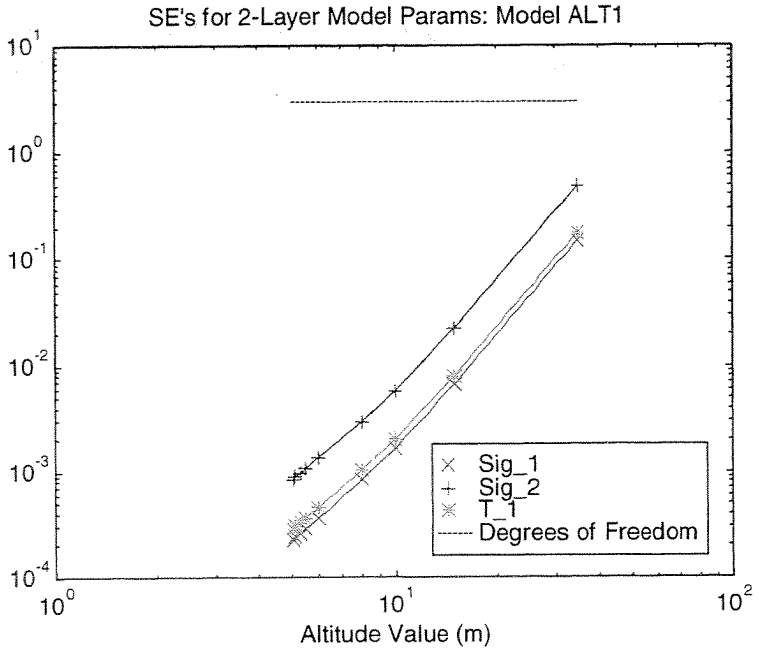

Figure 5.6.1: Variation of parameter error with bird altitude for 1 ppm EM error.

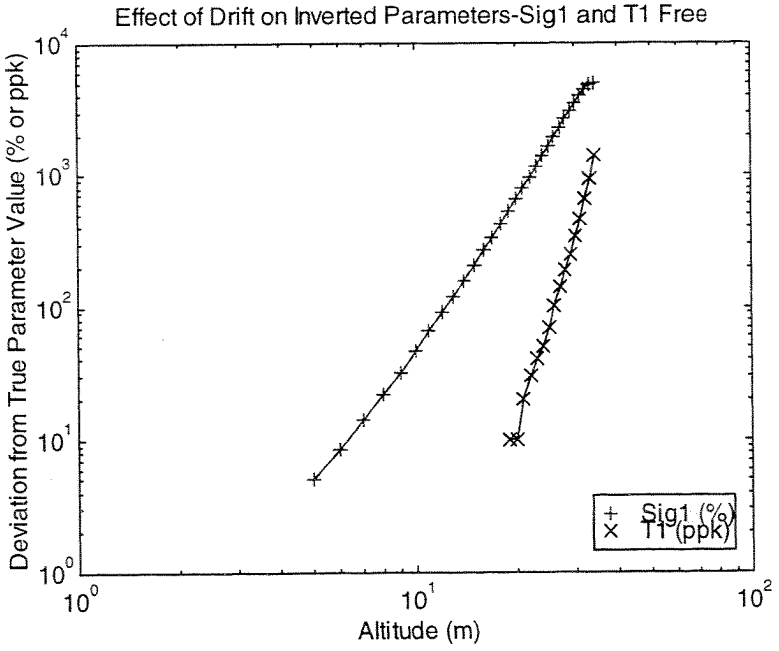

Figure 5.6.2: Variation of parameter error arising from 10 ppm drift error as a function of altitude with Sig1 and T1 free.

The second example (Figure 5.6.2) assumes a constant level of drift error of 10 ppm in all channels, and shows the deviation of Sig1 and T1 from their true values as fractional errors as the bird's altitude ranges from 5 m to 30 m. T1 errors below 10 ppk are not shown as they are less than 1 cm and were truncated by the inversion routine to zero. Note the steepness of both curves with respect to altitude: drift errors on this order become very important to T1 at altitudes above 20 m.

The third example (Figure 5.6.3) assumes a constant level of drift error of 10 ppm in all channels, and shows the behaviour of all three model parameters as the bird's altitude ranges from 5 m to 30 m.

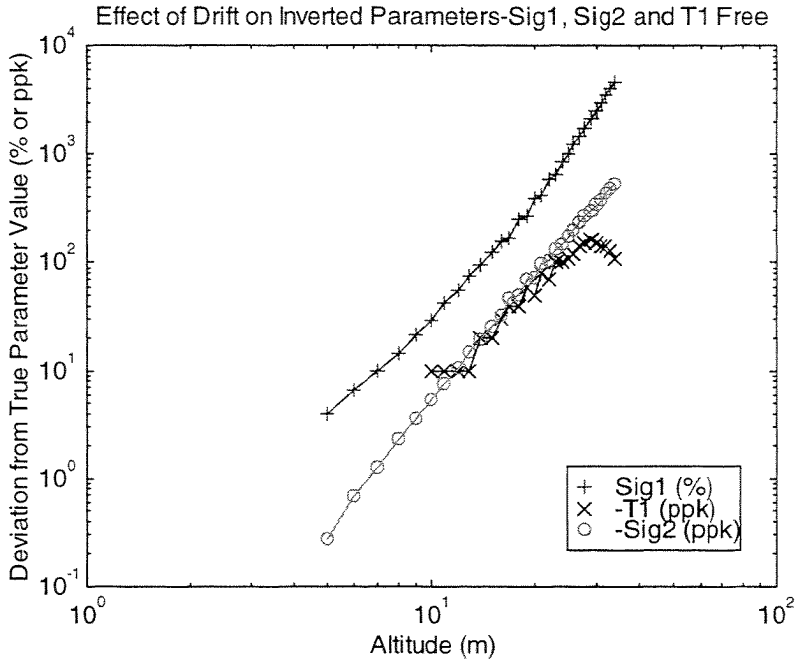

Figure 5.6.3: Variation of parameter error arising from 10 ppm drift error as a function of altitude with Sig1, Sig2 and T1 free. T1 errors below 10 ppk are not shown as they are less than 1 cm and were truncated by the inversion routine to zero. Errors in T1 appear at a lower altitude due to the greater number of free parameters in this case, but are limited to the 100 to 200 ppk range above about 23 m relative to the previous example.

An interesting feature of Figure 5.6.1 is that the ice thickness noise level drops below the precision of the laser altimeter at about 18 m altitude, assuming a 1 ppm average EM error. This emphasises the respective roles of laser and EM error over different altitude ranges in establishing the error in T1: laser error is independent of height, with a noise floor of about 1 cm, while the EM component is strongly height dependent. The next two figures further emphasise the role of altitude on parameter estimation in the presence of EM error.

Figure 5.6.2 and Figure 5.6.3 demonstrate that drift at the 10 ppm level is particularly important at altitudes above 20 m for snow plus ice thickness, and that ice conductivity estimates are strongly affected by drift at all altitudes, at least for the relatively thin ice of the Standard Model. Evidently, care must be taken with drift corrections and background measurement schedules if absolute estimates of ice conductivity are parameters of interest in the survey results. Real-time estimation of ice conductivity requires even more stringent background schedules and will be most accurate at relatively low survey altitudes (closer to 10 m than to the nominal 15 m).

6 Errors Due to inappropriate model parameterisation or values

6.1 Case 1: Rafted ice

Rafted ice affects the EM response by introducing a saline water layer between the rafted ice layers. The effect is to reduce the apparent thickness of the ice relative to the total thickness of ice present and/or to alter the apparent ice layer conductivity. The model used for this example consists of a 0.5 m layer of normal sea ice of conductivity 0.02 S/m, overlying a seawater layer of variable thickness and conductivity 2.5 S/m, which in turn overlies another layer of normal sea ice floating on deep seawater. In the first example, ice thickness only is allowed to vary, while in the second, ice conductivity and thickness are both allowed to vary.

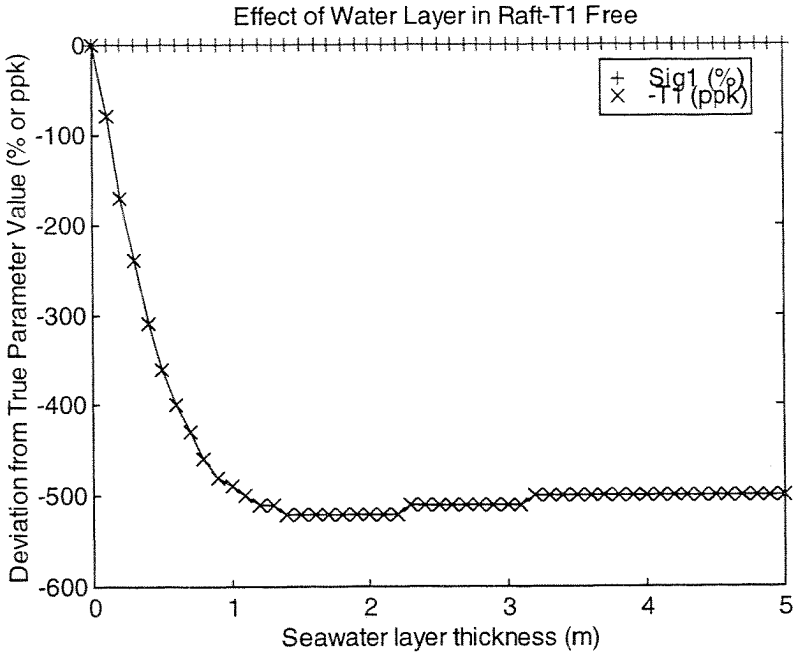

Figure 6.1.1: Errors in inversion of rafted ice model, inverted as a single ice layer over seawater. T1 only was left free during the inversion. The thickness of each rafted layer is 0.5 m, for a total ice thickness of 1 m.

In the first example, for very thin water layers, the total ice thickness is reproduced accurately. For water layer thicknesses over 1 m, the total ice thickness is underestimated by 500 ppk, which is the value of the lower ice layer's thickness: it is effectively screened from the EM system by the presence of the water layer. In the second example, where the ice conductivity has been allowed to vary, the ice conductivity absorbs some of the effect of the seawater layer, reducing the magnitude of the total ice thickness error slightly for thicker water layers. Note that the ice thickness is slightly overestimated, with a very high ice conductivity overestimate (over 3000%), for thin water layers. This may explain some high apparent ice conductivities observed over deformed ice.

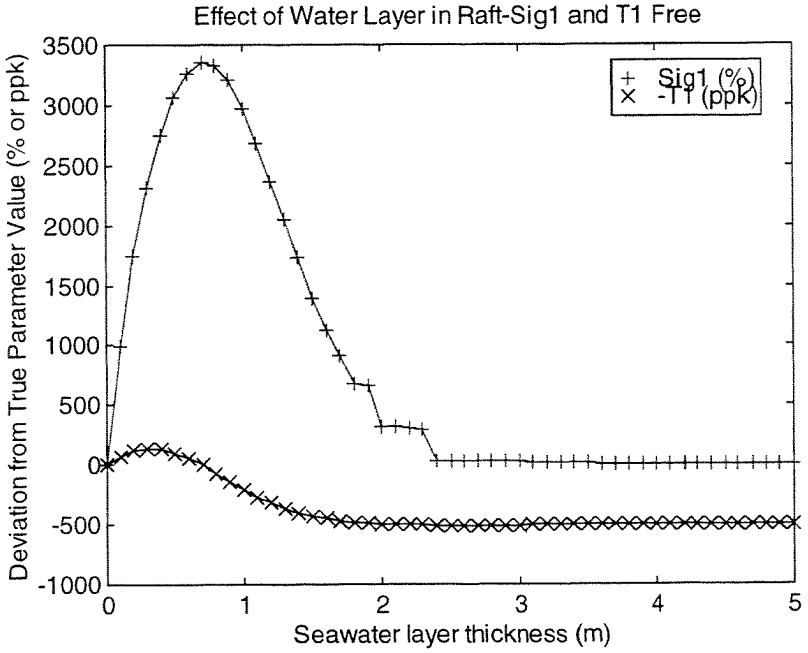

Figure 6.1.2: Errors in inversion of rafted ice model, inverted as a single ice layer over seawater. Sig1 and T1 left free during the inversion. The thickness of each rafted layer is 0.5 m, for a total ice thickness of 1 m.

6.2 Case 2: Conductivity layering in ice

Reports have appeared in the literature of cases in which contrasting conductivity of layers within the ice have been suggested as the source of model misfits and errors in the estimation of total ice thickness (Soininen *et al*, 1998). This example uses a three-layer model consisting of 0.5 m of highly resistive ice overlying a 0.5 m layer of ice possessing moderate but variable conductivity, floating on normal seawater, to investigate this assertion. While this model does not closely represent the Baltic Sea conditions discussed by Soininen *et al*, it is a potentially useful model for situations in which a thick snow layer has accumulated on top of

normal first-year sea ice, as might occur in Labrador Sea or Gulf of St. Lawrence waters.

The two plots for this case show the error in T1 (first example) and Sig1 and T1 (second example) as a function of the conductivity of the 0.5 m sea ice layer underlying a uniform1 mS/m, 0.5 m snow layer. In both cases, the total estimated snow plus ice thickness is within 1 cm of the true value for sea ice layer conductivities of less than 100 mS/m (a very high value for normal first-year sea ice of this thickness.) As expected, Sig1 estimate absorbs the majority of the effect of the variable ice conductivity, and falls within ± 75% of the actual sea ice conductivity of 20 mS/m over a lower-layer ice conductivity range of 0-200 mS.

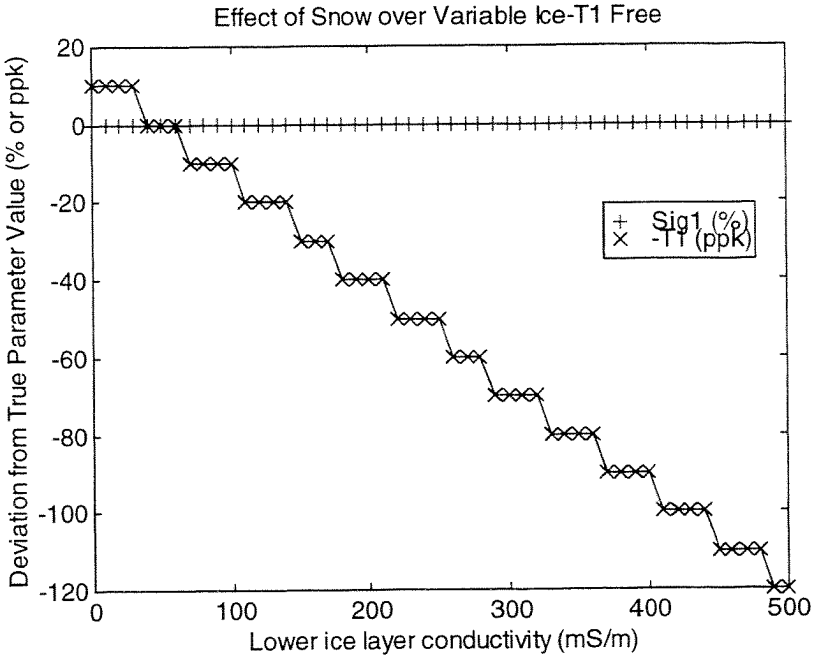

Figure 6.2.1: Errors in inversion of snow-covered ice layers due to assumption of uniform conductivity. T1 was the only free parameter in this case. The steps in the ice thickness error curve correspond to 1 cm increments in ice thickness error.

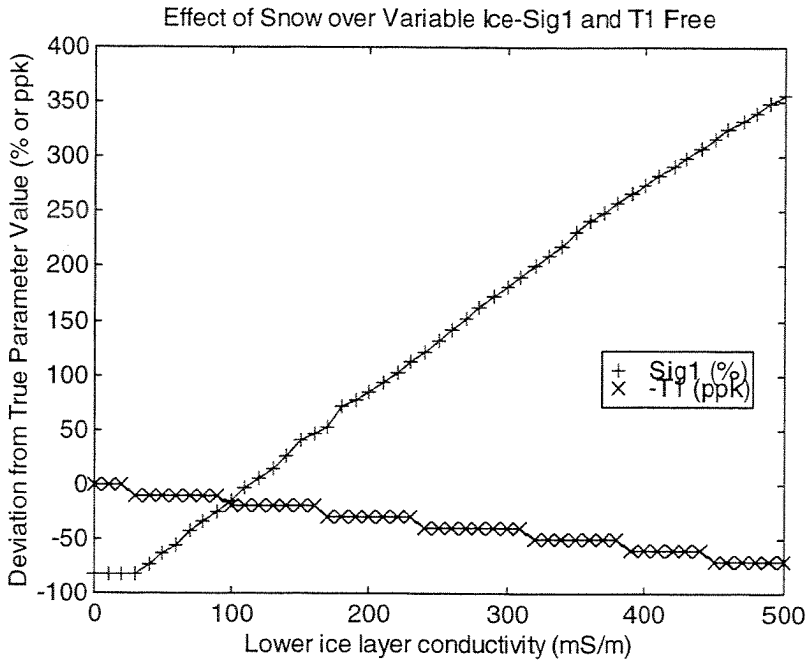

Figure 6.2.2: Errors in inversion of snow-covered ice layers due to assumption of uniform conductivity. Sig1 and T1 were both left free during this inversion. The steps in the ice thickness error curve correspond to 1 cm increments in ice thickness error.

7 Parameter equivalence issues

Parameter "equivalence" is a problem encountered during the inversion of data for model parameters wherein the inversion is unable to clearly distinguish between changes in one parameter (*e.g.* snow plus ice thickness) and another parameter (*e.g.* average ice conductivity.) This is more of an issue for EM interpretation in cases where thin conductive layers are present within a thick resistive section than in the ice measurement case.

The existence of an equivalence problem can be assessed through analysis of the "parameter eigenvector" and "singular value" matrices obtained during SVD analysis. Two cases were analysed using SVD methods in Section 5.3 above: these were the standard ice measurement case, and the ice measurement with bathymetry case.

The severity of equivalence is measured by the presence and degree of similarity of large double entries in the columns of the parameter eigenvector matrix. For example, negligible equivalence is present for the parameter related to an entry of 0.99 in a given column, since no other entries in that column will be larger than a few percent of that value. The converse situation is when two columns exist with entries approximating $\pm 1/\sqrt{2}$ in a pattern similar to the following five-parameter example:

SV's	1000	1	x	x	x
P1	x	x	x	x	x
P2	0.707	-0.707	x	x	x
P3	x	x	x	x	x
P4	0.707	0.707	x	x	x
P5	x	x	x	x	x

In this example, "x" symbols are used to indicate entries irrelevant to the point being made here. This pattern is present because the first column or eigenparameter actually determines the product of P2 and P4 (remember that the partial derivative matrix was computed for logarithmic parameters, and that addition of log(P2) and log(P4) corresponds to the log of the product log(P2*P4). The second eigenparameter determines the ratio P4/P2 in the same way. If the eigenparameters are sufficiently distinct, one can determine P2 by subtracting the second eigenparameter from the first, while P4 can be determined by adding the two eigenparameter. However, if as in this case they are highly equivalent and their respective singular values (SV's) are not both large enough to yield very small eigenparameter errors, even a tiny error in the input data used to invert for P2 and P4 will likely result in large swings in P2 and P4, though not in the product P2*P4. This is the fundamental expression of parameter equivalence.

In the straightforward ice measurement case (a three-parameter problem), weak equivalence may be seen between Sig_1 and T_1 in the first two columns: the equivalence is weak because the each of the four entries are numerically

different at the 1% or greater level and the two eigenparameters (the two columns of the eigenvector matrix) are associated with large singular values, indicating that they are both very well-determined. The third parameter, Sig_2, is uniquely determined, as the third eigenparameter has an entry of 0.96 associated with Sig_2, though its error will be higher than for the previous two eigenparameters due to the smaller singular value associated with that column.

In the five-parameter ice-thickness/bathymetry case, the same weak equivalence is seen in the first two eigenparameters for Sig_1 and T_1. A similar degree of weak equivalence is seen in the last two eigenparameters for Sig_3 and T_2. However, unlike the Sig1-T_1 equivalence, the last two eigenparameters are both associated with relatively small singular values: their relative sensitivity to data error are about 20 and 150 times that for the first eigenparameter. Hence equivalence effects are much more likely to be observed for these two parameters, which represent sub-ice water thickness and sea-bottom conductivity. This make sense physically, because the presence of conductive seawater shields the less-conductive sea-bottom from the transmitted field, so that reflections from the water-bottom interface and from the bottom material itself are weak. Thus, only small amounts of information come back to the EM sensor from the sea-bottom, and in the presence of noise or other errors, such small signals are easily biased by those errors.

8 EIS System Error Budgets

8.1 Calibration Error Budget

The theory underlying the estimation of the calibration error budget is straightforward, based on standard experimental error analysis techniques. The EM observed data at a given point in time are $\underline{o} \pm \Delta\underline{o}$, where the underscores indicate vector quantities. In the case of EIS, the $\underline{o}$ vector has two complex elements. The laser altimeter data is $l \pm \Delta l$, and the pitch and roll outputs from the TANS Vector orientation measurement unit are $P \pm \Delta P$ and $R \pm \Delta R$.

The EM response of a layered model with parameters $\underline{p} \pm \Delta\underline{p}$ (the layer thicknesses and conductivities) may be calculated as a function of the parameters, laser altitude and orientation measurements by

$$\underline{c} = \underline{c}(\mathrm{p}, \mathrm{l}, \mathrm{P}, \mathrm{R})$$

using an accurate numerical procedure. The ground truth calibration factors (GTCF's) may then be calculated as

$$\underline{G} \pm \Delta\underline{G} = \frac{(\underline{o} \pm \Delta\underline{o})}{(\underline{c} \pm \Delta\underline{c})}$$

For the *i*'th frequency, the error in the GTCF can be estimated by

$$\Delta G_i = G_i \cdot \left(\left(\frac{\Delta o_i}{o_i} \right)^2 + \left(\frac{\Delta c_i}{c_i} \right)^2 \right)^{1/2}$$

G_i is known to be within a few percent of unity, owing to the inherent accuracy of the system's hardware calibration. For the same reason, o_i and c_i have virtually equivalent amplitudes, which can also be used to simplify the calculation. The error ΔG in G due to errors in the observations and ground truth can be estimated by computing the total differential of the calculated response with respect to the various model inputs. A two-layer model with parameters σ_1, t_1 and σ_2 represents the conventional case:

$$\begin{aligned} \Delta c &= \frac{\partial c}{\partial l} \cdot \Delta l + \frac{\partial c}{\partial P} \cdot \Delta P + \frac{\partial c}{\partial R} \cdot \Delta R + \frac{\partial c}{\partial \sigma_1} \cdot \Delta\sigma_1 + \frac{\partial c}{\partial t_1} \cdot \Delta t_1 + \frac{\partial c}{\partial \sigma_2} \cdot \Delta\sigma_2 \\ &= A \cdot \Delta l + B \cdot \Delta P + C \cdot \Delta R + D \cdot \Delta\sigma_1 + E \cdot \Delta t_1 + F \cdot \Delta\sigma_2 \end{aligned}$$

The terms A-F will be used below during calculation of representative error estimates.

Given reasonable values for the error levels $\Delta\underline{o}$, Δl, ΔP, ΔR, of the various inputs to the calculation derived from experience with the system and the specifications of system components, and also for the ground truth measurements $\Delta\sigma_1$, Δt_1 and $\Delta\sigma_2$, ΔG may be estimated as follows:

$$\Delta G_i = \left(\frac{(O = \Delta o_i)^2 + (A \cdot \Delta l)^2 + (B \cdot \Delta P)^2 + (C \cdot \Delta R)^2 + (D \cdot \Delta \sigma_1)^2 + (E \cdot \Delta t_1)^2 + (F \cdot \Delta \sigma_i)^2}{o^2{}_i} \right)^{1/2}$$

Values for the partial derivatives A-F may be obtained by interpolation from the plots of these functions in Figure 5.1.2 -- Figure 5.1.8. Table 8.1.1 below summarises the calculation of the amplitude error for conventional ground truth calibration.

Table 8.1.1: Calibration noise calculation at 10 m altitude.

Quantity		Frequency		Units	Comment
		30,000	90000	Hz	EIS operating frequencies
	IP	5,740	6451	ppm	SM Response at 10 m altitude
	QD	1,276	851	ppm	SM Response at 10 m altitude
	Δ *o*	0.6	6	ppm	both IP and QD
	Δ *l*	0.01	0.01	m	1-Alpha specs
	Δ *P*	0.1	0.1	degree	Vector spects
	Δ *R*	0.1	0.1	degree	Vector spects
	Δ *σ1*	0.03	0.03	S/m	Estimated GT error
	Δ *t1*	0.03	0.03	m	Estimated GT error
	Δ *σ2*	0.025	0.025	S/m	Estimated GT error
	A	1200	1400		Dominant Component from SM
	B	2	2		Dominant Component from SM
	C	2	2		Dominant Component from SM
	D	200	290		Dominant Component from SM
	E	350	400		Dominant Component from SM
	F	70	40		Dominant Component from SM
	Δ *o*	0.6	6	ppm	Weak component of error
A x	Δ *l*	12	14	ppm	Dominant component of error
B x	Δ *P*	0.2	0.2	ppm	Negligible
C x	Δ *R*	0.2	0.2	ppm	Negligible
D x	Δ *σ1*	6	8.7	ppm	Minor component of error
E x	Δ *t1*	10.5	12	ppm	Major component of error
F x	Δ *σ2*	1.75	1	ppm	Weak component of error
	Δ *G*	0.002915	0.00327	dimensionless	Error in Ground Truth Cal. Factor

The results indicate that approximately 0.3% error may be expected in the amplitude of the GTCF's for a single sample. Averaging *n* samples together would reduce this random error by about $\sqrt{n}$. The dominant contributor to the overall error at a 10 m calibration altitude is the 1 cm laser precision, followed closely by the 3 cm error in t_1.

Repeating the calculation at 15 m altitude (Table 8.1.2) yields a slight increase in noise in the GTCF's, due primarily to the decrease in EM response. The dominant component has shifted from laser error to ice thickness surface measurement error.

Table 8.1.2: Calibration noise at 15 m altitude.

Quantity		Frequency		Units	Comment
		30,000	90000	Hz	EIS operating frequencies
	IP	2,106	2281	ppm	SM Response at 15 m altitude
	QD	337	215	ppm	SM Response at 15 m altitude
	Δ *o*	0.6	6	ppm	both IP and QD
	Δ *l*	0.01	0.01	m	1-Alpha specs
	Δ *P*	0.1	0.1	degree	Vector spects
	Δ *R*	0.1	0.1	degree	Vector spects
	Δ $\sigma 1$	0.03	0.03	S/m	Estimated GT error
	Δ *t1*	0.03	0.03	m	Estimated GT error
	Δ $\sigma 2$	0.025	0.025	S/m	Estimated GT error
	A	250	250		Dominant Component from SM
	B	2	2		Dominant Component from SM
	C	2	2		Dominant Component from SM
	D	200	290		Dominant Component from SM
	E	350	400		Dominant Component from SM
	F	70	40		Dominant Component from SM
	Δ *o*	0.6	6	ppm	Minor component of error
A x	Δ *l*	2.5	2.5	ppm	Minor component of error
B x	Δ *P*	0.2	0.2	ppm	Negligible
C x	Δ *R*	0.2	0.2	ppm	Negligible
D x	Δ $\sigma 1$	6	8.7	ppm	Major component of error
E x	Δ *t1*	10.5	12	ppm	Dominant Component of error
F x	Δ $\sigma 2$	1.75	1	ppm	Minor component of error
	Δ *G*	0.005856	0.007079	dimensionless	Error in Ground Truth Cal. Factor

The same derivation and calculation can be used to assess the effect of systematic data errors on the calibration by substituting the expected systematic errors into the calculation. The major contributor to systematic error is the laser altimeter, which is specified as having 5 cm accuracy (as opposed to the 1 cm specified precision and observed stability used above.) Systematic EM errors are assumed to consist primarily of approximately 5 ppm of drift in both inphase and quadrature, although in post-processed results, drift error may be expected to be much lower. The pitch and roll are assumed to be accurate within about 1 degree. The results are summarised in Table 8.1.3 below for the 10 m calibration altitude case. Laser altimeter error is by far the most significant component in this case, and would clearly remain so at 15 m and higher. The amplitude of the error in this case is on the order of 1% for both frequencies. It is worth noting

that, provided laser altimeter systematic errors do not change significantly with time, this error would be consistent from flight to flight. Thus, the act of calibrating the system absorbs the systematic errors from the various data inputs into the GTCF's. Measurements made with the system post-calibration should then be accurate to a level determined by the 0.3% precision of the calibration measurement and the noise levels of operational data inputs, rather than to the lower standard of the systematic calibration error.

Table 8.1.3: Systematic error calculation for EIS calibration.

Quantity		Frequency		Units	Comment
		30,000	90000	Hz	EIS operating frequencies
	IP	5,740	6451	ppm	SM Response at 10 m altitude
	QD	1,276	851	ppm	SM Response at 10 m altitude
	Δ *o*	5	5	ppm	both IP and QD
	Δ *l*	0.05	0.05	m	1-Alpha specs
	Δ *P*	1	1	degree	Vector spects
	Δ *R*	1	1	degree	Vector spects
	Δ $\sigma 1$	0.03	0.03	S/m	Estimated GT error
	Δ *t1*	0.01	0.01	m	Estimated GT error
	Δ $\sigma 2$	0.025	0.025	S/m	Estimated GT error
	A	1200	1400		Dominant Component from SM
	B	2	2		Dominant Component from SM
	C	2	2		Dominant Component from SM
	D	200	290		Dominant Component from SM
	E	350	400		Dominant Component from SM
	F	70	40		Dominant Component from SM
	Δ *o*	5	5	ppm	Minor component of error
A x	Δ *l*	60	70	ppm	Dominant component of error
B x	Δ *P*	2	2	ppm	Negligible
C x	Δ *R*	2	2	ppm	Negligible
D x	Δ $\sigma 1$	6	8.7	ppm	Minor component of error
E x	Δ *t1*	3.5	4	ppm	Minor component of error
F x	Δ $\sigma 2$	1.75	1	ppm	Negligible
	Δ *G*	0.010323	0.010895	dimensionless	Error in Ground Truth Cal. Factor

8.2 Operational Error Budget

Error levels during normal EIS operations may be derived in a manner similar to that used for estimation of calibration errors. Again, the computed response of a model specified for the parameter vector $\underline{p} \pm \Delta\underline{p}$ at laser altitude, pitch and roll values *l, P* and *R* is

$$\underline{c} = \underline{c}(\mathrm{p}, \mathrm{l}, \mathrm{P}, \mathrm{R})$$

The parameter vector is computed by inverting this model:

$$\begin{aligned} \underline{p} &= c^{-1}(\underline{o}, l, P, R) \\ &\equiv \underline{p}(\underline{o}, l, P, R) \end{aligned}$$

The error $\Delta\underline{p}$ in the parameter vector may be computed as

$$\begin{aligned} \Delta p_i &= \frac{\partial p_i}{\partial \underline{o}} \cdot \Delta\underline{o} + \frac{\partial p_i}{\partial l} \cdot \Delta l + \frac{\partial p_i}{\partial P} \cdot \Delta P + \frac{\partial p_i}{\partial R} \cdot \Delta R \\ &= J^{-1}{}_i \cdot \Delta\underline{o} + A \cdot \Delta l + B \cdot \Delta P + C \cdot \Delta R \end{aligned}$$

where $J^{-1}{}_i$ is the i'th row of the inverted matrix of partial derivatives ***J***:

$$J_{ij} = \frac{\partial o_i}{\partial p_j}$$

The most difficult part of the first expression above to estimate is the first element, corresponding to EM data errors $\Delta\underline{o}$. For EIS measurements over a reasonable altitude range over typical ice conditions, the matrix ***J*** is well-conditioned and invertible, so $\boldsymbol{J}^{-1}$ exists. For numerical reasons, the partial derivatives are actually computed with respect to the natural logarithm of the parameter values. This is corrected for below. For a 15 m altitude over the Standard Model, $\boldsymbol{J}^{-1}$ has the following values:

$$J^{-1} = \begin{bmatrix} .0012 & -.0011 & -.0032 & .0055 \\ .0077 & -.0045 & -.0181 & .0090 \\ .0007 & -.0028 & -.0051 & .0051 \end{bmatrix}$$

The three rows of this matrix correspond to σ_1, σ_2 and t_1, while the columns correspond to the inphase values of the observed EM data at 30 and 90 kHz, followed by the quadrature values of the EM data at 30 and 90 kHz. If the noise for the observed EM data is $\Delta\underline{o}$ = [0.6,6., 0.6,6.]^t, where the superscript "t" denotes the transpose operation, then the matrix-vector product becomes:

$$\begin{aligned} \Delta\ln(\underline{p})_{EM} &= \boldsymbol{J}^{-1}\, \Delta\underline{o} \\ &= [.0257, .0205, .0115] \end{aligned}$$

These must be corrected for the fact that the derivatives were computed with respect to the natural logarithms of the parameters. This is accomplished by multiplying each of the $\Delta\ln(\underline{p})$ values by the corresponding element of $\underline{p}$ to yield the $\Delta\underline{p}$ values relating to the EM observations:

$\Delta\underline{p}_{EM}$ = [.0005, .0515, .0115].

The remainder of the expression relates to errors in laser altimeter, pitch and roll. The effect of pitch and roll on the EM observations is negligible compared to their effects on bird altitude estimation.

Given reasonable values for the error levels $\Delta\underline{o}$, Δl, ΔP, ΔR, of the various inputs to the calculation derived from experience with the system and the specifications of system components, $\Delta\underline{p}$ is estimated as follows:

$$\Delta p_j = \left(\left(J_{ij}^{-1}\Delta o_i\right)^2 + (A\cdot\Delta l)^2 + (B\cdot\Delta P)^2 + (C\cdot\Delta R)^2\right)^{1/2}$$
$$= \left(\left(\Delta p_{jEM}\right)^2 + (A\cdot\Delta l)^2 + (B\cdot\Delta P)^2 + (C\cdot\Delta R)^2\right)^{1/2}$$

Values for the partial derivatives A-C are computed from the relevant portions of the model calculation. The only significant factors arise for j=3 (*i.e.* for ice thickness) from the calculation of true sensor height above the ice surface:

$$h_{vert} = l\cdot\cos P\cos R - axial\_offset\cdot\sin P\cos P\cos^2 R - vertical\_offset$$
$$\frac{\partial h_{vert}}{\partial l} = \cos P\cos R$$
$$\frac{\partial h_{vert}}{\partial P} = -l\cdot\sin P\cos R + axial\_offset\cdot\cos^2 R\left(\sin^2 P - \cos^2 P\right)$$
$$\frac{\partial h_{vert}}{\partial R} = -l\cdot\cos P\sin R + axial\_offset\cdot 2\cos R\sin R\sin P\cos P$$

where *axial_offset* (0.4 m) is the distance from the altimeter to the centre of the bird, and *vertical_offset* (0.0 m) is the distance of the altimeter datum from the axis of the bird. There is no significant contribution to ice or seawater conductivity error from modest pitch, roll or altitude errors.

Table 8.2.1 below summarises the error calculation for typical conditions, *i.e.* 15 m altitude over the Standard Model. Predicted errors for a single 10 Hz sample are 0.0005 S/m for ice conductivity, 0.0523 S/m for seawater conductivity, and 0.0153 m for ice thickness. These values appear to overestimate the latter two errors compared to the observed values, but it should be borne in mind that comparisons with ground truth are typically made between mean ground truth values and mean EIS ice thicknesses. In a 10 second sample, there are 100 EIS results: the random component of the error will drop by 10=√100 over such a sample, bringing "observed" random error levels down to .00005 S/m, .005 S/m and .0015 m. These values are actually smaller than those observed in comparisons with surface measurements (see Section 10 below).

Table 8.2.1: Operational error estimates for inverted parameters.

Parameters		Inverted J Matrix (15 m alt)				
ID	Value	IP30k	IP90k	QD30k	QD90k	<--Data ID
$\sigma 1$	0.02	0.00121	-0.00106	-0.00316	0.00554	Matrix row 1
$\sigma 2$	2.5	0.00767	-0.00452	-0.01815	0.00898	Matrix row 2
$t1$	1	0.00074	-0.00277	-0.00512	0.00513	Matrix row 3
l	15 m					
P	1 degree					
R	1 degree					

Input Errors	Frequency		Units	Comment
	30,000	90000	Hz	
Δ o_IP	0.6	6	ppm	IP EM error
Δ o_QD	0.6	6	ppm	QD EM error
Δ l	0.01		m	1-Alpha specs
Δ P	0.1		degree	Vector specs
Δ R	0.1		degree	Vector specs

Intermediate Results	Value		Units	Comment
Δ o_IP_att	0.6621	6.0065	ppm	EM errors adjusted for attitude effects
Δ o_QD_att	0.6007	6.0001	ppm	EM errors adjusted for attitude effects
A	0.999695		m/m	partial wrt laser altimeter output
B	-0.66138		m/degree	partial wrt pitch
C	-0.2615		m/degree	partial wrt roll

Computed Errors	Value	Units	Comment
Δ $\sigma 1\_EM$	0.0005	S/m	Only term for ice conductivity
Δ $\sigma 2\_EM$	0.0523	m	Only term for seawater conductivity
Δ $\tau 1\_EM$	0.0115	S/m	Major term for ice thickness
A x Δ l	0.0100	m	Major term for ice thickness
B x Δ P	-0.0012	m	Weak term for ice thickness
C x Δ R	-0.0005	m	Weak term for ice thickness

Parameter Errors	Value	Units	Comments
Δ $\sigma 1$	0.0005	S/m	Error in ice conductivity
Δ $\sigma 2$	0.0523	S/m	Error in water conductivity
Δ $\tau 1$	0.0153	m	Error in ice thickness

Other points of interest in this calculation include the following:

1. EM error drives essentially all error in the ice and seawater conductivities: laser, pitch and roll are negligible contributors.
2. EM error is the dominant error source for snow plus ice thickness calculations, with pitch and roll errors making very weak contributions. Laser altimeter noise contributes at the 1 cm level, as expected.

The variation of parameter noise levels for a variety of operational situations is shown in Table 8.1.1 below. Sensor altitude varies across the table, ranging from 7.5 m to 30 m. Error estimates are grouped by parameter, starting with noise in ice thickness T1. Four cases are presented: 0.02 S/m ice of 0.1, 1.0 and 2.0 m thickness, representing first-year ice of varying thicknesses, followed by a final case with 2 m thickness and 0.001 S/m conductivity, representing multi-year ice of moderate thickness. It is evident that noise levels increase rapidly for thin ice at high bird altitudes: at 20 m altitude, all cases show errors less than the system's 5 cm nominal accuracy.

The ice conductivity estimates for thin ice have higher noise levels than nominal even at 7.5 m altitude. This effect is due to the very small amount of ice traversed by the EM signal before being reflected at the ice-seawater interface, as well as a moderate amount of parameter equivalence (see Section 7). For thicker ice, the noise level drops rapidly.

The water conductivity estimates also suffer from increased noise at high sensor altitudes and for thin ice.

Table 8.2.2: Noise Budget for 7.5 to 30 m altitude: 3 free parameters

		Standard Error at Specified Altitude (m)					
Model Description	Parameter	7.5	10	15	20	25	30
	T1						
0.1 FY Ice	0.1	0.0101	0.0105	0.0183	0.0485	0.1152	0.2369
1 m FY ice	1	0.0101	0.0103	0.0153	0.0381	0.0904	0.1865
2 m FY Ice	2	0.0101	0.0101	0.0112	0.0222	0.0545	0.1176
2 m MY Ice	2	0.0101	0.0101	0.0101	0.0126	0.0276	0.0629
	Sig1						
0.1 FY Ice	0.02	0.0053	0.0152	0.0722	0.2227	0.5372	1.1058
1 m FY ice	0.02	0.0000	0.0001	0.0005	0.0015	0.0036	0.0072
2 m FY Ice	0.02	0.0000	0.0000	0.0001	0.0003	0.0007	0.0014
2 m MY Ice	0.001	0.0000	0.0000	0.0000	0.0000	0.0000	0.0001
	Sig2						
0.1 FY Ice	2.5	0.0049	0.0154	0.0781	0.2481	0.6080	1.2637
1 m FY ice	2.5	0.0031	0.0103	0.0523	0.1643	0.3987	0.8223
2 m FY Ice	2.5	0.0028	0.0093	0.0460	0.1413	0.3372	0.6871
2 m MY Ice	2.5	0.0015	0.0062	0.0339	0.1074	0.2604	0.5354

When two parameters, T1 and Sig1, are allowed to vary, with Sig2 fixed at 2.5 S/m, as shown in Table 8.2.3 below, noise in the free parameters drops significantly relative to the three-parameter case, owing to a reduction in parameter equivalence. This effect is particularly noticeable in the ice thickness.

This case is emphasised because it represents the normal set of free parameters for post-processing. Except under exceptional circumstances, the water conductivity is not allowed to vary because it is known *a priori* to be stable. Cases where this assumption may be invalid include estuarine conditions or situations where the ice cover is melting rapidly.

Table 8.2.3: Noise Budget for 7.5 to 30 m altitude: two free parameters

Model Description	Parameter		Standard Error at Specified Altitude (m) 7.5	10	15	20	25	30
	T1							
0.1 FY Ice		0.1	0.0101	0.0103	0.0140	0.0310	0.0708	0.1437
1 m FY ice		1	0.0100	0.0101	0.0112	0.0185	0.0394	0.0798
2 m FY Ice		2	0.0101	0.0102	0.0108	0.0122	0.0142	0.0162
2 m MY Ice		2	0.0101	0.0103	0.0117	0.0162	0.0254	0.0402
	Sig1							
0.1 FY Ice		0.1	0.0039	0.0107	0.0483	0.1458	0.3473	0.7092
1 m FY ice		1	0.0000	0.0001	0.0004	0.0012	0.0027	0.0055
2 m FY Ice		2	0.0000	0.0000	0.0001	0.0003	0.0006	0.0012
2 m MY Ice		2	0.0000	0.0000	0.0000	0.0000	0.0000	0.0001

Table 8.2.4: Systematic parameter error *vs.* drift and altitude: two free parameters.

Systematic error in ice thickness

	Altitude (m)					
Drift (ppm)	7.5	10	15	20	25	30
0.2	0.00	0.00	0.00	0.00	0.00	0.00
2	0.00	0.00	0.00	0.00	0.00	0.02
5	0.00	0.00	0.00	0.00	0.02	0.08
10	0.00	0.00	0.00	0.01	0.08	0.03
20	0.00	0.00	0.00	0.05	0.08	-0.15

Systematic error in ice conductivity

	Altitude (m)					
Drift (ppm)	7.5	10	15	20	25	30
0.2	0.000	0.000	0.000	0.000	0.000	0.000
2	0.001	0.002	0.007	0.022	0.054	0.119
5	0.002	0.005	0.021	0.062	0.153	0.328
10	0.004	0.009	0.042	0.129	0.329	0.480
20	0.007	0.019	0.086	0.278	0.480	0.480

Chi-Squared Misfit Due to Drift

	Altitude (m)					
Drift (ppm)	7.5	10	15	20	25	30
0.2	0.2	0.2	0.2	0.2	0.2	0.2
2	0.8	0.8	0.9	1.0	1.0	1.0
5	5.0	5.2	5.6	5.9	6.2	6.7
10	19.9	20.8	22.5	24.2	26.6	58.6
20	79.8	83.7	91.9	102.4	229.3	632.9

Drift is an important source of systematic error, as shown in Table 8.2.4 above, which shows errors induced in each parameter of the Standard Model as a function of altitude and drift magnitude. As in the previous table, only two

parameters were left free during the inversion. Altitude varies across the columns as in the previous table, and the parameters are again grouped into ice thickness and ice conductivity. Drift errors in the EM ranging from 0.2 to 20 ppm are listed for each parameter group. This table shows the worst-case effects of drift on these parameters, as both inphase and quadrature components are assumed to drift equally.

Another way to look at drift effects is to plot drift error in the free parameters as a function of time and altitude. The "bounding" model developed earlier for EM drift, *i.e.*.

$$Drift = 10 \cdot \sqrt{t}$$

was used in the construction of the following figures.

In Figure 8.2.1 to Figure 8.2.4, the effect of the drift prediction scheme used in real-time inversion (discussed in Section 5.4) is shown for early and late intervals in the background measurement schedule. While T1 errors are below the 1 cm level at 20 m sensor altitude in both cases, Sig1 errors become significant.

The "runaway" character of EM drift error under the present real-time drift prediction strategy is illustrated by the steadily increasing level of drift error as time progresses in all cases. This rapidly increasing level of drift error, together with the design aim of keeping real-time ice thickness errors to the order of 1 cm or better where possible, defines the background measurement schedule.

The rate of increase of EM drift drops rapidly with time (proportional to $1/\sqrt{t}$), so that much longer background measurement intervals are possible towards the end of a given flight relative to the first few intervals.

Figure 8.2.5 to Figure 8.2.8 show the improvements obtained by post-processing the dataset. Lower EM drift errors translate into much lower parameter errors, particularly for ice conductivity. These examples illustrate the importance of post-processing for minimisation of bias in ice conductivity.

Since during post-processing the EM drift errors at both the start and end of each interval are known, it is possible to achieve nearly zero drift errors at each end of the interval. This behaviour is clearly illustrated by these figures, where drift errors are essentially zero at the start and end of the measurement interval, peaking near the middle of the interval.

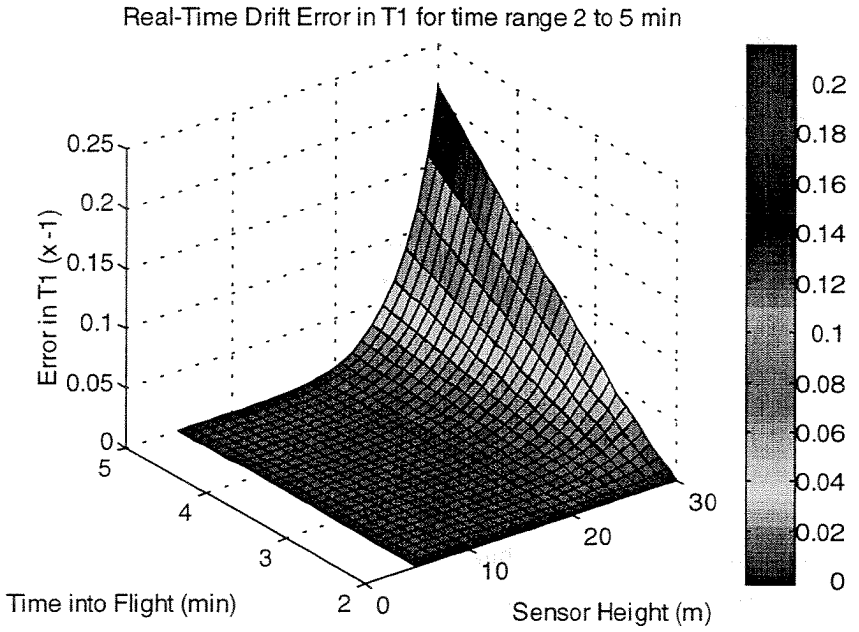

Figure 8.2.1: Drift-induced error in real-time ice thickness vs. time and sensor height.

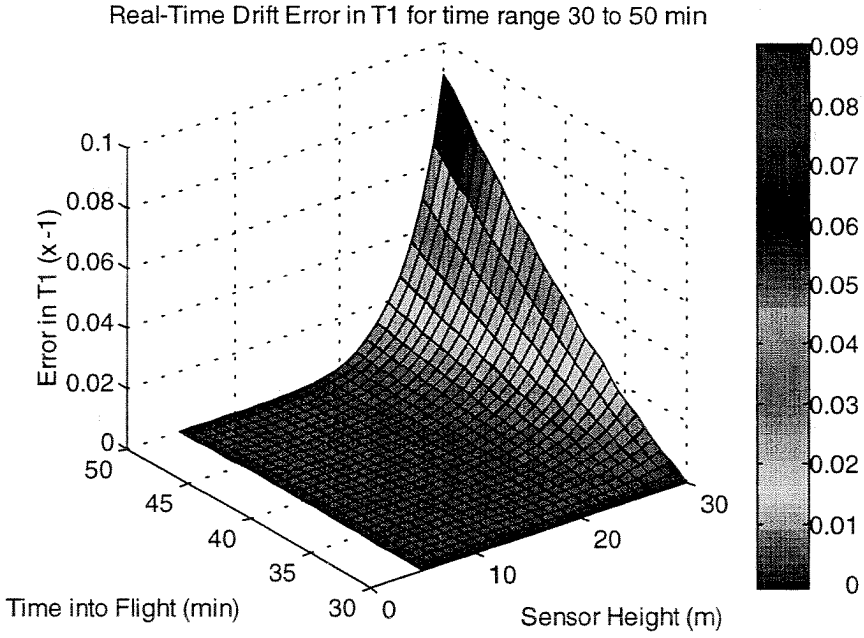

Figure 8.2.2: Drift-induced error in real-time ice thickness later in background schedule.

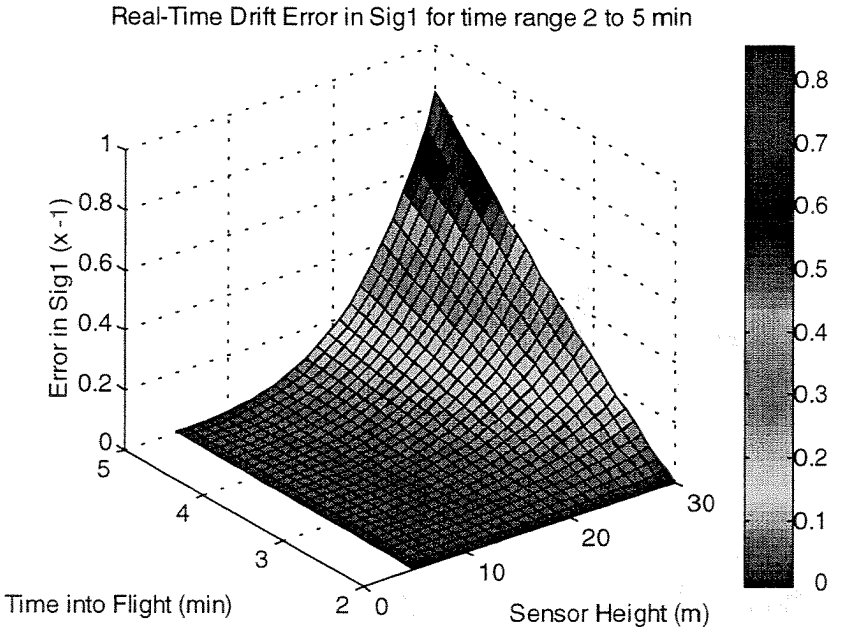

Figure 8.2.3: Drift-induced error in real-time ice conductivity vs. time and sensor height near start of background schedule.

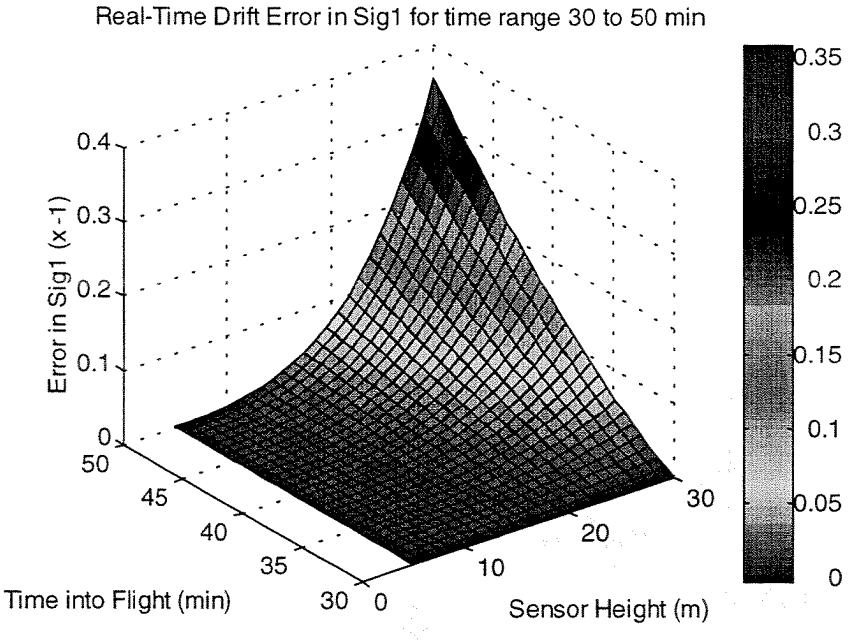

Figure 8.2.4: Drift-induced error in real-time ice conductivity later in background schedule.

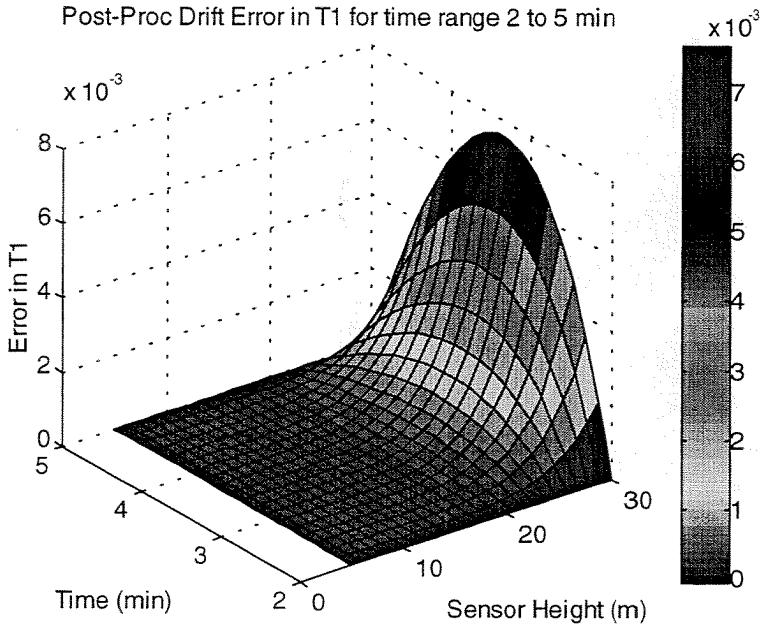

Figure 8.2.5: Drift-induced errors in post-processing ice thickness estimates early in background schedule.

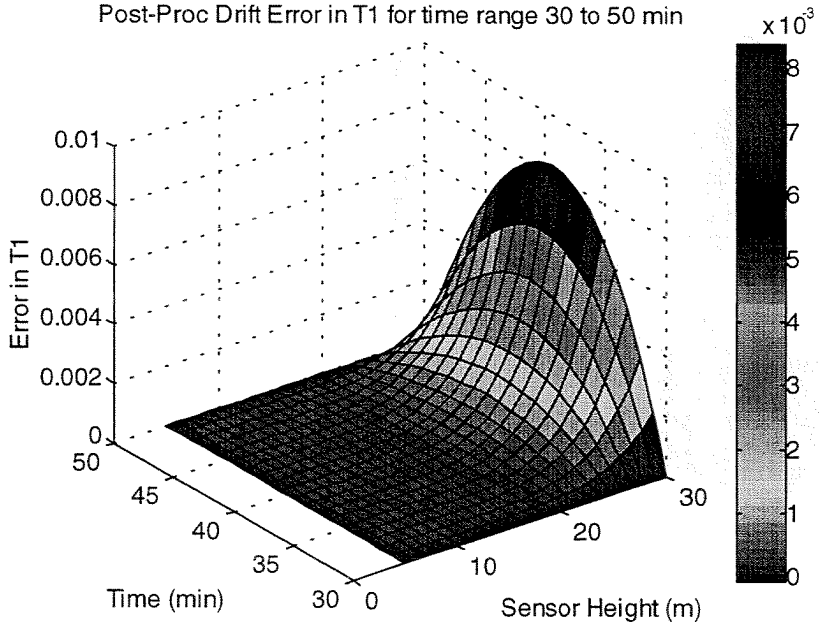

Figure 8.2.6: Drift-induced errors in post-processed ice thickness late in the background schedule.

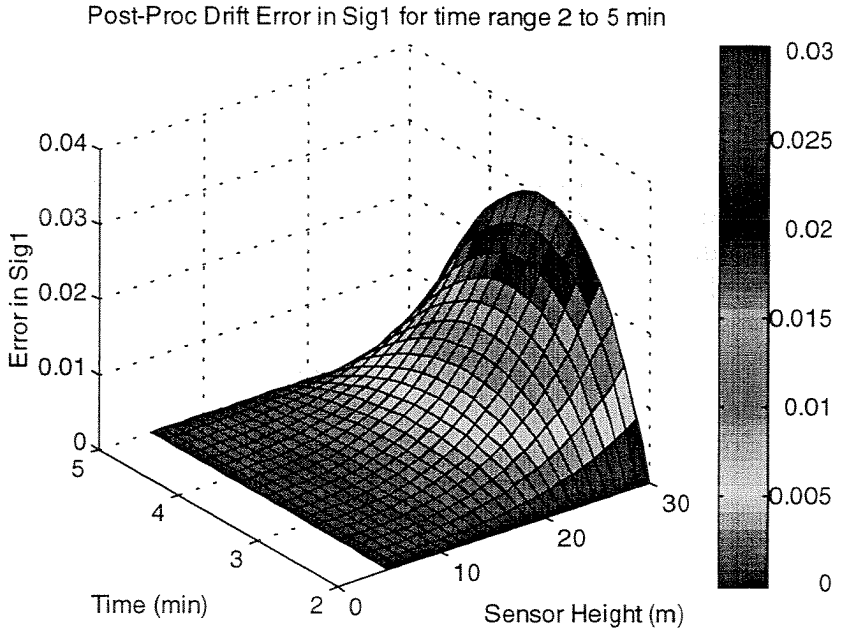

Figure 8.2.7: Drift-induced errors in post-processed ice conductivity early in the background schedule.

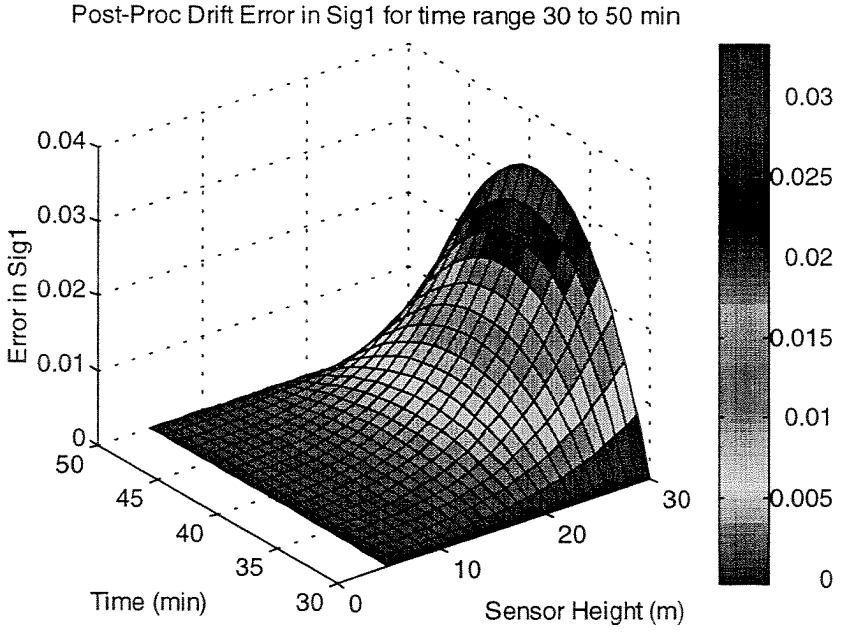

Figure 8.2.8: Drift-induced errors in post-processed ice conductivity late in the background schedule.

9 Field Examples of Calibration

9.1 Case 1: Conventional Calibration

The first example to be examined is for a conventional calibration over a marked line on ice in Hillsborough Bay during the 1997-98 ice season, and has been excerpted from the 1998 data report (Holladay and Prinsenberg, 1998). This calibration was prepared on February 22 using data from FLT004, line 20. The surface measurements used for the calculation are summarised in Table 9.1.1. There was no snow present on the ice (it had melted during a thaw) so that only ice thicknesses are provided.

Table 9.1.1: Surface measurements for Hillsborough Bay calibration line

Distance	Site #	Thickness	Distance	Site #	Thickness
0	1*	36	100	21*	36
5	2	36	105	22	38
10	3	37	110	23	40
15	4	37	115	24	36
20	5*	38	120	25*	36
25	6	35	125	26	39
30	7	37	130	27	36
35	8	38	135	28	36
40	9*	37	140	29*	37
45	10	39	145	30	38
50	11	35	150	31	39
55	12	36	155	32	38
60	13*	38	160	33*	36
65	14	36	165	34	39
70	15	38	170	35	36
75	16	40	175	36	39
80	17*	35	180	37*	38
85	18	35	185	38	38
90	19	37	190	39	38
95	20	35	195	40	38
			200	41**	40

* indicates a marker bag placed at the site

The calibration coefficients for the 30, 90 and 150 kHz operating frequencies as obtained in the field were:

Old calibration factors (in the bird, set up during the previous calibration in 1997):

(+1.0315 0.0194),(0.9806 0.3300),(1.3076 0.5778)

New calibration factors computed on Feb. 22, 1998 from FLT004, Line 20:

(+0.9953 0.0034),(0.9560 0.3104) (1.2994 0.5733)

Ratios (new/old):

(0.9646 - 0.0148i), (0.9714 - 0.0104i), (0.9935 - 0.0006i)

The above field calibration was checked after reprocessing of the dataset on two passes from this flight, lines 20 and 50:

The mean and SD of the incremental calibration factors computed for Line 020 were

(0.99546, -0.00071) (0.99787, -0.00167) (1.00206, 0.00069)

(0.00115, 0.00014) (0.00109, 0.00038) (0.00123, 0.00037)

These incremental changes are consistent with those generated in the field (a perfect match would consist of (1.0, 0.0) for each frequency). These values differ in amplitude by less than 0.5% from the field calibration in all cases.

As a consistency check, the mean and SD of Incremental Calibration Factors computed for Line 050 are:

(0.99969, 0.00192) (0.99318, 0.00807) (0.98146, -0.00425)

(0.00066, 0.00007) (0.00066, 0.00025) (0.00088, 0.00028)

Again, these results match the field calibration very well, to within 0.1% at 30 kHz, .7% for 90 kHz, and 1.9% at 150 kHz.

These two sets of incremental factors match well (to better than 0.5% in amplitude) between Line 20 and Line 50 at 30 and 90 kHz but differ at the 2% level at 150 kHz. The reasons for the differences are not known, but are consistent with typical noise levels for the three frequencies. The results from the first pass will be used for later comparisons. To put these differences into perspective, at 15 m altitude over 1 m ice, an difference of 1% in the amplitude of the calibration factors at both frequencies being used for inversion (30 and 90 kH) corresponds to a difference of about 5.2 cm in snow plus ice thickness and 2.6 mS/m in ice conductivity. The 0.5% differences observed in this case yields a systematic difference of about 2.6 cm in ice thickness and 1.3 mS/m in ice conductivity. These differences are on the same order as errors in surface measurements and laser altitude.

Combining the pre-98 calibration factors with the observed incremental factors yielded the following mean bird calibration factors:

(0.99157, 0.00383) (0.95579, 0.30762) (1.30359, 0.57886)

The differences between the factors determined in post-processing and those prepared manually on February 22 and used for subsequent real-time acquisition are approximately 0.4% 0.2% and 0.2% in amplitude for the three frequencies. As a further check, tests were performed to evaluate the differences in inverted data corrected with these two calibrations. The differences were found to be negligible, as expected.

This analysis indicated that it was not necessary to recalibrate FLT010-086 before re-inversion for the 1998 Data Report. FLT004-007 were recalibrated using the field-generated incremental factors

(0.9646 - 0.0148i), (0.9714 - 0.0104i), (0.9935 - 0.0006i)

The above field calibration was checked after reprocessing of the dataset on two passes from this flight, lines 20 and 50:

The mean and SD of the incremental calibration factors computed for Line 020 were

(0.99546, -0.00071) (0.99787, -0.00167) (1.00206, 0.00069)

(0.00115, 0.00014) (0.00109, 0.00038) (0.00123, 0.00037)

These incremental changes are consistent with those generated in the field (a perfect match would consist of (1.0, 0.0) for each frequency). These values differ in amplitude by less than 0.5% from the field calibration in all cases.

As a consistency check, the mean and SD of Incremental Calibration Factors computed for Line 050 are:

(0.99969, 0.00192) (0.99318, 0.00807) (0.98146, -0.00425)

(0.00066, 0.00007) (0.00066, 0.00025) (0.00088, 0.00028)

Again, these results match the field calibration very well, to within 0.1% at 30 kHz, .7% for 90 kHz, and 1.9% at 150 kHz.

These two sets of incremental factors match well (to better than 0.5% in amplitude) between Line 20 and Line 50 at 30 and 90 kHz but differ at the 2% level at 150 kHz. The reasons for the differences are not known, but are consistent with typical noise levels for the three frequencies. The results from the first pass will be used for later comparisons. To put these differences into perspective, at 15 m altitude over 1 m ice, an difference of 1% in the amplitude of the calibration factors at both frequencies being used for inversion (30 and 90 kH) corresponds to a difference of about 5.2 cm in snow plus ice thickness and 2.6 mS/m in ice conductivity. The 0.5% differences observed in this case yields a systematic difference of about 2.6 cm in ice thickness and 1.3 mS/m in ice conductivity. These differences are on the same order as errors in surface measurements and laser altitude.

Combining the pre-98 calibration factors with the observed incremental factors yielded the following mean bird calibration factors:

(0.99157, 0.00383) (0.95579, 0.30762) (1.30359, 0.57886)

The differences between the factors determined in post-processing and those prepared manually on February 22 and used for subsequent real-time acquisition are approximately 0.4% 0.2% and 0.2% in amplitude for the three frequencies. As a further check, tests were performed to evaluate the differences in inverted data corrected with these two calibrations. The differences were found to be negligible, as expected.

This analysis indicated that it was not necessary to recalibrate FLT010-086 before re-inversion for the 1998 Data Report. FLT004-007 were recalibrated using the field-generated incremental factors

(0.9646 -0.0148), (0.9714 -0.0104), (0.9935 -0.0006)

for the 30, 90 and 150 kHz data to make them consistent with the rest of the dataset.

Figure 9.1.1 and Figure 9.1.2 below show the EIS result on which the February 22 calibration was based (Line 20) and a subsequent pass (Line 50). Laser altimeter spikes are present near –100 and +230 m during the second pass, generated by specular reflection of the laser beam from the surface of small melt pools on the ice and the consequent loss of reflected signal. These artefacts were left in to illustrate the large amplitude of the laser spikes, which were eliminated in real-time data by a bird software change on March 18. Spikes were removed during post-processing from data files gathered prior to this date.

The correspondence between the mean airborne and surface measurements was good, to within 2.5 cm for both passes. Registration to the surface measurement line was accomplished through manual "fiducial" marks placed on the system's hardcopy chart output during data acquisition. This procedure is not as precise as registration from video imagery, but over flat ice surfaces it is the best approach available, in the absence of differentially corrected GPS positions.

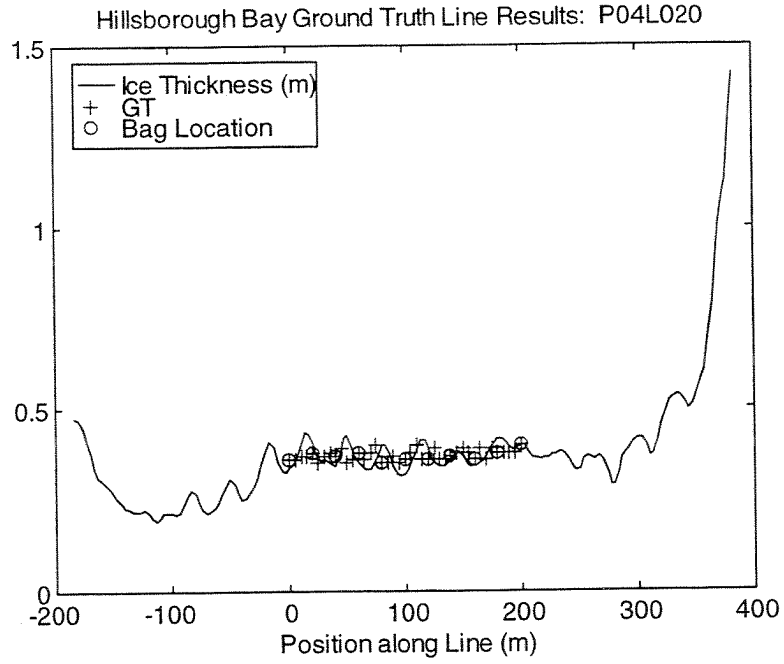

Figure 9.1.1: EIS-observed ice thickness over 1998 Hillsborough Bay calibration line. Surface measurements are presented as crosses. Circles mark bag locations or other known features.

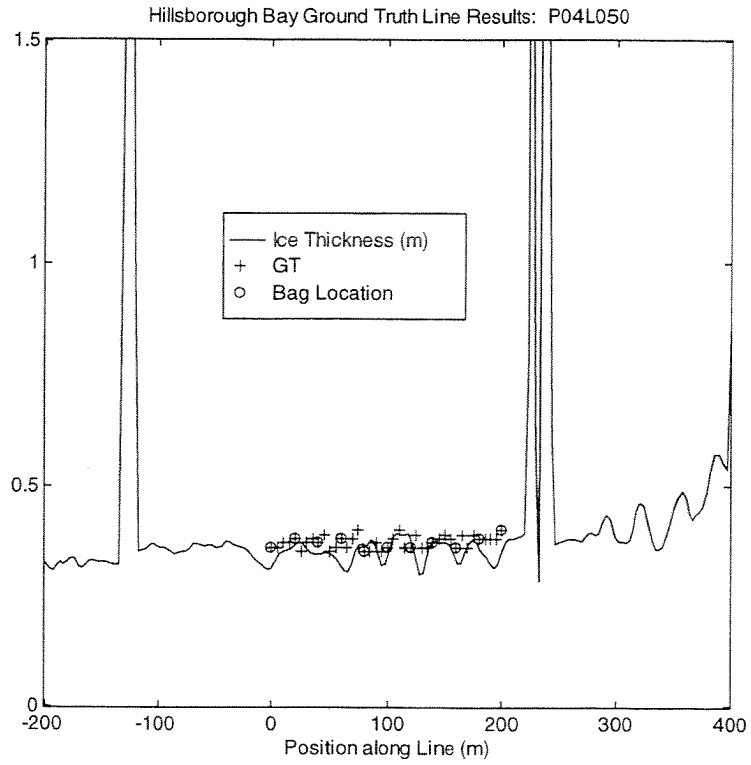

Figure 9.1.2: A subsequent pass over the 1998 calibration line. Surface measurements are presented as crosses. Circles mark bag locations or other known features. Spikes near the –100 and 230 metre positions are due to laser altimeter effects.

9.2 Case 2: Open-Water Calibration

Another system calibration test was performed using four patches of open water encountered during FLT074, after the laser spike rejection software had been installed in the bird. This yielded the following set of incremental calibration factors (relative to FLT004 Line 20 calibration):

A	(0.99433, -0.00254)	(0.98211, 0.00683)	(0.96753, -0.00413)
B	(1.00285, 0.00098)	(0.98974, 0.00731)	(0.97507, -0.00527)
C	(1.00116, -0.00067)	(0.98818, 0.00700)	(0.97678, -0.00557)
D	(0.99765, -0.00017)	(0.98359, 0.00833)	(0.97369, -0.00480)

Differences from FLT004, L20 were:

A (	0.0019	+0.0030i)	(0.0169	-0.0094i)	(0.0366	+0.0064i)
B (	-0.0066	-0.0005i)	(0.0092	-0.0099i)	(0.0291	+0.0076i)
C (	-0.0049	+0.0011i)	(0.0108	-0.0095i)	(0.0274	+0.0079i)
D (	-0.0014	+0.0006i)	(0.0154	-0.0109i)	(0.0305	+0.0071i)

These differences had percentage means and SD's (in amplitude) of

mean	(-0.28 +0.10i)	(1.31 -0.99i)	(3.09 +0.73i)
SD	0.41	.037	0.41

which are considerably larger than the differences between the L20 and L50 factors on the Hillsborough Bay calibration line, as well as the difference between the February 22 field calibration and the PCCalQW calibration, both of which were based on FLT004, Line 20. These differences are also systematic, with the real components varying linearly with frequency (see Figure 9.2.1.)

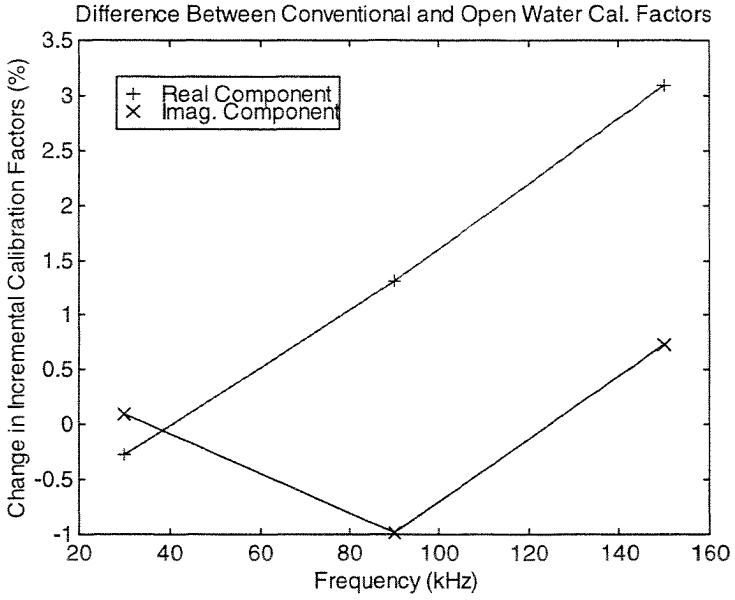

Figure 9.2.1: Plot of differences in real and imaginary parts of calibration factors between conventional and open-water calibration. The real part varies linearly with frequency.

It is possible that these open-water calibration factors are superior in systematic accuracy to those obtained over marked lines, despite their higher noise levels, as suggested in the Calibration Error Budget section above. To investigate this possibility, the mean factors derived from the above, *i.e.*

mean	(0.9990, .0006)	(.9859, .00737)	(.9733, -.00494)
SD	(0.0038, .0015)	(.0036, .00067)	(.0040, .00063)

were applied to several datasets, including the data for the lines used above to check the field calibration factors and the relevant flight lines re-inverted. The results are given in the next few figures.

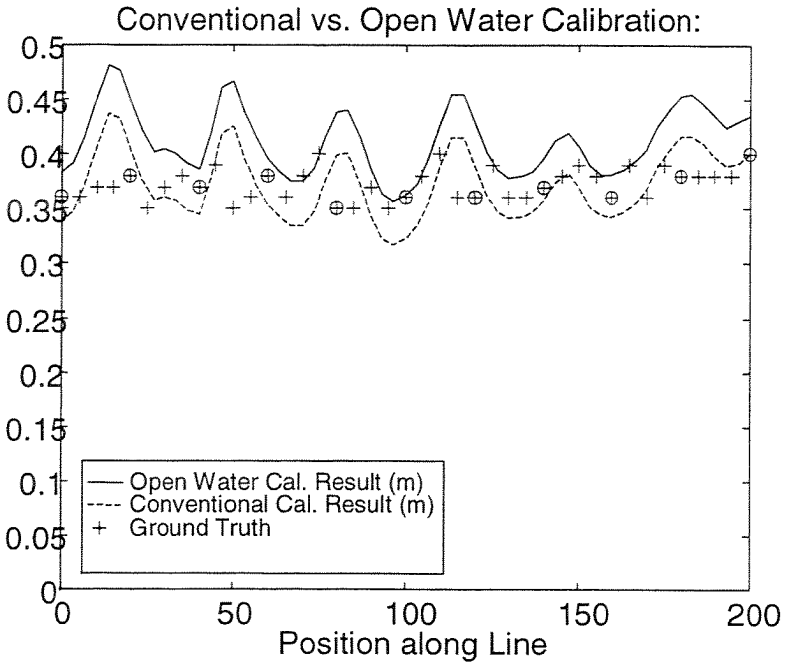

Figure 9.2.2: Snow plus ice thickness along the 1998 Hillsborough Bay, PEI calibration line, estimated using conventional (lower trace) and open-water calibration factors (upper trace).

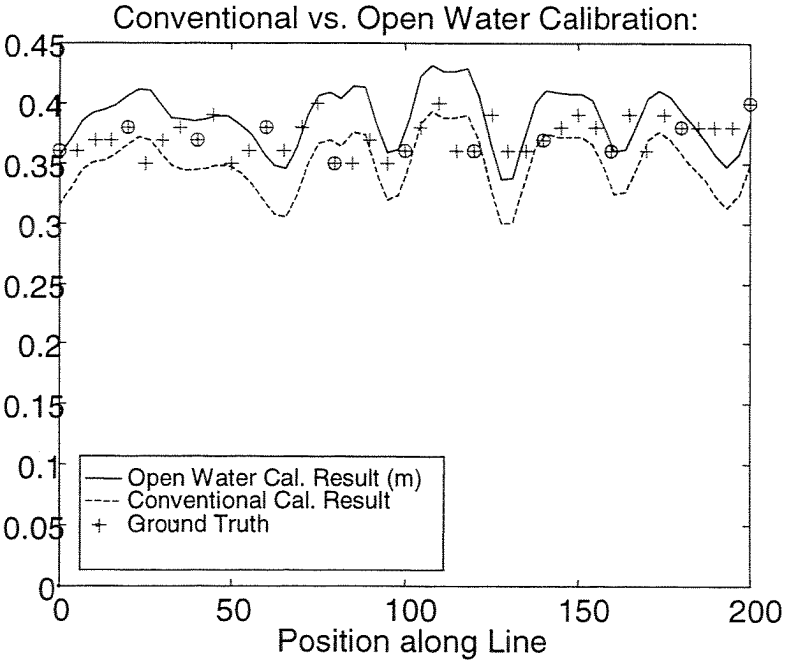

Figure 9.2.3: A later pass along the 1998 calibration line. The open-water factors (upper trace) in this case yield a better fit to the surface measurements than do the conventional factors.

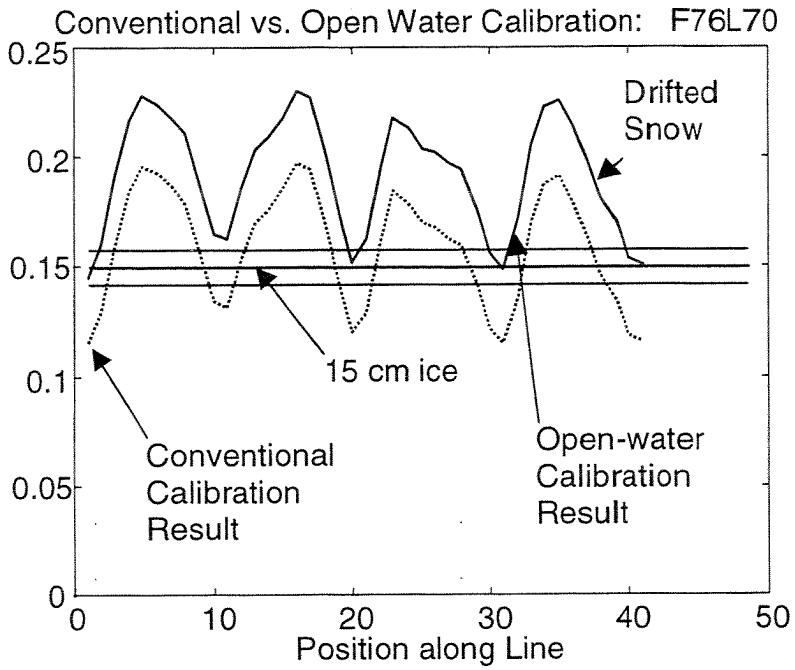

Figure 9.2.4: Open-water and conventionally-calibrated results over thin (15 cm ice plus drifted snow) at north end of 1998 Egmont Bay marked floe. Thin lines above and below the 15 cm level represent the 1 cm uncertainty in ground-truth measurement.

Figure 9.2.4 is notable in that the refrozen lead ice profiled by the system was known from surface measurements to be very uniform in thickness at 0.15 m, overlain by narrow snow drifts of maximum depth 10 cm. The EIS results reproduce the amplitude of the snow drifts remarkably well, and the thicknesses minima obtained with the OWC mostly fall within the ±1 cm uncertainty of the 15 cm ice thickness measurement. The CC results have a mean value of 15.9 cm, and the minima all fall below the 15 cm minimum thickness observed at this site.

To summarise, the comparison for F4L20 indicates precise agreement between the Conventional calibration (CC) method and the surface measurements, as expected. The Open-water calibration (OWC) method yields results which are slightly greater in thickness: in F4L50 and F76L70, the OWC approach yields estimated snow plus ice thicknesses which agree more closely with surface measurements than do the CC results. The fitting error is larger for OWC than CC results in the first two examples, but smaller in the F76L70 case. Ice conductivities are not very well determined in any of these examples, due to the modest ice thickness. The results of the OWC-CC comparison are listed in Table 9.2.1 below.

Table 9.2.1: Comparison of Conventional and Open-Water calibration results.

Measurement Type (cm or mS/m, as appropriate)	F4L20	F4L50	F76L70
Ground Truth			
Ice Thickness	37.2 +/- 1.5	37.2 +/- 1.5	15 +/- 1
Snow Thickness	0	0	0 - 10 cm drifts
Conductivity	20 (assumed)	20 (assumed)	20 (assumed)
Conventional Calibration			
Snow plus ice Thickness	37.2 +/- 3	34.9 +/- 2.4	15.9 +/- 2.6
Average Conductivity	1	1	1
Chi-Squared value for fit	9.5	166	840
Open-Water Calibration			
Snow plus ice Thickness	41.2 +/- 3.7	38.8 +/- 2.4	19.2 +/- 2.6
Average Conductivity	1	1	17
Chi-Squared value for fit	1608	398	104

10 Operational Examples

10.1 Case 1: 1996 Labrador Validation Line

EIS profiles over the CART1 surface measurement line set up during the 1996 Labrador field work (Moucha *et al*, 1998) highlight a number of the complexities which occur over deformed ice, including footprint averaging and 2D effects. Rafting and the effects of entrained seawater may also be an issue in this case.

The EIS system used ground truth calibration factors from the final calibration from the 1995 Resolute field project, set up at the end of that field work based on high-quality data obtained over smooth, flat ice. The system's calibration appeared to have been extremely stable, with no change necessary for the Labrador field program.

The CART1 surface measurement line was the first to be flown during the 1996 field work. It was located northwest of Huntingdon Island in deep water. The line was profiled with EIS on March 10 and 11. The surface measurements were made on March 10 during the airborne data acquisition.

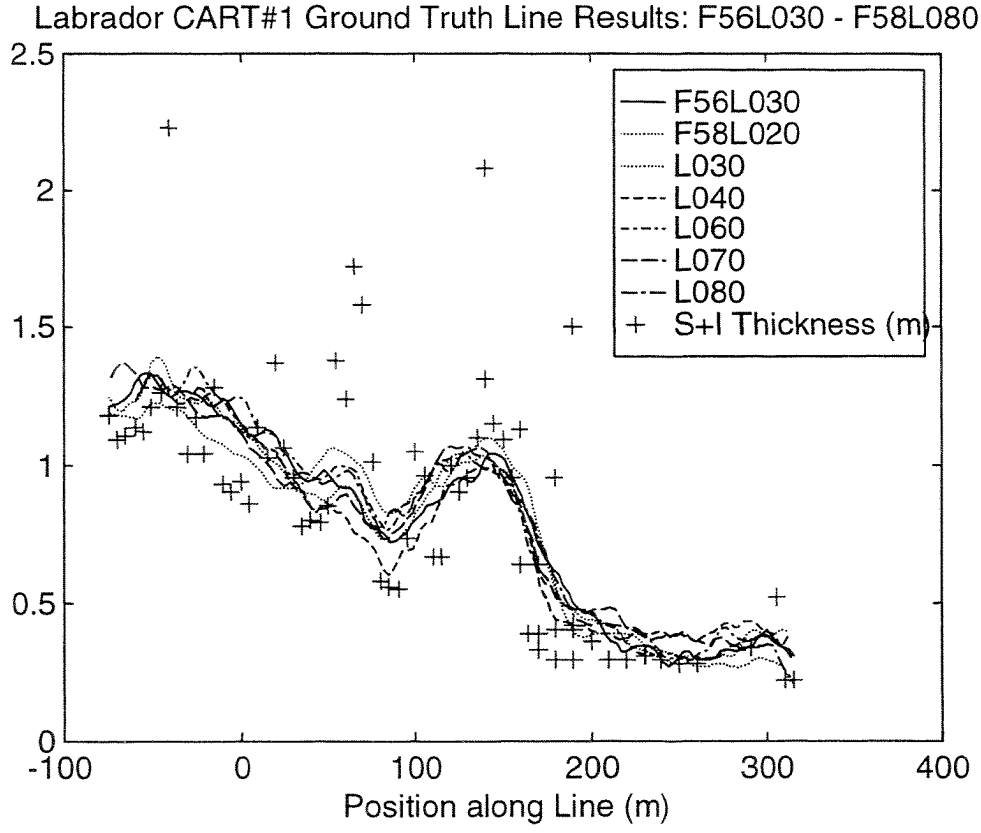

Figure 10.1.1: Surface measurements on CART1 line with EIS snow plus ice thickness results.

The EIS results, as expected, smooth out short-wavelength variations in snow plus ice thickness such as the ridges near 60 and 140 m. These variations are associated with the edge of the landfast ice, which appears to have been deformed by the storm activity that broke up much of the landfast ice in the area. However, ice features which are broader than the EIS footprint of approximately 30 m are reflected in the EIS results, which are highly repeatable from pass to pass. The system's footprint effect is particularly visible at the steep margin near 160 m.

The passes were flown at 16.8 ± .9, 11.3 ± .6, 11.4 ± 1.2, 12.1 ± 1.6, 13.7 ± 1.2, 14.6 ± 1.4 and 13.5 ± 1.6 m (1σ). The average snow plus ice thickness along this line as estimated by surface measurements is 0.765 ± .433 (1σ), while the EIS averages ranged from 0.69 to 0.72 ± .7. The mean thickness for all passes was 0.784 m, with a standard deviation in the mean of .007, reflecting the extremely repeatable nature of the EIS profiles. The systematic difference of 0.019 m between the surface measurements and the EIS results is certainly acceptable, particularly in view of the complex ice structure along the line.

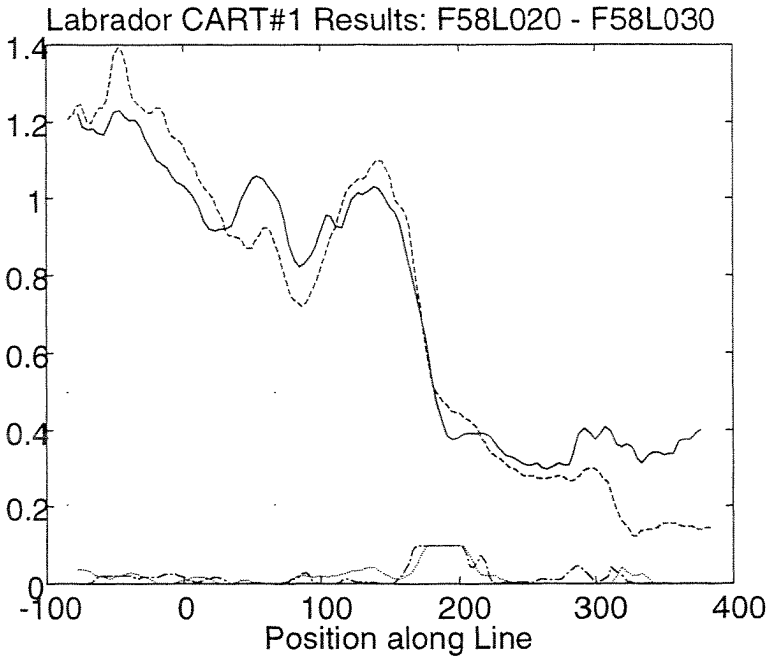

Figure 10.1.2: Estimated thickness and conductivity profiles for two selected passes over the CART1 line.

The estimated conductivity profiles for F58L020-030 are plotted at the bottom of Figure 10.1.2. They indicate enhancements in ice conductivity between 160 and 210 m along the line (reaching the 0.1 S/m limit in this case) and from about 280 to 320 m. The thick landfast ice to the left of the figure is estimated to be fairly resistive, ranging from about 0.01 to 0.03 S/m. Note that the enhanced conductivity near 200 m does not coincide with the full width of the ridged zone,

but rather spans the vicinity of the margin between thick, older ice and newly formed thin ice. The enhancement near 300 m is probably due to rafting effects.

The CART2 line (Figure 10.1.3) was located in the bay south of Huntingdon Island. It has morphology similar to CART1, likely arising from the same series of events that created the CART1 ice margin structure.

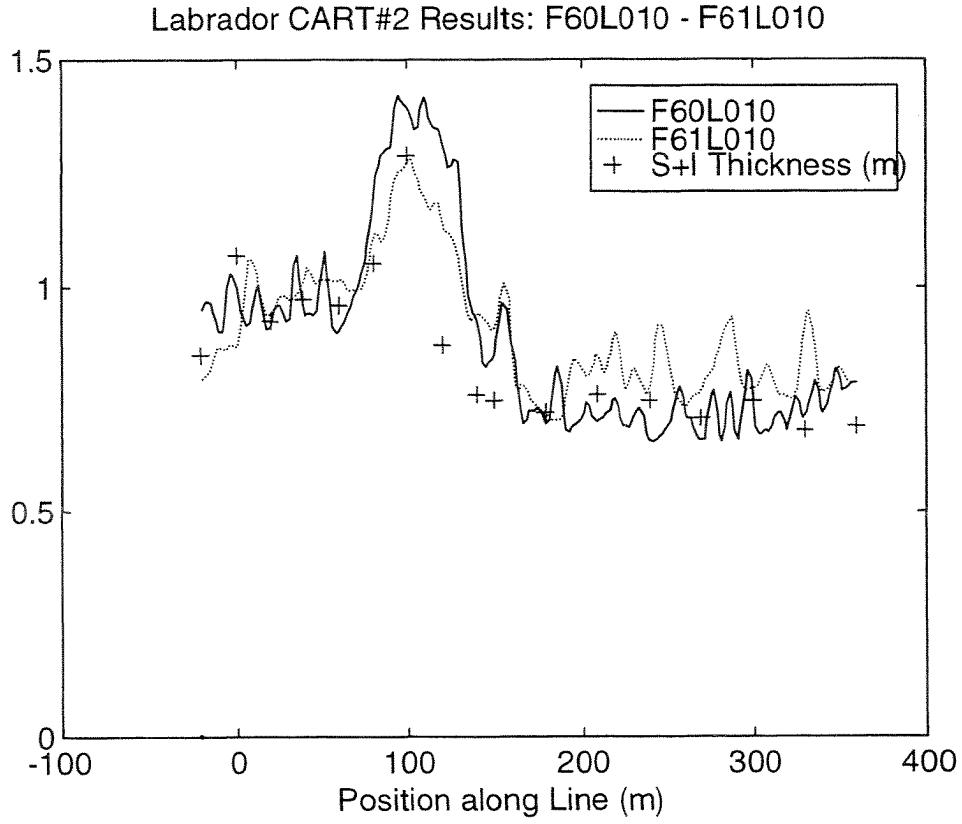

Figure 10.1.3: EIS profiles over CART2 surface measurement line.

The mean thicknesses for the two EIS profiles (flown at 15.4 ± .4 and 12.7 ± .7 m) over this line are 0.86 ± .21 and 0.90 ± .14 m, while the mean auger hole snow plus ice thickness estimate is 0.90 ± .17. The mean EIS thicknesses match the mean auger measurements to within 0.04 and 0.00 m, both of which are within system specifications.

The excess variability observed in the EIS results over the thinner portion of Figure 10.1.3 compared to that of the ground truth measurements appears to derive from a combination of aliasing of the ground truth measurements and snow drift effects. The section of ice in question was covered with a substantial snow layer, with drifts elongated along the flight line. Slight deviations of the bird's flight path from the surface measurement line (which was not marked or ground-truthed before the flight) could then have sampled substantially different

snow thicknesses between FLT060 and FLT061. The same effect may have been responsible for the change in the apparent ridge thickness near 100 m.

10.2 Case 2: 1998 Egmont Bay Validation Line

Multiple passes over a marked line set up on a drifting floe in the Northumberland Strait were obtained during the 1998 field program. This case includes a number of effects, including rafting confirmed by surface measurements and 2D features.

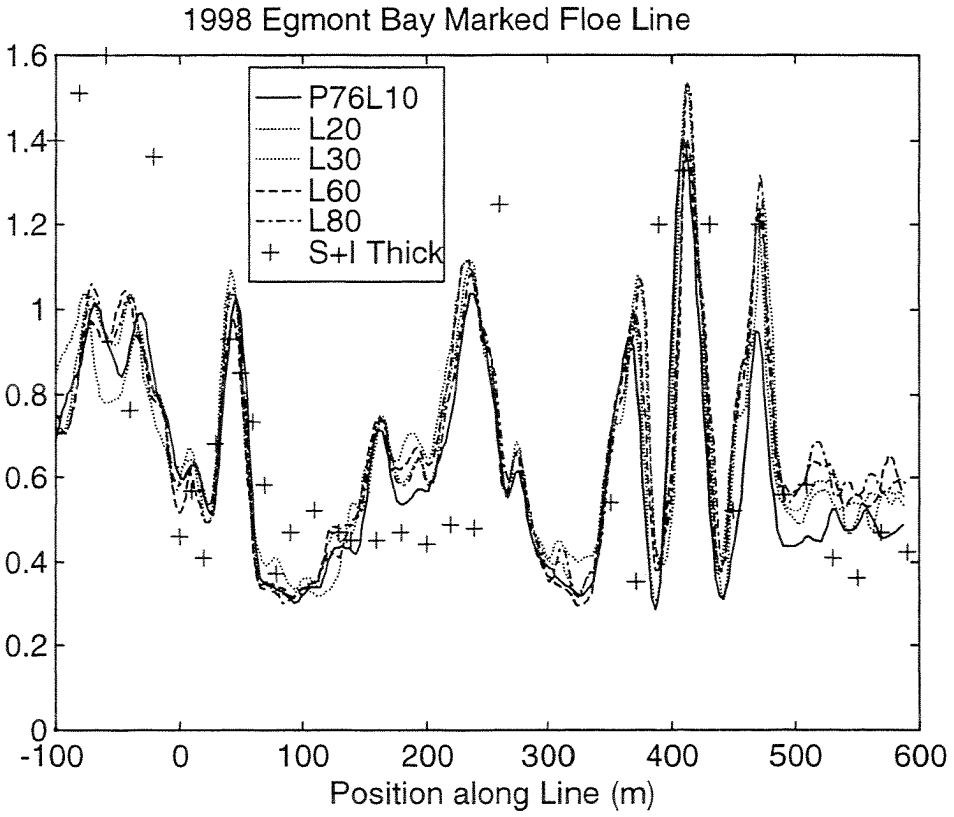

Figure 10.2.1: Composite of five airborne thickness profiles over the Egmont Bay floe line. Surface measurements are presented as crosses.

The conventional EIS calibration discussed in Section 9.1 above was used for this example, which is of particular interest in that it shows the strong coherency and repeatability of the airborne measurements over the complex floe structure. It also shows the degree of correspondence between surface and airborne measurements expected for such a structure. There do exist zones of disagreement between surface and airborne measurements, such as the section between –100 and –40 m along the line. It is likely that the feature responsible for this thickness disparity was a narrow ridge of total thickness 1.2-1.4 m, aligned with the survey line. This is supported by the small snow thickness observed at several of the auger sites and by the much lower average thickness

of the floe. A feature having this geometry would not have been accurately captured by the airborne measurements unless its width was greater than 10-30 m.

Another point of systematic difference between the airborne and ground measurements occurs near +200 m. The ground truth indicates a consistent 0.45 to 0.5 m snow plus ice thickness, while the airborne data suggests at least 10 cm greater thickness and considerably more variability. It is possible that a large rafted block exists beneath this section of the floe, perhaps just off-line which was not detected in the auger holes but which does increase the EM-estimated thickness. Rafted conditions were observed at several auger holes between 390 and 470.

The mean altitudes of the passes used in this figure were 12.7 ± 2.1, 10.3 ± .9, 10.6 ± 1.6, 10.8 ± .9, and 13.1 ± .6 m (1σ). The mean of the EIS-determined mean thicknesses for this line was 0.66 ± 0.02 m, with a mean standard deviation value for the five passes of 0.243 ± .005 m. The surface measurements averaged 0.75 ± .38 m. The 0.09 m disparity between the airborne and surface measurements is not surprising in light of the complex three-dimensional character of the floe and the known and inferred presence of substantial amounts of rafting. The excellent match between the EIS results and the auger-measured thickness of the thin refrozen lead north of this floe (see Figure 9.2.4) supports the assertion that possible errors in the system's calibration were not responsible for the majority at least of the disagreement of the airborne and surface measurements for this line.

Figure 10.2.2 shows a pair of somewhat longer profiles, which extend over the main line and out to the 15 cm floe off the north end of the marked floe. This figure, plotted versus sample number rather than position as in the previous figure, includes EIS-estimated ice conductivity profiles with the thickness profiles. The ice conductivity parameter was allowed to vary up to 0.5 S/m, rather than restricting it to 0.1 S/m as has been the convention for routine EIS processing.

Several zones of high bulk ice conductivity were observed, coincident with highly deformed sections of ice. The ice conductivity estimates display excellent coherence between the two passes, and are is clearly well-determined and stable, particularly above values of 0.1 S/m. It would appear that a range of ice conductivity values extending to even higher values could be allowed and would improve the overall degree of fit. A combination of ridging and rafting effects appear to be responsible for the high estimated conductivities: relatively flat, thin sections of ice display much lower conductivities, consistent with the conductivity estimate used for calibration of the system on the Hillsborough Bay lines discussed earlier.

Rafting is known to be present (through auger observations) at the sharp series of ridges associated with rafting at the 400 m point in the last figure and which appear between samples 140 and 200 on this figure. This zone is seen to be

associated with high ice conductivity estimates, as expected. This suggests that the preceding zone of high conductivities, centred on sample 100, may also be associated with rafting. Such an association was postulated based on the observation that EIS thickness estimates were considerably larger than surface snow plus ice thickness measurements between 150 and 250 m in Figure 10.2.2.

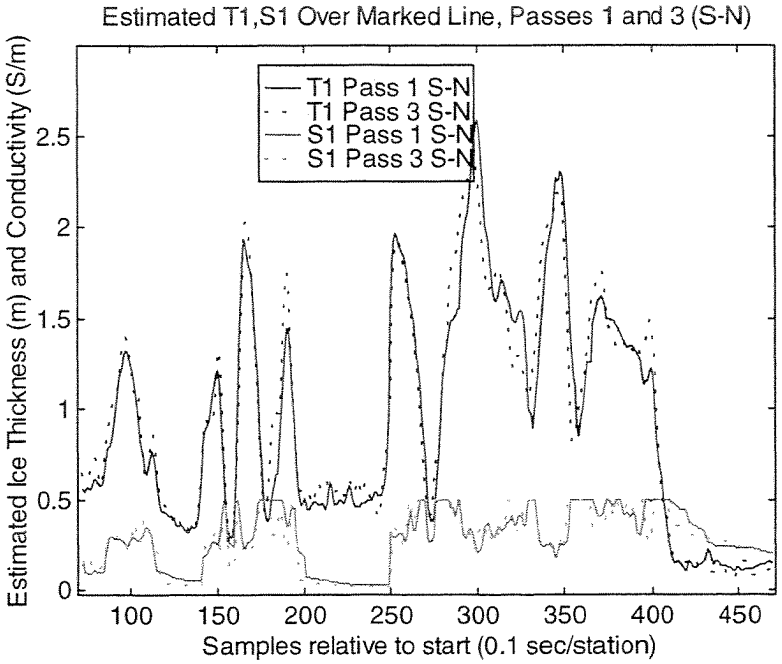

Figure 10.2.2: Estimated ice thickness and conductivity profiles for two passes over Egmont Bay floe, with extension to the north.

10.3 Case 3: 1995 First Year/Multi-Year Line ("Site A") near Resolute, NWT

This example comes from the Site A first-year/multi-year survey data acquired during the 1995 Resolute field program (Holladay *et al*, 1998), which was performed in conjunction with the SIMMS'95 experiment (Misurak *et al,* 1995). The calibration factors used to compute these ice properties from the EM data were prepared at the conclusion of the field program and applied during post-processing to the dataset, based on high-quality data obtained over smooth, flat ice.

Site A was a surface measurement line that crossed a margin between FY and MY ice at approximately right angles. The snow plus ice profile over the FY/MY margin is compared to the surface data collected on April 27th and 30th in Figure 10.3.1. This plot includes results from 21 airborne passes over the survey line, executed at altitudes of 15.2 ± 1.1, 17.5 ± .6, 14.9 ± 1.5, 15.7 ± .4, 12.1 ± .7, 12.6 ± .7, 11.3 ± .9, 15.3 ± 1, 15.9 ± 1.0, 14.5 ± .7, 12.2 ± .6, 14.1 ± 1.4, 12.5 ± .9, 10.2 ± .6, 11.3 ± 1.8, 12.1 ± 1.2, 19.3 ± .91, 20.8 ± .5, 16.4 ± .8, 13.3 ± .5, and

26.2 ± .8 (1σ, note the erratum in the Remarks column of p. A-5 of Holladay *et al*, 1998 for Line 900). The consistency of the thickness and conductivity results from pass to pass and between flights is striking. The short wavelength fluctuations in FY ice thickness are due to drifted snow which were profiled by the laser altimeter. The low degree of coherence of these short-wavelength features, relative to the high degree of consistency of large ice structures in these profiles, is ascribed to variations in flight path and the short scale length of the drifts. The high degree of accuracy expected for EIS-estimated ice thickness results is borne out by the consistency of these results and their close correspondence to the surface measurements. The mean of the mean thicknesses along each of the 21 profiles was 2.92 ± .03 m (1σ), while the mean and standard deviation of the standard deviations was 1.41 ± .03 m. The mean snow plus ice from surface measurements was 3.09 ± 2.65 m, or 3.07 ± 2.65 m using trapezoidal integration of the snow plus ice thickness data along the line. The difference between the mean airborne and surface measurements is thus 0.09 to 0.11 m.

While this difference is larger than for the preceding examples, it should be noted that virtually all of the difference arises from the multi-year portion of the line. The EIS and surface measurements along the first-year part of the line from 0-200 m are 1.92 ± .03 (mean and SD of means for 21 lines) *vs* 1.95 ± .13 m: these results thus match within one standard deviation of the EIS data. The EIS and surface measurements along the multi-year of the line from 260 to 480 m are 3.96 ± 0.07 m *vs* 4.20 ± .79 m. Note that the average standard deviation of the EIS results over the MY ice was 0.45 m, compared to 0.79 for the surface measurements. The 0.24 cm discrepancy between the EIS and surface measurement thicknesses observed over the over multi-year is ascribed to the high degree of lateral heterogeneity present in this ice, which was heavily ridged and hummocky, rather than to problems with EIS or surface measurement data quality. An exhaustive gridded surface measurement program of the sort described by Kovacs and Holladay (1989) would probably be required to fully control spatial aliasing effects in the surface measurement results and achieve a good match between the two datasets.

Figure 10.3.2 is a plot of the bulk ice conductivity estimated from the same 21 airborne EIS passes during post-processing of the data. The first-year ice to the left of the figure displays estimated ice conductivities lying for the most part within the 15 to 30 mS/m range, with a few profiles exhibiting greater variance. The multi-year ice at right displays a much lower average conductivity, clustered between 3 and 10 mS/m. The degree of scatter in the conductivity estimates is much greater than for ice thickness, as expected. Note that the estimated conductivities in the MY ice are lower for the hummocks at 350 and 450 m than for the melt pools near 300 and 400 m, also as expected.

The enhancement of ice conductivity visible at the FY-MY margin may be due to excess brine remaining trapped in the block structure despite exposure to the Arctic winter. A more likely possibility is that drifted snow, known to be present at

the margin, insulated the ice surface, increasing its average temperature sufficiently to enhance brine volumes within the ice and thus increase its conductivity.

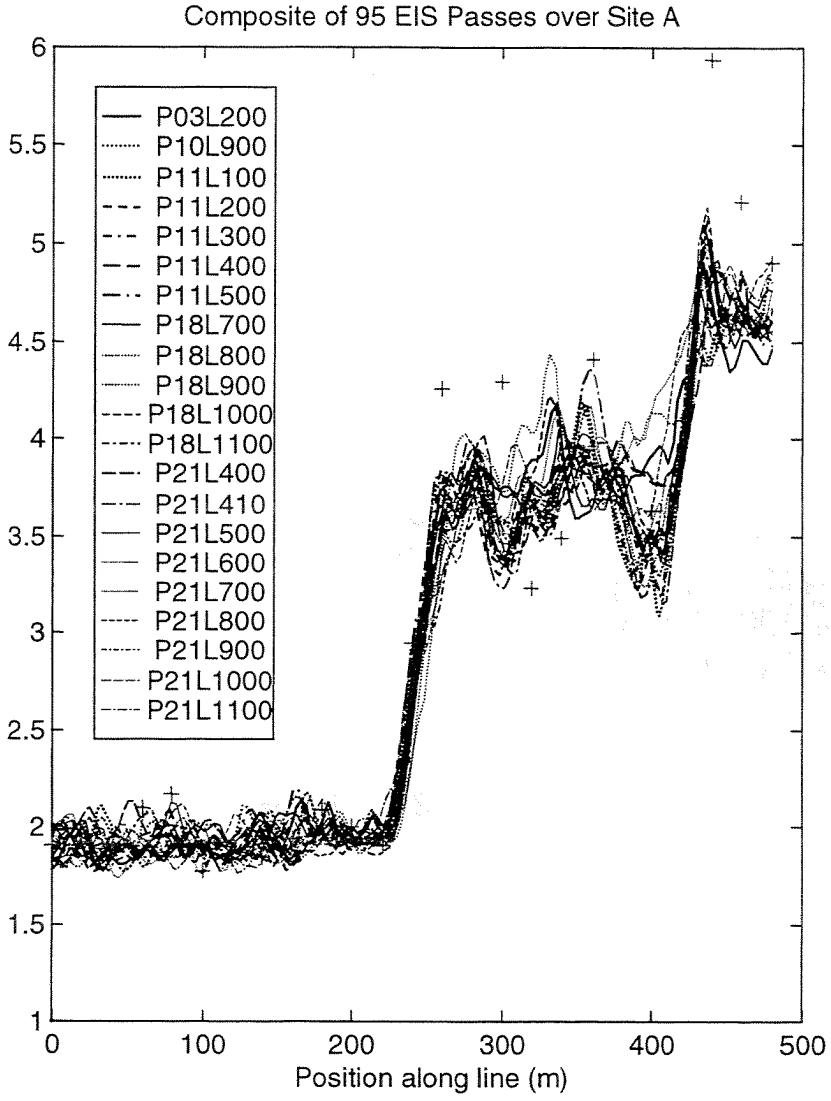

Figure 10.3.1: EIS results for multiple passes over Resolute Site A and snow plus ice thickness surface measurements (cross symbols) along profile.

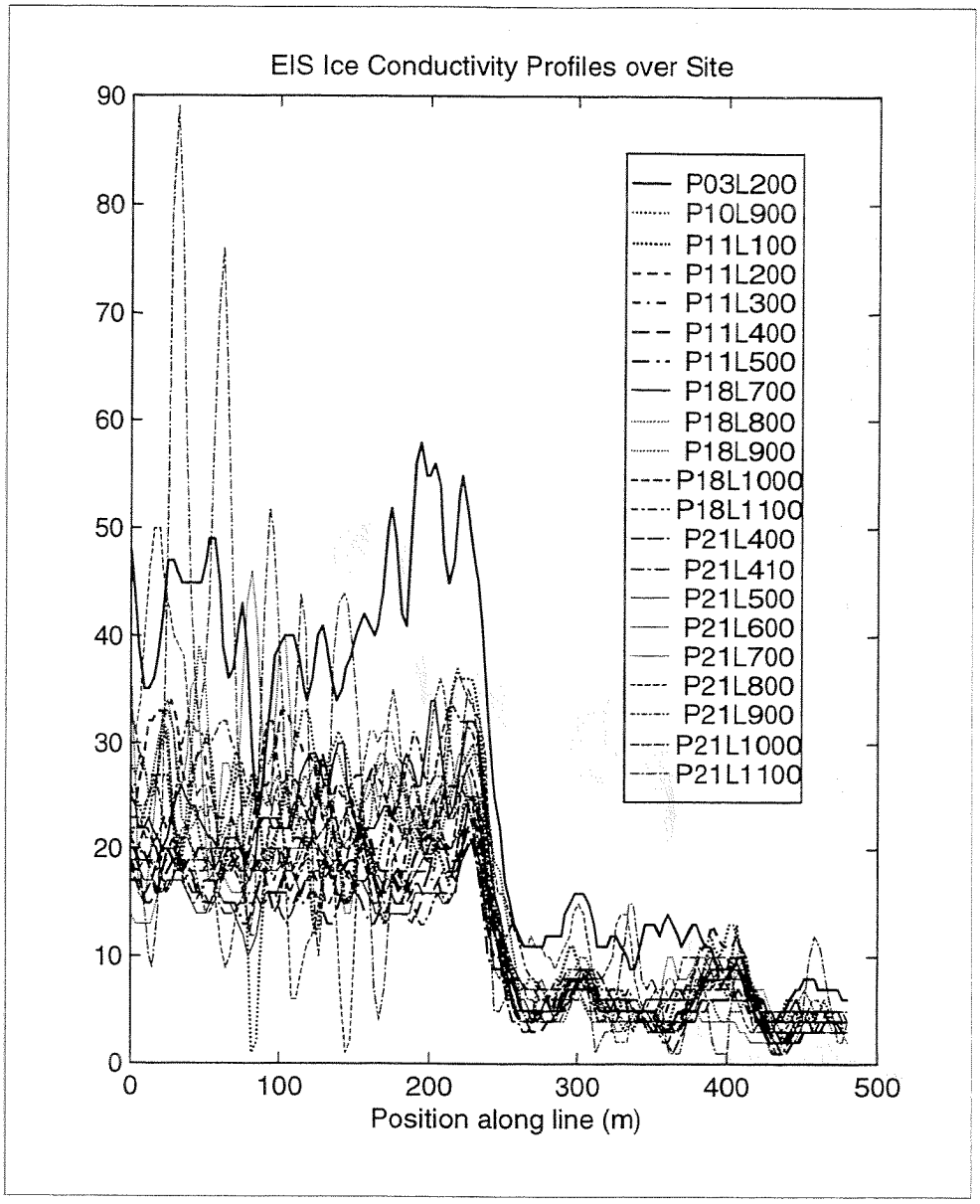

Figure 10.3.2: EIS-estimated ice conductivity profiles (mS/m), Resolute Site A.

11 Quality Index

11.1 Calculation of Quality Index

Assessment of EIS data by non-expert users has been complicated by the multiple factors that must be considered. For example, sensor altitude has a strong influence on the accuracy of EIS ice property estimate, as does the amount of EM drift present at the time of observation. Other factors that must be considered are the normalised inversion fitting error and the time rate of change of the sensor's pitch and roll.

A preliminary "quality index," for use in assessment of field data, has been constructed as indicated below, comprising a weighted sum of functions of the above factors. As drift is not directly measurable while the bird is at survey altitude, the real-time and post-processing drift models developed in Section 5.4 have been used as conservative estimates of drift.

$$Q = 10\left[1-\left\{\alpha\cdot\frac{|\Delta T|}{.01}+\beta\cdot\log_{10}\left(\frac{|\Delta S|}{.001}\right)+\kappa\cdot|\Delta PR|^2+\eta\cdot\frac{RMN}{.01}\right\}\right]$$

where

$$\Delta T = D\cdot(h/40)^{3.9}/5$$

$$\Delta S = D\cdot(h/41)^{8}/5$$

$$D_{PP} = 10\cdot\left[\left\{\sqrt{t}-\sqrt{t_{\min}}\right\}-\left\{\left(\sqrt{t_{\max}}-\sqrt{t_{\min}}\right)\cdot\frac{(t-t_{\min})}{(t_{\max}-t_{\min})}\right\}\right]$$

$$D_{RT} = 10\cdot\left[\left\{\sqrt{t}-\sqrt{t_{prev}}\right\}-\left\{\left(\sqrt{t_{\min}}-\sqrt{t_{prev}}\right)\cdot\frac{(t-t_{prev})}{(t_{\min}-t_{prev})}\right\}\right]$$

and where all times t_{xxx} are measured in minutes relative to the initial background measurement of the flight, weights α=0.1, β=0.3, κ=0.02, and η=0.08, and

t = time of quality index estimate,

t_{min} = time of background at beginning of current measurement interval,

t_{max} = time of background at end of current measurement interval,

t_{prev} = time of background measurement beginning previous interval,

ΔT = ice thickness error model with respect to sensor altitude and EM drift,

ΔS = ice conductivity error model with respect to sensor altitude and EM drift,

D = drift error model (one of the two below),

D_{RT} = conservative drift error model for real-time acquisition, and

D_{PP} = conservative drift error model for post-processing.

The value of the Quality index as defined above indicates performance as follows: a Q index of 10 corresponds to top-quality results, with expected errors of <1.5 cm and < .001 S/m, while Q=5 corresponds to "fair" results, with potentially poor conductivity estimates and errors in T1 of a few cm. At the low end of the scale, Q=1 indicates ice thickness errors ranging up into decimetres and ice conductivity being poorly determined. As such, the Q scale is non-linear in T1 and roughly logarithmic in conductivity. This definition of Q provides fine detail at the "good" end of the scale, rather than at the poor end.

11.2 Examples

The following figures show the quality factor Q as computed for the real-time and post-processed results of a survey line from 1998 FLT076, over Egmont Bay in the Northumberland Strait.

It should be noted that the real-time inversion used a fixed ice conductivity of 0.02 S/m, while the post-processed example below estimated both ice thickness and conductivity.

In rubbled and rafted sections of the floe, the real-time RMN error was large due to the fixed and incorrect ice conductivity, decreasing the Quality index value in those sections. The Quality index is much higher on average in the post-processed case due to this effect, although orientation and altitude effects diminish the index in the initial section before 12.7 minutes.

While the present formulation of the Quality index remains open to adjustment and improvement, the approach certainly simplifies discrimination between EIS data of poor, good and excellent quality, and thus constitutes a significant step forward.

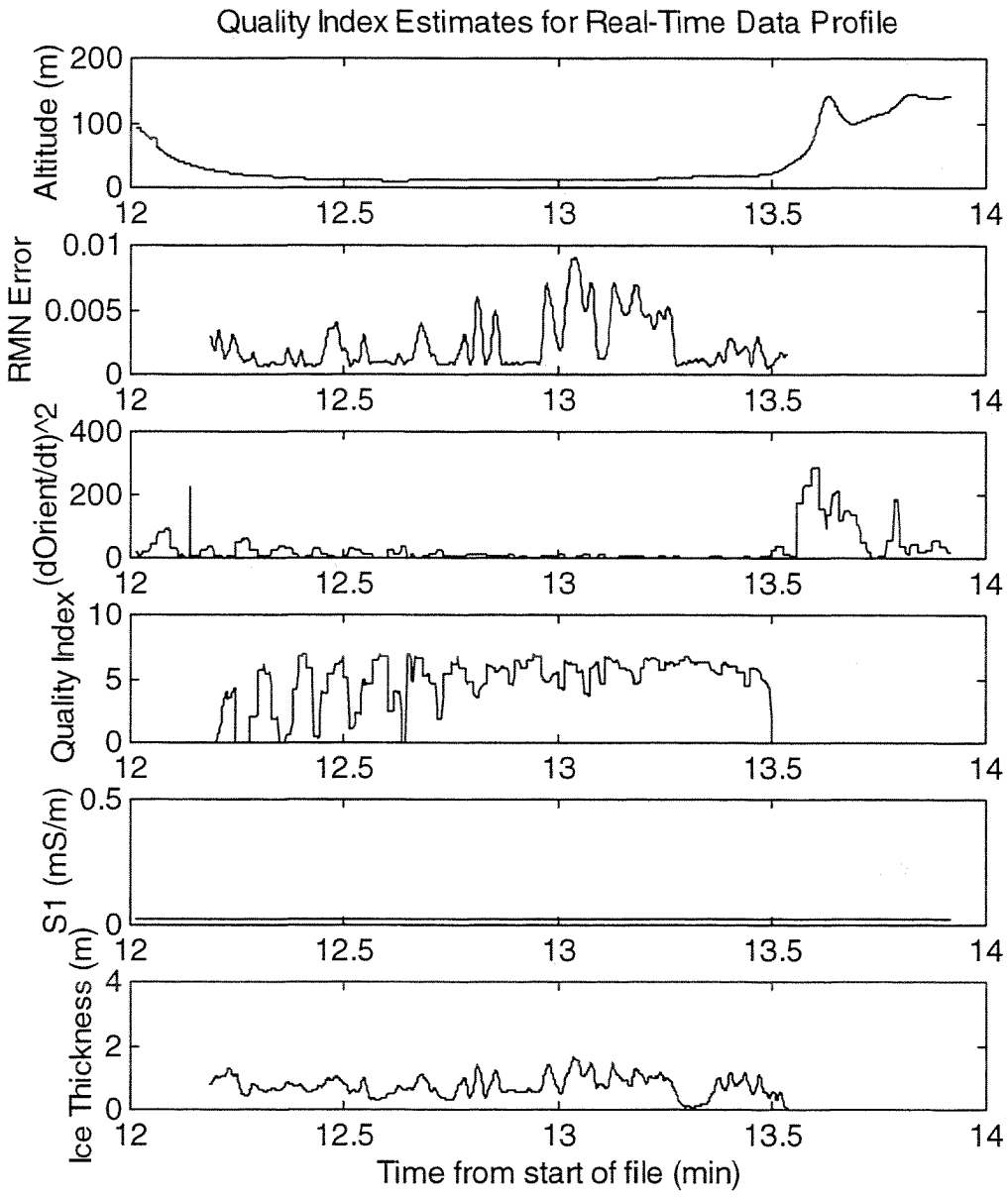

Figure 11.2.1: Quality index, with observed and computed parameters for test line after real-time processing.

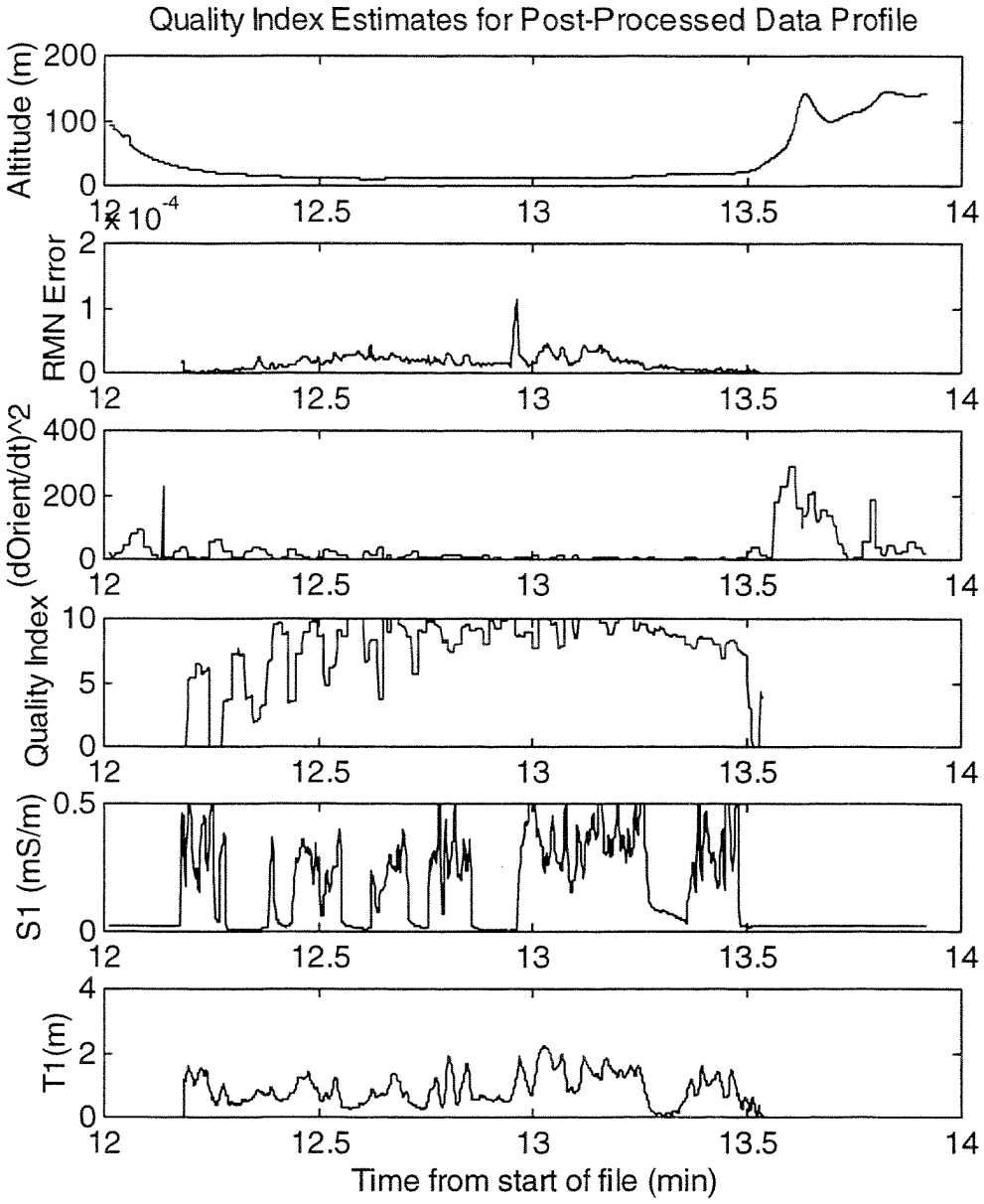

Figure 11.2.2: Quality index, observed and computed quantities for test line after post-processing.

12 Conclusions and Recommendations:

12.1 Calibration

The "hardware calibration" of the EIS sensor is very stable, displaying apparently negligible changes from year to year. The validity of this observation should be assessed further during system operations by careful measurement of the system calibration at the beginning of each ice season and/or field program. Provided that the new estimated calibration closely approximates the previously existing one (*i.e.* to within the expected error level of the calibration), changes to the sensor's internal calibration factors should probably be avoided in the interest of consistency, with the new calibration results being logged to permit future analysis of long-term trends. The conditions prevailing at the time of each calibration flight should be recorded, particularly the air temperature at the surface measurement site, in order to facilitate such analysis.

The accuracy of the "conventional calibration" method currently being used for the EIS system can maximised by setting up the surface measurement line on ice which is flat and snow-free, with at least 6 m of seawater beneath the ice. It is important to obtain estimates of the seawater conductivity beneath the ice in cases where rain, melt water or river flow could create a layer of reduced water conductivity beneath the ice. Maintaining a stable altitude of approximately 10 m over the measurement line during acquisition minimises the effect of drift, which may be further improved by performing a careful drift correction in post-processing before computing the calibration factors. Obtaining precise estimates of ice and water conductivity at the time of airborne data acquisition, and ensuring that the bird is flown straight and level over the ice, will also improve the accuracy of the ground-truth calibration factors.

Since flat, snow-free ice conditions with ice thick enough for helicopter landings (desirable for safe acquisition of surface measurements) are rare in the Gulf of St. Lawrence, alternative methods have been considered. The most attractive of these in view of its simplicity is to perform the calibration measurements over relatively deep, open seawater. Provided that the surface is rough enough (*e.g.* with ripples, or traces of brash ice) for stable laser altimeter operation, acquisition of an accurate altitude above the seawater surface is straightforward. The "calibration model" in this case is a uniform conductive halfspace. Provided that the water is indeed uniform in conductivity with depth and that the conductivity is well known, it should be possible to perform an accurate calibration with relatively little effort. The accuracy of the process is improved by the fact that calibration at the EIS operating frequencies is relatively insensitive to small changes in seawater conductivity.

It is therefore recommended that a comparison of conventional and open-water calibration be performed in the near future. Unless unexpected problems with open-water calibration appear as a result of this comparison, open-water

calibration may prove to be the most accurate and cost-effective way to calibrate the system in Labrador Sea and Gulf of St. Lawrence waters, or wherever patches of deep open seawater are present.

12.2 Operational error

Real-time data can be transmitted to users as soon as the helicopter lands. This gives it substantial value for operational purposes. Although real-time data uses a predicted drift correction, the quality of this correction improves as a flight progresses and can be further improved by increasing the number of background measurements. The rapid processing and turnaround capabilities of the DFO field processing computer and EIS-specific software should permit improvements in data accuracy and throughput.

An interesting possibility has been raised, based on the observation that the EM drift of the system appears to behave approximately as the square root of time since start-up. With some effort, it may be possible to improve both real-time drift prediction and post-processing drift corrections by fitting the known drift behaviour to a set of suitable "basis functions" to yield a smooth drift prediction or estimate that would significantly improve upon the linear approximation currently used. The risk in doing this is that such a fitting process would add to the complexity of the drift prediction and thereby increase the chances of error. This risk can be offset by using previously recorded flight data to test first the new prediction algorithm and then the user interface changes (if any) required to implement and control it.

In the longer term, a more detailed experimental analysis of EM drift in the system would be highly desirable. While many drift sources have been identified, none have been adequately quantified. It appears from existing observations that most EM drift derives from thermal effects, particularly in the bird shell and in the receiver antennas. Gaining a better understanding of these effects would permit engineering changes which could dramatically simplify system operation through the elimination or near-elimination of the requirement for system background measurements. This would improve real-time ice conductivity and thickness accuracies while increasing the productive proportion of each survey flight.

A clear result of the operational error analysis is that maintaining a low operating altitude for the bird yields substantial benefits in terms of system accuracy, especially for thin ice conditions, due to the much higher signal levels obtained at low altitudes. The optimal altitude range for EIS data acquisition is 10-15 m. Below this range, the demands on the pilot become unacceptably high and the risk of a surface strike increase, while above this range, EM error replaces laser altimeter error as the dominant error source in ice properties estimation. The main drawback to low-altitude operation is that it places greater demands on the helicopter pilot, particularly under low-contrast conditions or at the end of a long mission, when the effort required to maintain a given bird altitude increases

substantially. The tools used by the pilot for bird altitude monitoring at present are the EIS laser altimeter output and the helicopter's radar altimeter, although visual cues are sometimes useful as well. An "analogue" bird altitude readout utilising both laser and radar altimeter data for safety, perhaps coupled with bright visual "alarm" indicators to warn the pilot that the bird is approaching the upper or lower limits of the bird altitude "window," would reduce pilot effort substantially. Such a device would provide a disproportionately high increase in data quality and consistency for the modest cost involved, and would decrease the risk of surface strikes by the bird while surveying.

The user interface software in the helicopter computer should be altered to compute and display the Quality index, and to send this data to the operator's laptop. The Monitor program on the laptop would also have to be altered to display the Quality index. Access to the Quality index should significantly improve the operator's ability to monitor system performance in real time.

13 Acknowledgements

Support for this project was provided by the Panel on Energy Research and Development and by the Canadian Coast Guard.

References

Holladay, J.S. and S.J. Prinsenberg, 1999a. Airborne Electromagnetic Sea Ice Sounding Measurements During 1998 Gulf of St. Lawrence Field Program. Can. Contract. Rep. Hydrogr. Ocean Sci. 53: vi + 118 p.

Holladay, J.S. and S.J. Prinsenberg, 1999b. Airborne Electromagnetic Sea Ice Sounding Measurements During 1997 Gulf of St. Lawrence Field Program. Can. Contract. Rep. Hydrogr. Ocean Sci. 52: vi + 45 p.

Holladay, J.S, R. Lo and S.J. Prinsenberg, 1997, Bird orientation effects in quantitative airborne electromagnetic interpretation of pack ice thickness sounding, Oceans'97 Conference Proceedings, Halifax, NS.

Holladay, J.S. and R.Z. Moucha, 1998. Electromagnetic/laser ice thickness data from the Labrador Shelf, 1994, Can. Contract. Rep. Hydrogr. Ocean Sci. 49: v + 340 p.

Holladay, J.S., R.Z. Moucha and S. Prinsenberg, 1998, Airborne Electromagnetic Sea Ice Sounding Measurements During SIMMS'95, Can. Contract. Rep. Hydrogr. Ocean Sci., in press 50: vii + 179 p.

Kovacs, A. and J.S. Holladay, 1989, Development of an Airborne Sea Ice Thickness Measurement System and Field Test Results, CRREL Report 89-19, U.S. Army Corps of Engineers Cold Regions Research and Engineering Laboratory, Hanover, NH.

Kovacs, A, J.S. Holladay, and C.J. Bergeron, 1995, The footprint/altitude ratio for helicopter electromagnetic sounding of sea-ice thickness: comparison of theoretical and field estimates, Geophysics **60**, 374-380.

Misurak, K.M., C.P. Derksen, E.F. LeDrew and D.G. Barber, 1995. SIMMS 1995 data report, Earth Observations Laboratory Tecnical Report ISTS-EOL-SIMS-TR95-003, University of Waterloo.

Moucha R.Z, J.S. Holladay and S.J. Prinsenberg, 1998, Airborne Electromagnetic Sea Ice Sounder Measurements During RADARSAT Validation Project 1996. Can. Contract. Rep. Hydrogr. Ocean Sci. 51: vii + 349 p.

Peterson, I.K., S.J. Prinsenberg and J.S. Holladay, 1997. Comparison of Electromagnetic sea ice thickness measurements with RADARSAT imagery in the Gulf of St. Lawrence. Proceedings of GER'97: Geomatics in the Era of RADARSAT, Ottawa, Canada, May 25-30, 1997: 5pp.

Prinsenberg, S.J., I.K. Peterson and J.S. Holladay, 1996. Comparison of Airborne Electromagnetic Ice Thickness Data with NOAA/AVHRR and ERS-1/SAR Images. Atmosphere-Ocean 34(1): 185-205.

Prinsenberg, S.J., J.S. Holladay and L.A. Lalumiere, 1993. 1992 Electromagnetic/Radar Ice and Snow Sounding Project over the Newfoundland Shelf in 1992. Can. Techn. Rep. of Hydrogr. and Ocean Sc., No 144: vii + 59pp.

Prinsenberg, S.J., J.S. Holladay, J.R. Rossiter and L.A. Lalumiere, 1992. 1991 Beaufort Sea EM/Radar ice and snow sounding project. Can. Techn. Rep. of Hydrogr. and Ocean Sc., No 139: vi + 61pp.

Rossiter, J.R. and J. Scott Holladay, 1994, Ice Thickness Measurement, in *Remote Sensing of Sea Ice and Icebergs*, S. Haykin, E.O. Lewis, R.K. Raney and J.R. Rossiter, Eds, John Wiley and Sons, Toronto, pp 141-176.

Soininen, H, T. Jokinen, M. Oksama, and I. Suppala, 1998, Sea ice thickness mapping by airborne and ground EM methods, Exploration Geophysics, AEM'98 Special Edition, Australian Society of Exploration Geophysicists.